NASA TECHNICAL NOTE NASA TN D-2889

NASA TN D-2889

A WIND-TUNNEL STUDY OF GROUND-WIND LOADS ON LAUNCH VEHICLES INCLUDING THE EFFECTS OF CONDUITS AND ADJACENT STRUCTURES

by George B. McCullough and William J. Steinmetz

Ames Research Center
Moffett Field, Calif.

NATIONAL AERONAUTICS AND SPACE ADMINISTRATION • WASHINGTON, D. C. • JULY 1965

NASA TN D-2889

A WIND-TUNNEL STUDY OF GROUND-WIND LOADS ON LAUNCH VEHICLES INCLUDING THE EFFECTS OF CONDUITS AND ADJACENT STRUCTURES

By George B. McCullough and William J. Steinmetz

Ames Research Center
Moffett Field, Calif.

NATIONAL AERONAUTICS AND SPACE ADMINISTRATION

For sale by the Clearinghouse for Federal Scientific and Technical Information
Springfield, Virginia 22151 – Price $3.00

A WIND-TUNNEL STUDY OF GROUND-WIND LOADS ON LAUNCH VEHICLES INCLUDING THE EFFECTS OF CONDUITS AND ADJACENT STRUCTURES

By George B. McCullough and William J. Steinmetz
Ames Research Center

SUMMARY

Steady ground winds were simulated at Reynolds numbers up to 5-1/2 million based on the diameter of the upper stage. Measurements were made of the dynamic and steady-state bending moments.

It was found that circular conduits near the upstream stagnation line produced large dynamic response, whereas conduits on the lateral meridians tended to nullify the adverse effect of an upstream conduit. Fairing an upstream circular conduit to the vehicle with generous fillets also reduced its adverse effect.

A rectangular umbilical mast directly upstream of a model produced a violent sinusoidal response of nearly constant amplitude. The magnitude of the response was reduced by increasing the spacing between the mast and the vehicle or by the addition of a plate to the upper portion of the mast which effectively increased the width of the wake of the mast.

Selected data from tests of models of several specific vehicles are shown to illustrate the trends revealed by the tests of the simplified models. The effects observed with the simplified models are, in most cases, less pronounced for the more realistic specific vehicles.

A brief statistical investigation of several selected vibration records suggested that the lateral dynamic response can be characterized as the sum of a sine wave plus a narrow-band gaussian noise. It was indicated that the lateral unsteady forces contain a damping component and are thus coupled to model motion.

INTRODUCTION

The response of launch vehicles standing on the launch pad to natural wind excitation has been a matter of growing concern to engineers in recent years. Due to the lack of fundamental understanding of the aerodynamics of bluff bodies, it has not been possible to predict accurately the response of a vehicle to ground winds. Even wind-tunnel tests provide incomplete information, since a steady rather than a turbulent wind environment is simulated. In addition, the capability of present day wind tunnels to duplicate full-scale

Reynolds numbers for the proposed large-diameter vehicles of the future is limited. Hence, the demand for adequate design criteria has prompted a surge of investigations into the phenomenon of ground-wind induced oscillations of launch vehicles.

In 1958, Fung was the first to report measurements of the unsteady forces on a circular cylinder at supercritical Reynolds numbers (ref. 1); in addition, he obtained data for the same cylinder subjected to forced oscillations of various amplitudes (ref. 2). Fung's results indicated that the unsteady forces induced on a circular cylinder at supercritical Reynolds numbers are random rather than periodic as in the case of subcritical Reynolds numbers.

The results of reference 3 represent an extension of Fung's work in that pressures at several stations along a cantilevered circular cylinder were measured. The influence of tip shape on the aerodynamic forces acting on a cylinder is considered in references 4 and 5. Information regarding the axial correlation of the fluctuating pressures acting on the models, which reveals the three-dimensional character of the flow, is presented in all three references. In addition to presenting measured pressure data, Bohne (ref. 5) developed an analytical method of predicting ground-wind response.

The effects of model geometry (nose shape, fineness ratio, and stage-diameter ratio) and structural properties (damping, stiffness, and mass) on the response of launch vehicles were studied systematically in reference 6. The method and the aims of the investigation differed somewhat from the studies mentioned above. An attempt was made to define the response of launch vehicles to a steady ground wind. To accomplish this goal, the model response rather than the aerodynamic input was the principal quantity analyzed (although some pressure measurements are presented and discussed). It was found that the dynamic response in the wind direction was small, but the lateral dynamic response varied greatly in magnitude with model geometry and wind speed. Large lateral responses, in some instances, were attributed to nose shapes of medium bluntness, such as hemispheres or shallow cones, especially those with roughness on the upper stage. In addition, a limited investigation of the effects of conduits indicated that protuberances can induce large lateral oscillations.

The present investigation is a study of the effects of conduits and umbilical towers on the response of launch vehicles and, hence, represents an extension of the work of reference 6. The bulk of the data was obtained from two simple axisymmetric models. Most of the conduit-effect data were obtained from a model with an upper stage diameter equal to one-half the lower stage diameter. Tubular conduits were added to the upper stage of this model in arrangements of one, two, three, and four conduits. Most of the tower-effect data were obtained for a constant-diameter model utilizing two towers of different design. Circumstances prevented an all-inclusive investigation of tower effects, and the quantity of data is limited, but it is believed that important tower effects were revealed. It should be pointed out that since only model response was measured, only gross characteristics of the aerodynamic exciting forces can be deduced.

In addition to the results obtained from the systematic investigation of the two simple models, data for several specific launch vehicles are presented

to illustrate or clarify trends. The data for these "realistic" vehicles are intended to put the basic model results into proper perspective.

Since an analysis of random data is not complete without some consideration of statistics, the statistical characteristics of the response of the simple models are discussed briefly in the text.

The investigation was conducted in the Ames 12-Foot Pressure Wind Tunnel. Reynolds numbers, based on the diameter of the upper stage, up to 5-1/2 million were attained.

NOTATION

The models of this investigation represent vehicles that are standing vertically on the launch pad prior to firing. The wind vector is perpendicular to the model axis of symmetry. To an observer looking upwind, positive lateral and dragwise bending-moment vectors (right-hand screw rule) are forward and to the right, respectively. The moment center is the intersection of the tunnel floor fairing and the model axis of symmetry as shown in figure 1.

A frontal area of model exposed to wind, sq ft

C_l steady-state lateral bending-moment coefficient, $\dfrac{\text{mean lateral bending moment}}{qAy_A}$

$C_{l,d}$ dynamic lateral bending-moment coefficient, $\dfrac{(M_l)_{max}}{qAL}\,Nr\sqrt{\zeta_l\,\dfrac{V}{fD}}$

$C'_{l,d}$ modified dynamic lateral bending-moment coefficient, $\dfrac{[(M_l)_r]_{max}}{qAL}\,Nr\sqrt{\zeta_l\,\dfrac{V}{fD}}$

C_m steady-state dragwise bending-moment coefficient, $\dfrac{\text{mean dragwise bending moment}}{qAy_A}$

$C_{m,d}$ dynamic dragwise bending-moment coefficient, $\dfrac{(M_m)_{max}}{qAL}\,Nr\sqrt{\zeta_m\,\dfrac{V}{fD}}$

D diameter of upper stage, ft

f frequency of fundamental bending mode in lateral plane, cps

k "sine" parameter, $\dfrac{\sqrt{2\overline{(M_l)_p{}^2}}}{\sqrt{\overline{(M_l)_r{}^2}}}$

L length of model exposed to wind, ft

M	generalized mass for fundamental bending mode, $\int_o^L \phi^2 m \, dy$, slugs
M_l	dynamic lateral bending-moment response, ft-lb
$(M_l)_{max}$	maximum dynamic lateral bending moment measured during data sample, ft-lb
$(M_l)_p$	periodic (sinusoidal) component of dynamic lateral bending-moment response, ft-lb
$(M_l)_{peak}$	peak amplitude of dynamic lateral bending-moment response, ft-lb
$(M_l)_r$	random (gaussian) component of dynamic lateral bending-moment response, ft-lb
$\left[(M_l)_r\right]_{max}$	maximum dynamic lateral bending moment measured during data sample, random component, ft-lb
M_m	dynamic dragwise bending-moment response, ft-lb
$(M_m)_{max}$	maximum dynamic dragwise bending moment measured during data sample, ft-lb
m	mass per unit length, slugs/ft
N	structural parameter, $\dfrac{\int_o^1 \phi^2 m \, d(y/L)}{\int_o^1 \phi m (y/L) d(y/L)}$
P	frequency distribution or probability distribution
q	free-stream dynamic pressure, psf
R	free-stream Reynolds number, $\dfrac{\rho V D}{\mu}$
r	generalized fineness ratio, $\dfrac{1}{\int_o^1 \phi (x/L) d(y/L)}$
t	time, sec
V	free-stream velocity, fps
x	diameter at arbitrary model station, ft
y	distance from moment center to arbitrary model station, ft
y_A	distance from moment center to center of area, ft

ζ_l ratio of damping to critical damping for lateral fundamental bending mode

ζ_m ratio of damping to critical damping for dragwise fundamental bending mode

μ free-stream viscosity, slugs/ft sec

ξ normal coordinate of fundamental bending mode, tip deflection, ft

ρ free-stream density, slugs/cu ft

ϕ normalized mode shape of fundamental bending mode

ω circular frequency of fundamental bending mode in lateral plane, $2\pi f$, radians/sec

$\overline{(\ )}$ mean, $\frac{1}{T}\int_0^T (\ )dt$

$\dot{(\ )}$ first derivative with respect to time, t

$\ddot{(\ )}$ second derivative with respect to time, t

MODELS

The models, supplied by General Dynamics/Astronautics, San Diego, California, were made in circular tubular sections of aluminum alloy. The sections were flanged internally and bolted together with steel bolts in tension. Internal steel weights, screwed and clamped in place, simulated a realistic mass distribution. All models used the same bottom or first-stage section which was secured to a spool-shaped support pedestal with a Marman clamp. The pedestal was bolted to a 4-inch-thick steel base plate which, in turn, was bolted to the wind-tunnel structure. When the clamp was loosened, the model could be rotated to any desired orientation with respect to the wind.

The heavy steel base plate and the lower portion of the support pedestal were covered by a fairing or false floor to a height of 3-1/2 inches. The upper portion of the pedestal and the clamp was exposed to the windstream. This was not considered a significant disadvantage, however, because of the short moment arm of the exposed area.

The two "simplified" models will be referred to as the "two-diameter" model and the "constant-diameter" model. The two-diameter model necked down to an upper-stage diameter one-half that of the first stage, whereas the constant-diameter model was of substantially constant diameter throughout its length. Both of these models were derived from models of specific vehicles by removing all surface protuberances, filling screw holes, and polishing and buffing the surface so that the model components were essentially smooth circular cylinders with conical noses. Most of the tests with the

constant-diameter model were made with artificial roughness consisting of 16 vertical strips of 0.003-inch-thick by 1/2-inch-wide cellulose tape applied to the model in a staggered arrangement. The staggered tapes were thought to be conducive to a random aerodynamic excitation, uncorrelated along the portion of the model covered with tape. Sketches of the two simplified models are shown in figure 1 and photographs in figure 2.

The conduits used in conjunction with the simplified models were circular rods, 1/4 inch in diameter, attached to the outer surface of the model with flat-head machine screws as shown in figure 2. (A few tests were made with an upstream conduit held away from the surface with spacers; with a "faired" conduit; and, with a 1/8-inch-diameter conduit.)

In addition to tests of the isolated models, tests were made in conjunction with two different umbilical towers. Dimensioned photographs of the towers are shown in figure 3. The towers were bolted to the false floor and guyed to the walls of the wind tunnel with steel cables as shown in figure 2(b). Although the presence of guy wires upstream of the model was not desirable, it is believed that they had only a small effect on the response of the models because tests of the same model-tower configuration with different guy wire arrangements showed no discernible effect of the wires. Sketches of the geometric relationship of the towers to the models in plan view and the wind direction sign convention are shown in figure 4.

The specific vehicles for which data are shown will be referred to as models A, B, C, D, and E. Sketches are shown in figure 5 and photographs in figure 6. It might be noted that a few tests of the simplified constant-diameter model were made incorporating the vertical stiffeners that covered the center section of model A (fig. 6(a)).

The index mark noted in figure 5(b) represents a reference mark at the base of the model. Its purpose is to delineate the orientation of the model with respect to the wind; hence, the index mark will be evident in the model sketches shown in subsequent figures.

INSTRUMENTATION

The instrumentation consisted of four strain-gage bridges installed inside the pedestal near the level of the tunnel floor. The gages were arranged in pairs on the streamwise and lateral meridians so as to be sensitive to streamwise and lateral bending. Since the pedestals did not rotate with the model, the gages were always alined orthogonally with respect to the windstream.

A 20-kc carrier-amplifier unit powered the bridges and amplified the output signals. The output signals were fed to three separate recording devices: a recording oscillograph, a magnetic tape recorder, and a digital readout apparatus which provided the mean square, arithmetic mean, and the maximum for each record. The circuitry of the digital readout apparatus is described in reference 6.

MEASUREMENTS

Test Methods

The output signals from the strain gages in the model-support pedestal consisted of a fluctuating voltage which in most cases varied randomly in amplitude with an approximately sinusoidal wave form. Occasionally the signal was of nearly constant amplitude. The recording oscillograph and magnetic tape recorder provided continuous records of the voltage for later analysis. Data records were 1 minute long. Short samples of typical records are shown in figure 7. Except for rare cases the predominant response frequency was close to the natural first-mode bending frequency of the model.

The manner of making a run was to take data at successively increased values of tunnel velocity until visual observation of the monitoring oscilloscopes indicated that the design bending moment was being approached. Rough plots of the peak lateral bending moment were made during the test and any anomalies or peaks in the curve were measured in detail before the tunnel was stopped.

Test Variables

Since the investigation was designed to reveal the effects of conduits and umbilical masts in different orientations, model configuration and wind direction were the principal parameters of the investigation. For each run Reynolds number was a variable. The relation between Reynolds number and tunnel velocity was changed by changing tunnel pressure. Most runs were made with a tunnel pressure of 4.7 atmospheres ($\rho \approx 0.011$), but a lower pressure was also employed ($\rho \approx 0.007$). The free-stream Mach number was limited to 0.3 to avoid major compressibility effects.

Damping was changed by coating the support pedestal with a thick layer of a viscous paint-like material designed to increase damping. The pedestal in figure 6(e) is coated.

Calibrations

The strain gages in the support pedestals were calibrated by pulling on the model with known loads. The mode shapes and structural damping were determined by shaking the models with an electromagnetic shaker in the lateral and streamwise planes with no air flow in the wind tunnel.

Mode shape.- The mode shapes of the models were computed from the output of a "roving" accelerometer temporarily attached to several axial stations along the length of the models while they were shaken at constant amplitude. Fundamental mode shapes of the simplified models are shown in figure 8.

Damping.- The model damping was determined by recording the decay of the bending moment after the shaker had been mechanically disconnected from the

model. A simple but effective quick release mechanism had been incorporated in the shaker rod for this purpose. Damping was measured at frequent intervals throughout the investigation. Typical results are shown in figure 9. The maximum value of damping appropriate to a particular run is shown on the data plots.

Data Reduction

The dynamic response data were reduced to the coefficient form derived in the appendix of reference 6, that is, $C_{l,d}$ and $C_{m,d}$ in the lateral and streamwise planes, respectively. A constant value of the coefficient represents a dynamic bending moment increasing with V/fD. For a constant bending moment, the dynamic moment coefficient varies inversely with V/fD. For example, a $C_{l,d}$ of 20 at a V/fD of 5 may represent approximately the same bending moment as a $C_{l,d}$ of 2 at a V/fD of 30. The coefficient, intended to be a measure of the oscillatory aerodynamic input to the models, is based on the geometric and structural properties of the model and certain assumptions regarding the nature of the input forces. A statistical analysis of the lateral dynamic response is contained in Results and Discussion.

The form of the steady-state moment coefficient is conventional. The distance from the measuring station to the center of projected area was taken as the length dimension in the denominator. Hence, if the center of pressure should coincide with the center of area, the steady-state moment coefficient becomes equivalent to the corresponding steady-state force coefficient. Previous experience has shown that this is frequently the case.

Corrections were applied to the measured dynamic pressures to account for the blockage of the models and wakes.

RESULTS AND DISCUSSION

Because the lateral dynamic bending moment is the least predictable component of the total load experienced by a missile standing on the launch pad, most of the discussion presented herein will be concerned with this component of the load. In addition, selected steady-state lateral and dragwise data will be presented.

The dynamic data are plotted against the reduced velocity, V/fD. Increasing values of V/fD represent increasing wind speed (and Reynolds number) because the frequency f and the diameter D are constant for any one model configuration. A scale of Reynolds number, based on the upper stage diameter, is shown along the bottom of the plots. This scale is approximate because of minor variations in tunnel density.

Two-Diameter Model

Base runs were made with the two-diameter model devoid of conduits, protuberances, or nearby towers for various wind directions in order to verify the symmetry of the model. Data are shown in figure 10. The results are reasonably consistent except for a peak in $C_{l,d}$ at V/fD of 16 for one orientation and at V/fD of 42 for another. These inconsistencies are well beyond experimental error and it will be shown later that peaks of comparable magnitude can result from an extremely small asymmetry. Otherwise the value of $C_{l,d}$ is substantially constant at a little greater than 2, whereas $C_{m,d}$ is approximately one-quarter of this value.

It might be noted that the peak in the 0° data at V/fD of 42 (referred to above) is indicated by arrowheads extending from two data points. This means is utilized throughout the report to indicate that an emergency stop of the wind-tunnel drive system was necessitated by a rapid approach to the design bending moment.

Effect of one conduit on the dynamic lateral bending moment.- Tests were made with one conduit on the upper stage of the two-diameter model. Figure 11(a) shows the lateral dynamic response obtained for various wind directions with maximum tunnel density ($\rho \approx 0.011$). With the wind from 0°, large peaks ($C_{l,d} \approx 26$) appear in the response curve in the vicinity of V/fD of 16 and 17 (Reynolds number about 1.3 million), which made it unsafe to proceed to higher tunnel speeds. The oscillations corresponding to these peaks were of nearly constant amplitude. With the wind from -5°, the large peak is greatly reduced and occurs at a higher V/fD. For still greater angles, only minor peaks appear, but since some of these are at high V/fD, they represent large base bending moments.

Of special interest are the peaks with the wind from -135° and -145°. Attempts to define these peaks by taking data at a few intermediate points resulted in a still higher peak in one case (-135°), and in the disappearance of the peak in the other case (-145°).

Tests were also made with reduced tunnel density ($\rho \approx 0.007$) for four wind directions. These results are shown in figure 11(b). Reducing the density and, hence, Reynolds number for a given wind speed had the effect of moving the peak to a higher value of V/fD corresponding approximately to the same Reynolds number as for the higher density tests. (The peak for the -5° wind direction may have been passed over inadvertently.)

With the intention of isolating the flow around the nose from the flow around the cylinder directly beneath it, a few tests were made with a horizontal circular plate installed just beneath the nose. The plate was twice the diameter of the upper stage. Tests were made with a single conduit on the upstream stagnation line and 135° from it, respectively. Tests were also made with the conduit faired and with increased model damping. The results are shown in figure 12. By comparison with figure 11 it can be seen that the horizontal plate had no significant effect on the lateral dynamic response of the model with the unfaired conduit.

The faired conduit configuration was achieved by stretching 2-inch-wide cellulose tape over the conduit with the outer edges of the tape adhering to the cylindrical surface of the upper stage thus providing generous fillets on both sides of the conduit. This modification completely removed the large peaks in the $C_{l,d}$ curve with the conduit on the stagnation line. There was a slight peak which failed to repeat with decreasing tunnel speed with the conduit at 135° to the wind. Since the flow separator plate produced no benefit, whereas the conduit fairing greatly reduced the severity of the lateral oscillations, it seems evident that the aerodynamic excitation originated along the upper stage and was triggered by the presence of the cylindrical conduit. It is surmised that the unfaired conduit shed separated flow into the main flow around the model, thereby inducing the aerodynamic excitation, whereas the faired conduit did not.

A support pedestal, coated with a damping compound was used to increase model damping from the normal range of 0.004-0.005 to approximately 0.010. With the lower damping and the unfaired conduit on the upstream stagnation line, large amplitude sinusoidal oscillations were recorded. With increased damping, the response was relatively calm and random. Hence, the existence of coupling between the model motion and the excitation is suggested. This phenomenon has been noted previously in the literature (e.g., refs. 6 and 7).

Tests were made with one conduit on the lower stage for two wind directions. Results are shown in figure 13. The effects are similar to those observed with the conduit on the upper stage except that with the wind from 0° the magnitude of the oscillations was reduced and it was possible to proceed to higher wind speeds. With reduced wind-tunnel density no significant peaks were observed.

Effect of small protuberances on the dynamic lateral bending moment.- A comparison plot showing the effect of surface irregularities less prominent than a 1/4-inch-diameter (0.06 D) conduit is shown in figure 14. The smallest of these, a 1/2-inch-wide strip of 0.003-inch-thick cellulose tape on the upstream stagnation line, produced only minor peaks in the $C_{l,d}$ curve. A 1/8-inch-diameter conduit on the upstream stagnation line produced a peak in the response curve at a Reynolds number of about 2 million for both the high- and low-density tests. A vertical row of five equally-spaced round-head machine screws (head diameter, 3/16 inch) on the upstream stagnation line produced a peak in the response curve at a Reynolds number of approximately 1.8 million. It will be recalled that the lateral dynamic response with the 1/4-inch-diameter conduit on the upstream stagnation line exhibited peaks at a Reynolds number of about 1.3 million (fig. 11). In all cases studied, a protuberance on the upstream stagnation line induced relatively large lateral oscillations at a Reynolds number of approximately 75,000 based on the diameter of the disturbing element.

With the wind from -135°, the 1/8-inch-diameter conduit induced a moderate, nonrepeating peak characteristic of conduits in this location.

Effect of two conduits on the dynamic lateral bending moment.- Tests were made with two conduits on the upper stage of the two-diameter model with two

different angular spacings of the conduits: 90° and 180°. The lateral dynamic response data are shown in figure 15. With the 90° spacing, no large peaks were found. Even for a wind direction of -45° which placed one conduit on the upstream stagnation line, no extraordinary oscillations were observed. Apparently the presence of the second conduit 90° from the wind vector nullified the adverse effect of the upstream conduit. With the 180° conduit spacing, only the 0° wind direction produced a large (and insurmountable) peak.

It is interesting to note that the two orientations which placed one or two conduits ±135° from the forward stagnation line produced peaks at relatively high values of V/fD.

Effect of three conduits on the dynamic lateral bending moment.- Lateral dynamic response data for the model with three conduits at 90° intervals are shown in figure 16. The only orientations which produced significant peaks in the data were the two which placed conduits 135° from the stagnation line. These peaks were difficult to repeat.

Effect of four conduits on the dynamic lateral bending moment.- Characteristics of the model with four equally spaced conduits on the upper stage are shown in figure 17. The lateral dynamic loads were low with this configuration except with the wind from 45°. In this case, with conduits ±45° and ±135° from the forward stagnation line, several peaks in the $C_{l,d}$ curve are apparent.

From the foregoing results, it is evident that a launch vehicle with several external conduits is less likely to encounter large lateral dynamic loads than a vehicle with just one conduit. Arrangements involving conduits at opposite meridians in a plane normal to the wind vector are particularly free of oscillations.

Effect of conduits on the steady-state lateral bending moment.- The variation of the lateral steady-state moment coefficient with wind direction for two values of Reynolds number is shown in figure 18 for arrangements involving one, two, three, and four conduits. For the single-conduit arrangement the sense of the lateral steady-state force was apparently away from the side with the conduit. For the two-conduit configurations the direction of the force was away from the side with the forward conduit. In general, a conduit near 67° from the forward stagnation line has the largest effect, a conduit near the upstream stagnation line has more influence than one near the rear stagnation line, and the sense of the lateral force is away from the side with the dominant conduit.

Effect of conduits on the steady-state dragwise bending moment.- Plots of the dragwise steady-state bending-moment coefficient for the basic model and several conduit arrangements are shown in figure 19. As might be expected, configurations with conduits ±90° from the upstream stagnation line attained the highest drag coefficient ($C_m \approx 0.6$) and the basic model exhibited the lowest ($C_m \approx 0.5$).

Effect of tower.- Data from four runs made with tower 2 directly upstream of the two-diameter model are shown in figure 20. The tower was placed in two locations: the "normal" distance from the vehicle and twice the normal distance (fig. 4). In both locations the tower was tested with and without a "fix," which consisted of a flat plate 2.62 D wide by 0.22 L long located on the upstream face of the tower and flush with the top of the tower. The tower induced a large peak in $C_{l,d}$ at a V/fD of 13. Moving the tower upstream reduced the magnitude of the peak and moved the peak to a V/fD of 15. The addition of the plate reduced the magnitude of the peak, especially with the tower in its normal position, and induced another peak at a higher V/fD. It might be noted here that the character of the model response with tower 2 directly upstream was somewhat unusual; that is, at the V/fD at which $C_{l,d}$ peaked, the model response was approximately sinusoidal. For V/fD values surrounding the critical value, the model response exhibited a beat frequency approximately equal to the difference between model frequency and the vortex shedding frequency of the tower. It was assumed that the tower vortex shedding frequency is directly proportional to the wind speed, V, and inversely proportional to the tower width and that the shedding frequency and model natural frequency coincide at the V/fD at which $C_{l,d}$ is maximum. The beating characteristic of the response was not peculiar to the two-diameter model but was observed when tower 2 was directly upstream of any model.

Tower 2 upstream of the two-diameter model induced no appreciable steady-state lateral moments but caused a dragwise steady-state moment coefficient of approximately -0.1.

Constant-Diameter Model

It was hoped that the constant-diameter model would exhibit a flat dynamic response, and thereby provide a good base against which to assess the effects of nearby towers. Such proved not to be the case as can be seen in figure 21. Data for the basic model with the longitudinal stiffeners are characterized by a peak in $C_{l,d}$ at a V/fD of 8 for both tunnel densities. Attempts to eliminate the peak by the addition of roughness to the nose and upper stage proved fruitless, but tape on the nose did reduce the peak somewhat, indicating that the nose was a major source of the excitation.

Another attempt was made to eliminate the peak by machining off the longitudinal stiffeners and bringing the cross section of the model to a true circular section with a surface finish comparable to that of the two-diameter model. That the results were disappointing is evident in figure 22. A very high peak in the lateral oscillations was encountered at a V/fD of 8.

Still another attempt was made to eliminate large peaks in the lateral response curve of the constant-diameter model by the addition of surface roughness in the form of staggered tapes as described in Models. Figure 23 shows that the response was greater than was the case with the integral stiffeners on the upper stage (fig. 21). It may be noted that the addition of a circular plate, twice the diameter of the model, just beneath the nose, greatly reduced the oscillatory response as is shown in figure 23. A similar effect is

reported in reference 6, and indicates that there was an interaction between the flow field around the nose and that around the cylindrical body.

Because of time limitations, it was decided to conduct the remainder of the investigation utilizing the roughened model. Attention will no longer be called to the staggered roughness tapes adopted as part of the standard constant-diameter model configuration.

Effect of conduits on the dynamic lateral bending moment.- A few tests were made with conduits applied to the upper portion of the constant-diameter model. Results are shown in figure 24. With a single conduit upstream, the dynamic lateral bending-moment coefficient reaches a value of 34.5, well above the 21 recorded for the basic model (fig. 23). Two conduits ±90° from the wind were effective in reducing the peak response below that of the basic model. Adding spacers under the single upstream conduit provided a gap of 0.087 inch between the conduit and the model greatly reduced the response. It should be noted that although a conduit on the upstream stagnation line has been shown to affect the dynamic lateral response of both the constant-diameter model and the two-diameter model, the influence of the nose area of the basic constant-diameter model has been shown to be significant; whereas for the two-diameter model, the excitation was shown to be independent of the nose region.

Effect of towers on the dynamic lateral bending moment.- The effect of tower 1 on the lateral dynamic response of the constant-diameter model was explored and data are presented in figures 25, 26, and 27. For the basic model (fig. 25) the tower had little effect except for a wind direction of -22½°. In this orientation, the tower "arm" was directly upstream of the model and the large response peaks were greatly reduced. It is possible, therefore, that there may be some similarity between this tower effect and the effect of a conduit with spacers on the upstream stagnation line (fig. 24). The low-density runs for all wind directions show a peak in the $C_{l,d}$ curve at a V/fD of 16 which did not appear in the tests of the basic model without the tower (fig. 23).

With two conduits on the upper stage in a plane normal to the wind (fig. 26) there were no significant peaks in the response curves. With one conduit on the upstream stagnation line and tower 1 directly upstream (fig. 27) the oscillations were greatly reduced below those experienced by the model without the tower (fig. 24). This result is inexplicably in sharp contrast to the effect of tower 1 on the basic model (figs. 23 and 25(a)).

Several runs were made utilizing tower 2 in conjunction with the constant-diameter model. Figure 28 presents data for tower 2 directly upstream of the basic model and the model with two conduits ±90° from the wind. In both cases a large peak in the $C_{l,d}$ curve at a V/fD of 6 is apparent. Since the response of the model with conduits on opposite meridians without the tower (fig. 24) was relatively low, the large response experienced with tower 2 is obviously an effect of the tower. The data presented for the two-diameter model (fig. 20) and the data shown in figure 28 verify that tower 2, when directly upstream of a model, induced large excitation at a reduced velocity of 10 based on the tower width.

Effect of tower on the steady-state bending moments.- Steady-state data for the basic model and the model with two conduits ±90° from the upstream stagnation line, each in conjunction with tower 1, are illustrated in figure 29. The effect of the tower directly upstream of the model is to decrease the drag-wise bending moment and to exert proportionately less influence as the wind vector rotates to 90° from the tower. The effect of tower 1 on the steady-state lateral moment is also quite clear. When the tower is in the range 0°-45° from the wind vector, the lateral force is in the direction toward the tower; with the wind vector 45°-90° to the tower, the sense of the lateral force is away from the tower.

Models of Specific Vehicles

The data presented in the foregoing sections have defined the influence of conduits and adjacent umbilical masts or towers in conjunction with the two-diameter model and the constant-diameter model. In addition to the above, however, there is a large body of data from tests of specific launch vehicles (ref. 8) which will be drawn upon to illustrate the trends discussed previously. These data will put realistic bounds on the results obtained for the simplified models.

Effect of conduits.- Figure 30 illustrates conduit effects in connection with Model C. This model had two external conduits spaced 90°. One was a cylindrical conduit and the other faired. For wind directions which placed the cylindrical conduit at or near the upstream stagnation line or 135° from the stagnation line there were peaks in the response curves. For other orientations, even the one which placed the faired conduit at the upstream stagnation line, the response curves were flat.

Figure 31 shows the effect of damping on the lateral dynamic response of Model A. The model response in this orientation was greater than for any other wind direction and was probably due to the presence of a cylindrical conduit on the lower stage in the upstream position. The adverse effect of the upstream conduit was not eliminated by the presence of the faired conduit at 90°. With the lowest value of damping, the response was nearly sinusoidal and violent. As the damping was increased the response became less violent and more random in nature. It will be recalled that a similar effect was noted in connection with the simplified two-diameter model (see fig. 12).

In figure 32 is shown a comparison of the lateral dynamic response of four constant-diameter configurations, all of which employed the same conical nose which has been shown to be a source of aerodynamic excitation. The four models are: the simplified constant-diameter model in smooth condition (without roughness tapes); the constant-diameter model before the integral stiffeners were machined off; Model A; and Model B which had a longer section of external stiffeners than Model A, but no protuberances on the upper stage. The data show that as the constant-diameter model became more cluttered with protuberances, the lateral dynamic response decreased. It is surmised that in this case the external protuberances acted as spoilers and fixed the regions of boundary-layer separation, thereby stabilizing the flow pattern and reducing the unsteady aerodynamic input.

In figure 33 are shown some effects of changes to the nose of Model E. This model had a relatively blunt ogival nose and was tested with and without an insulating blanket. The unblanketed nose was smooth, but the blanket simulation consisted of a series of concentric corrugations representing air ducts in the fabric blanket. An external pipe or vent interconnected these air ducts as shown in figure 6(f). The model was tested with two angular locations of the nose pipe. The lateral dynamic response was low and flat for the smooth nose. With the blanket which effectively roughened the nose, the response was greater, especially with the nose pipe at 172°. (In this rearward position it is doubtful that the nose pipe itself had any effect.) This is in accord with the findings of reference 6 which showed that roughness below noses of medium bluntness caused large response. With the nose pipe around to the side at -98° the response was reduced, possibly because the pipe acted as a spoiler and stabilized the flow in the vicinity of the nose.

Figure 34 shows the variation of C_m and C_l with wind direction and was crossplotted from tests of Model C in several orientations for a Reynolds number of about 3.7 million. The variation of C_m is somewhat erratic but averages out about 0.6. The steady-state lateral force is, in general, away from the side with the conduit and is typical of many models.

Effect of towers.- In figures 35, 36, and 37 are shown the effects of wind direction on Models B, D, and E, respectively. It will be noted that the response of Model B was rather large for certain positive wind directions (fig. 35), the response of Model D was relatively small throughout the entire range of wind angles (fig. 36), while Model E experienced large oscillations at all positive angles (fig. 37). It is thus apparent that factors (i.e., nose shape, conduits, protuberances, etc.) other than the presence of the tower influenced the response of these models. Only one consistent effect can be charged to the tower itself and this effect is not revealed in the figures. That is, for wind directions with tower 1 in the near-upstream vicinity of the models, relatively large second mode oscillations were observed at the higher velocities. The critical wind direction in this respect was invariably -22.5°. It might be noted that at this wind direction, the tower 1 "arm" was directly upstream of the models. Except for this particular model-tower 1 configuration, the model responses were primarily in the fundamental mode. Information regarding second mode characteristics was insufficient to provide quantitative results.

Figure 38 shows the effect of modifications to the basic structure of tower 2 on the dynamic response of Model D. The original tower model was solid on all four sides, and when mounted directly upstream induced such a violent response that it was impossible to determine the peak of the $C_{l,d}$ curve. The dynamic dragwise moment response was unusually high. Rectangular cutouts in the upstream face and sides of the tower, either fully open or covered with an expanded metal mesh as shown in figure 3(b), did not reduce the lateral dynamic response enough to permit the peak values to be determined, but did reduce the dragwise response. Shortening the tower in the open rectangle configuration by cutting off the top 8 inches reduced the lateral dynamic response sufficiently so that the peak in the $C_{l,d}$ curve could be defined.

Further tests were made with the tower in the mesh-covered configuration because it was believed that this degree of solidity most nearly represented the actual tower. Various "fixes" for the tower in this configuration were tried and the results are shown in figure 39. Perforated and solid plates of various heights and widths were attached to the downstream face of the tower near the top. The most effective fix of those tried was a solid plate 2.62 D wide and 0.23 L long attached flush with the top of the tower.

Statistics

In the preceding sections, the experimental results were presented in a form intended to show the variation of model response with wind speed. It is intended now to explore the statistical nature of the data and thus to gain further insight into the nature of the observed random phenomenon. It should be noted that only the lateral component of the dynamic response was analyzed.

Electronic statistical analyzer.- The characteristics of the hybrid analog-digital computer used in the statistical analysis of the lateral dynamic response are discussed in detail in reference 9. Selected magnetic tape records of the response signal were analyzed by the computer system. The computer scanned a 45-second sample from each 60-second data record and counted the number of peaks (in the rectified signal) which exceeded preselected voltage levels. The results for each record analyzed were plotted in the form of a "frequency distribution" defined as the proportion of the total number of peaks which exceeded the preset voltage levels. It might be noted (with reference to succeeding figures) that, for the data analyzed, one peak represents approximately 0.0005 of the total number.

For several response records, both a computer and a manual analysis were performed. The results for two samples are shown in figure 40. Even though the two records analyzed were apparently considerably different in statistical character, the frequency distributions yielded by the two methods agree well.

As used in this report, the term "probability distribution" is defined as the probability that a peak will exceed an arbitrary value. Hence, the probability distribution for the peaks of a sine wave is given as follows:

$$P(\zeta^2 > \zeta'^2) = \begin{cases} 1, & 0 \leq \zeta'^2 < 2 \\ 0, & \zeta'^2 \geq 2 \end{cases}$$

where

$$\zeta = \frac{(M_l)_{peak}}{\sqrt{\overline{M_l^2}}}$$

It will be noted in figure 40 that the solid vertical line at a value of the abscissa of 2 is redundant. If, however, the distribution shown is thought of as that which approaches (in a limiting sense) the probability distribution for

the peaks of a sine wave, no difficulties arise. In any case, it is believed that the representation shown, while somewhat ambiguous mathematically, is graphically lucid. Hence, that representation will be employed in subsequent figures.

In order to maintain confidence in the computer-analyzer, an arbitrarily chosen response record was analyzed twice daily throughout the period of analysis. The results for several such analyses are shown in figure 41. Since a slightly different sample of the record was analyzed each time, some variation in results was anticipated. The apparent increase in scatter with increased values of the abscissa is attributable to the semilog scale employed. In fact, it may be noted that the actual scatter decreases with increasing values of the horizontal coordinate. This result verifies a similar finding in reference 9.

Because of the good agreement between the computer- and manually-derived frequency distributions and the demonstrated consistency of the computer, it is believed that the computer results are reliable.

Analysis.- The following discussion is concerned with the lateral component of dynamic response of the simplified models. The results are qualitative in the sense that no attempt has been made to relate particular frequency distributions to specific configurations.

Rice (ref. 10) has developed an expression for the probability density of the envelope of a signal consisting of a sine wave plus a narrow-band gaussian noise (see appendix A). It is assumed that the probability distribution of the cyclic peak values and the probability distribution of the envelope are identical. The distributions are certainly identical for the two limiting cases; that is, for a sine wave and for a narrow-band gaussian signal (see, e.g., ref. 11). The above assumption is used to compare the probability distribution for the peaks of a sine wave plus narrow-band gaussian noise with the frequency distributions for several typical data samples in figure 42. The good (qualitative) agreement between the experimental frequency distributions and Rice's theoretical probability distribution indicates that, for most cases, the lateral dynamic response of the simplified models can be considered to be composed of sinusoidal and gaussian components.

Since the fundamental mode dominated the model response, the equation of motion for the system can be written as follows:

$$M\ddot{\xi} + 2\zeta_1\omega M\dot{\xi} + \omega^2 M\xi = \Xi$$

Some information concerning the individual terms in the above equation has been gained and discussed in previous sections of the report. For example, the frequency of model response was observed to vary only slightly ($|\Delta\omega/\omega| < 0.05$) during testing, except for the rather special configurations with tower 2 upstream of a model. The damping coefficient for the models was, to some degree, nonlinear (see fig. 9). It will be recalled that, in several instances, the model damping was varied for a given model configuration. It was found that, in general, as the model damping was increased, the sinusoidal component of the response was diminished, thus indicating a dependence of the aerodynamic

input upon model response. Indeed, it is suggested that an aerodynamic damping term is operative. Hence, for the models tested, the following functional relations can be stated:

$$M \neq M(\xi, \dot{\xi}, \ddot{\xi}, \ldots)$$

$$\omega \neq \omega(\xi, \dot{\xi}, \ddot{\xi}, \ldots)$$

$$\zeta_1 = \zeta_1(\xi, \dot{\xi}, \ddot{\xi}, \ldots)$$

$$\xi = \xi(t) = a \cos \omega t + \xi_r(t)$$

$$\Xi = F(\xi, \dot{\xi}, \ddot{\xi}, \ldots)\dot{\xi} + G(t)$$

where ξ_r is the random (gaussian) component of the model response, F is the aerodynamic damping coefficient, and G is the motion-independent constituent of the aerodynamic forcing function.

Now, it can be reasoned from observations discussed in previous sections of the report (see also ref. 6) that the influence of model motion on the aerodynamic input force is greatest as the model response tends to sinusoidal and is negligible when the model response is gaussian. Although the form of the aerodynamic damping, F, cannot be uniquely determined from observations of model response, the occurrence of a random (gaussian) response with no influence on the aerodynamic input implies that, in this case,

$$F = 0$$

$$G(t) = N(t)$$

where N is a gaussian noise. It would thus seem that a reasonable expression for the aerodynamic input force acting on a given model for a particular wind speed is given by:

$$\Xi = F(\xi, \dot{\xi}, \ddot{\xi}, \ldots)\dot{\xi} + N(t)$$

It is interesting to note that Caughey (ref. 12) considered a specific form of the function F. He showed that the response (with ζ_1 constant) can be characterized as the sum of a sinusoidal (self-excited) component and a narrow-band gaussian component, centered at the natural frequency of the system. Reed (ref. 7) conducted an analog computer study with another expression for the aerodynamic damping which showed that the response can be either random or sinusoidal depending on the relative magnitudes of the structural and aerodynamic damping coefficients. The analytical investigations cited above lend credence to the form of the aerodynamic input force deduced from the experimental evidence of the present investigation.

To summarize, two aspects of the phenomenon of ground-wind induced oscillations of launch vehicles have been clarified in the above analysis:

1. The lateral dynamic response of the simplified models, for most cases studied, can be characterized as the sum of a sine wave and a narrow-band gaussian noise centered at the fundamental model frequency.

2. The aerodynamic input to the simplified models, subjected to a steady wind, is, in general, a motion-coupled phenomenon. The coupling between the aerodynamic forces and the model response is accomplished through an aerodynamic damping force, the magnitude of which depends upon the geometry of the vehicle (conduit location, surface roughness, nose shape, etc.) and Reynolds number.

A modified dynamic lateral bending-moment coefficient incorporating the above results is developed and discussed in appendix B.

SUMMARY OF RESULTS

Tests were made to determine the effects of external conduits and adjacent structures on the dynamic response of two simplified models of launch vehicles to steady ground winds. Measurements were made of the dynamic and steady-state bending moments at the base of the models for Reynolds numbers up to 5-1/2 million. Data from tests of models of several specific vehicles illustrate the effects of conduits and nearby umbilical masts as applied to realistic configurations. Statistical analyses were made of selected vibration records. The results presented herein apply specifically to these models and should not be generalized as being applicable to all vehicles.

The data are summarized in the following paragraphs:

A circular conduit on the upstream stagnation line caused a large lateral dynamic response over a narrow range of velocities. The motion of the model associated with these large responses was nearly sinusoidal and of constant amplitude, suggestive of a motion-coupled phenomenon, in contrast to the more usual random-amplitude response. Fairing the circular conduit with generous fillets greatly reduced the lateral response. A circular conduit on either or both lateral meridians greatly reduced the adverse effect of a conduit on the upstream stagnation line. For this reason, multiple conduit arrangements were less likely to produce a large response than a single conduit. A limited amount of evidence suggested that the excitation induced by a single conduit on the upstream stagnation line occurred at a Reynolds number of approximately 75,000 based on the diameter of the protuberance.

A conduit located 135° from the upstream stagnation line also produced a peak in the lateral dynamic response curve. These peaks proved difficult to define.

Lateral steady-state moments appeared in conjunction with conduits arranged unsymmetrically about the meridian plane. The most effective conduit in this respect was in the vicinity of 67° from the upstream position. Conduits near the upstream stagnation line were more effective than conduits near the rear. The sense of the lateral force was away from the side with the dominant conduit.

An investigation of the effects of adjacent towers revealed that a rectangular mast directly upstream of any model induced extremely large dynamic loads. Increasing the distance between the mast and the vehicle or increasing the width of the wake from the mast by means of a solid plate normal to the wind reduced the magnitude of the response.

Data for models of specific vehicles, in general, corroborated the results determined from the simplified models, but the effects were less pronounced for the more realistic specific vehicles.

The statistical analysis indicated that the dynamic lateral response of the simplified models can be characterized as the sum of a sine wave and a narrow-band gaussian noise. It was inferred that a damping component of the aerodynamic forces is responsible for the aforementioned character of the response. These results accent the need for models that are dynamically as well as geometrically scaled when investigating the dynamic response of specific launch vehicles to a steady wind. Hence the importance of knowledge of full-scale structural properties, particularly damping, is clear.

Ames Research Center
National Aeronautics and Space Administration
Moffett Field, Calif., April 16, 1965

APPENDIX A

PROBABILITY DISTRIBUTION OF THE ENVELOPE OF THE SUM OF A DISCRETE SINUSOID AND A NARROW-BAND GAUSSIAN PROCESS

Consider the function described as follows:

$$M_l = (M_l)_p + (M_l)_r$$

where $(M_l)_p = A \cos \omega t$ and $(M_l)_r$ is a sample function from a stationary narrow-band (centered at ω) gaussian random process. Now, the frequency distributions presented in this report show the proportion of the total number of peaks which exceeded a given value during a sample. Then, in order to compare the experimental response data with the function displayed above, it is necessary to determine the probability distribution of the cyclic peak values for that function.

It is convenient to define the following:

$$\xi = \frac{(M_l)_{env}}{\sqrt{\overline{(M_l)_r^2}}}$$

$$\eta = \frac{(M_l)_{env}}{\sqrt{\overline{M_l^2}}}$$

$$\zeta = \frac{(M_l)_{peak}}{\sqrt{\overline{M_l^2}}}$$

$$k = \frac{\sqrt{\overline{2(M_l)_p^2}}}{\sqrt{\overline{(M_l)_r^2}}}$$

Rice (ref. 10) showed that the probability density of ξ is given by:

$$p(\xi) = \xi \exp\left[-\frac{1}{2}(\xi^2 + k^2)\right] I_o(k\xi)$$

where I_o is the modified Bessel function of zero order. Then, the probability that ξ will be above a given value ξ' is given by:

$$P(\xi') = \int_{\xi'}^{\infty} p(\xi)d\xi = \int_{\xi'}^{\infty} \xi \exp\left[-\frac{1}{2}(\xi^2 + k^2)\right] I_o(k\xi)d\xi$$

The probability distribution, $P(\eta')$, may be easily determined by making use of the relation:

$$\overline{M_1^2} = \overline{(M_1)_p^2} + \overline{(M_1)_r^2}$$

or

$$\frac{\overline{M_1^2}}{\overline{(M_1)_r^2}} = \frac{\overline{(M_1)_p^2}}{\overline{(M_1)_r^2}} + 1 = \frac{1}{2}k^2 + 1 = \frac{\xi^2}{\eta^2}$$

then

$$\xi = \eta\sqrt{\frac{1}{2}k^2 + 1}$$

hence

$$P(\eta') = P(\xi')$$

where

$$\eta' = \frac{1}{\sqrt{\frac{1}{2}k^2 + 1}}\xi'$$

The probability distribution of the cyclic peak values is not necessarily represented by the probability distribution of the envelope. However, it might be noted that for a narrow-band gaussian signal, these two distributions are identical (e.g., see ref. 11). For the case under discussion here, it will be assumed that:

$$P(\zeta') = P(\eta')$$

for $\zeta' = \eta'$. The probability distribution, $P(\zeta')$, for several values of the sine parameter, k, is shown in figure 43. The computations for each k were carried out as follows:

(a) An arbitrary value of ξ' was chosen.

(b) Reference 13 was used to determine $P(\xi')$.

(c) The probability, $P(\zeta')$, was then computed from the relation:

$$P(\zeta') = P(\xi')$$

where

$$\zeta' = \frac{1}{\sqrt{\frac{1}{2}k^2 + 1}}\,\xi'$$

APPENDIX B

DEVELOPMENT OF A MODIFIED DYNAMIC LATERAL BENDING-MOMENT COEFFICIENT, $C'_{l,d}$

The coefficient, $C_{l,d}$, derived in reference 6 has been utilized in this report to represent the unsteady lateral response of the models tested. As noted in reference 6 this characterization, insofar as it represents the aerodynamic input forces, is dependent upon several assumptions. Utilizing the results of the above discussion regarding lateral response statistics, it is possible to substitute an empiricism for one of the assumptions used in deriving $C_{l,d}$ and thus obtain a representation of the random aerodynamic input forces which is more realistic.

The equation of motion for the aerodynamically excited model is assumed to be of the form:

$$M\ddot{\xi} + 2\zeta_l \omega M\dot{\xi} + \omega^2 M\xi = F(\xi,\dot{\xi},\ddot{\xi}, \ldots)\dot{\xi} + N(t)$$

where $N(t)$ is a small gaussian noise force. It is presumed that the linearization technique employed in reference 12 may be applied regardless of the specific form of F and, hence, that this nonlinear differential equation can be replaced by two approximately equivalent linear differential equations as follows:

$$M\ddot{\xi}_p + \omega^2 M\xi_p = 0$$

$$M\ddot{\xi}_r + 2\zeta_l \omega M\dot{\xi}_r + \omega^2 M\xi_r = N(t)$$

where $\xi_p = a \cos \omega t$ is the periodic part of the solution and ξ_r is the randomly varying (gaussian) part of the solution. The development of the dynamic coefficient, $C_{l,d}$, given in reference 6 can now be duplicated to yield a revised coefficient, $C'_{l,d}$, which represents that portion of the unsteady aerodynamic input force which is independent of model motion. Specifically, the revised form of the dynamic lateral bending-moment coefficient is given by:

$$C'_{l,d} = \frac{\left[(M_l)_r\right]_{max}}{qAL} Nr \sqrt{\zeta_l \frac{V}{fD}}$$

where $\left[(M_l)_r\right]_{max}$ is the maximum value of the random component of bending-moment response recorded during a sample. It should be noted that when the sinusoidal component of the response signal, $(M_l)_p$, is zero, $C_{l,d}$ and $C'_{l,d}$ are identical.

The coefficient, $C'_{l,d}$, for a given sample was determined experimentally in the following manner:

(a) The frequency distribution for each sample was fitted to a sine plus random probability distribution using figure 43 and one point of the frequency distribution, thus determining an appropriate value of the sine parameter, $k = \sqrt{2\overline{(M_l)_p^2}} \Big/ \sqrt{\overline{(M_l)_r^2}}$.

(b) Since the mean square of the bending-moment signal, $\overline{M_l^2}$, was measured for each data sample, use may be made of the relation derived in appendix A:

$$\frac{\overline{M_l^2}}{\overline{(M_l)_r^2}} = \frac{1}{2}k^2 + 1$$

That is,

$$\overline{(M_l)_r^2} = \frac{\overline{M_l^2}}{\frac{1}{2}k^2 + 1}$$

(c) The peaks occurring during each 45-second sample analyzed totaled approximately 990; then,

$$P\left\{\frac{\left[(M_l)_r\right]_{max}}{\sqrt{\overline{(M_l)_r^2}}}\right\} \approx \frac{1}{990} \approx 0.001$$

Since $(M_l)_r$ has been assumed to be gaussian, the maximum value, $\left[(M_l)_r\right]_{max}$, can be estimated from the Rayleigh distribution; that is, for a probability of 0.001:

$$\frac{\left[(M_l)_r\right]_{max}}{\sqrt{\overline{(M_l)_r^2}}} \approx 3.7$$

or

$$\left[(M_l)_r\right]_{max} \approx 3.7\sqrt{\overline{(M_l)_r^2}}$$

(d) Finally, the revised (or modified) dynamic lateral bending-moment coefficient for a given sample was computed from the relation:

$$C'_{l,d} = \frac{\left[(M_l)_r\right]_{max}}{(M_l)_{max}} C_{l,d} = \frac{\left[(M_l)_r\right]_{max}}{qAL} Nr\sqrt{\zeta_l \frac{V}{fD}}$$

The $C_{l,d}$ and $C'_{l,d}$ representations for several data samples are shown in figures 44 and 45, respectively. The mean and standard deviation of the data scatter were computed and are indicated in each figure. (The data for tower 2 upstream of the two-diameter model were not included in the analysis of scatter since the aerodynamic forces in this case were periodic rather than random.) For the data analyzed, the scatter is significantly reduced (by a factor of 3 to 4) through the use of the modified coefficient. Hence, it is concluded that the mathematical model for the ground-wind phenomenon, utilized in the derivation of the modified coefficient, is more accurate than the model originally assumed.

REFERENCES

1. Fung, Y. C.: Fluctuating Lift and Drag Acting on a Cylinder in a Flow at Supercritical Reynolds Numbers. Tech. Rep. EM 8-5, Space Technology Lab., May 7, 1958. (Also published J. Aero./Space Sci., vol. 27, no. 11, Nov. 1960, pp. 801-814.)

2. Fung, Y. C.: The Fluctuating Lift Force Acting on a Cylinder Subjected to Forced Oscillations Perpendicular to a Flow at High Reynolds Numbers. Tech. Rep. EM 8-19, Space Technology Lab., Sept. 11, 1958.

3. Schmidt, Louis Vincent: Measurements of Fluctuating Air Loads on a Circular Cylinder. PhD Thesis, California Institute of Technology, 1963.

4. Blackiston, Harry Spencer, Jr.: Tip Effects on Fluctuating Lift and Drag Forces Acting on a Circular Cylinder Perpendicular to an Air Flow. Aeronautical Engineer Thesis, California Institute of Technology, 1963.

5. Bohne, Q. R.: Ground Wind-Induced Loads on Launch Vehicles. ASD-TDR-62-371, Boeing Co., Seattle, Jan. 1964.

6. Buell, D. A., McCullough, G. B., and Steinmetz, W. J.: A Wind-Tunnel Investigation of Ground-Wind Loads on Axisymmetric Launch Vehicles. NASA TN D-1893, 1963.

7. Reed, Wilmer H., III: Models for Obtaining Effects of Ground Winds on Space Vehicles Erected on the Launch Pad. Conference on the Role of Simulation in Space Technology, Virginia Polytechnic Institute, Blacksburg, Virginia, Aug. 17-21, 1964.

8. Gaffney, E. F.: Ground Wind Loads Wind Tunnel Tests on Several Atlas Vehicles. GDA 63-0999, General Dynamics/Astronautics, San Diego, April 1964.

9. Cameron, William D.: Hybrid Computer Techniques for Determining Probability Distributions. Presented at International Symposium on Analogue and Digital Techniques Applied to Aeronautics, Liege, Belgium, Sept. 9-12, 1963.

10. Rice, S. O.: Mathematical Analysis of Random Noise. Bell Syst. Tech. J., vol. 24, no. 1, Jan. 1945, sec. 3.10, pp. 98-107. (Also published in Wax, Nelson, Ed.: Selected Papers on Noise and Stochastic Processes. Dover Pub. Inc., N. Y., 1954, pp. 236-245.)

11. Crandall, Stephen H., and Mark, William D.: Random Vibration in Mechanical Systems. Academic Press, New York, 1963, pp. 48-53.

12. Caughey, T. K.: Response of Van Der Pol's Oscillator to Random Excitation. J. App. Mech., vol. 26, Sept. 1959, pp. 345-348.

13. Marcum, J. I.: Table of Q Functions. Res. Memo. RM-339, The Rand Corp., Jan. 1, 1950.

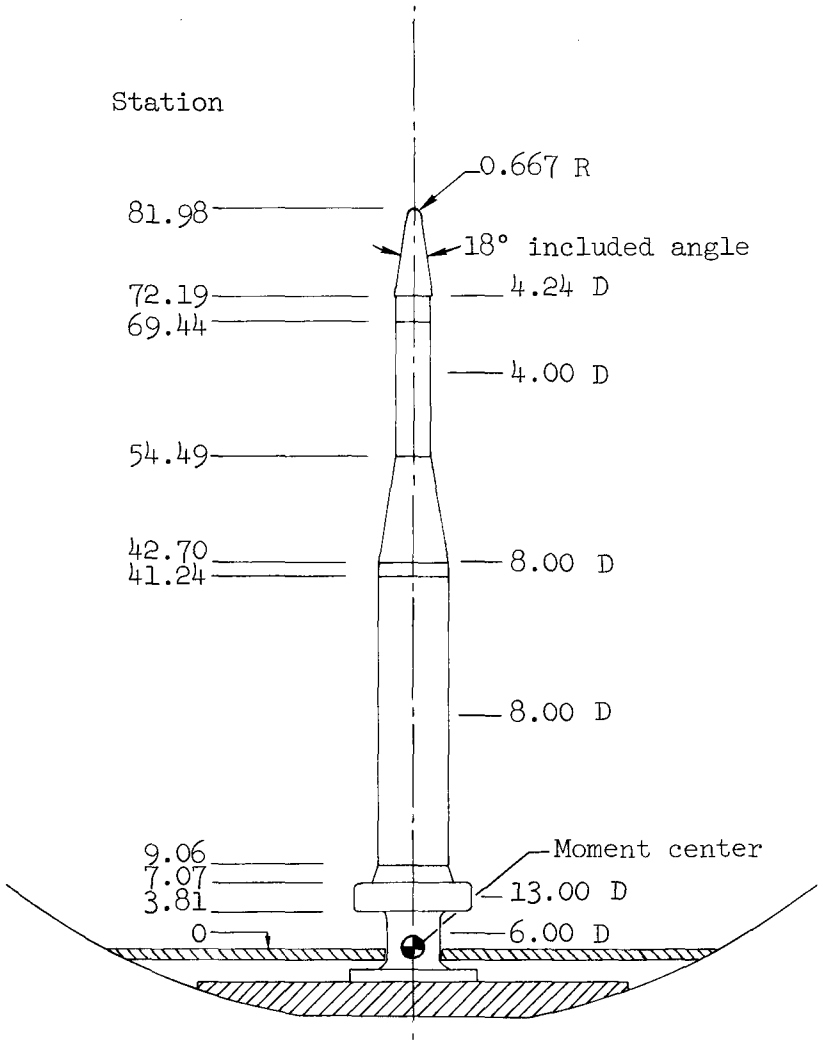

(a) Two-diameter model.

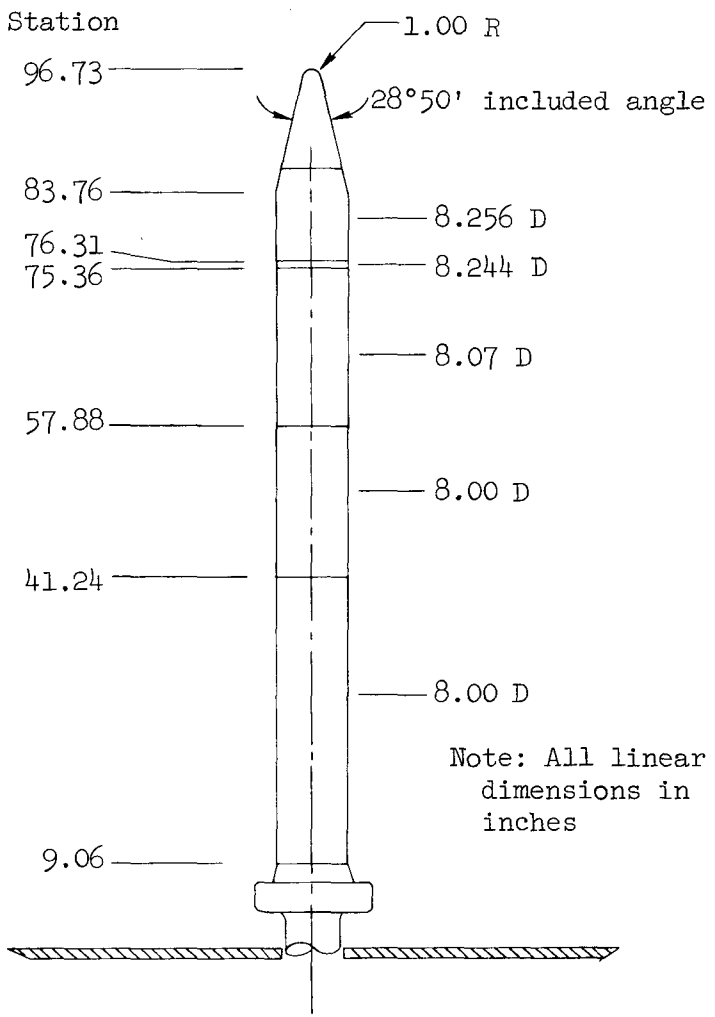

(b) Constant-diameter model.

Figure 1.- Sketches of the simplified models.

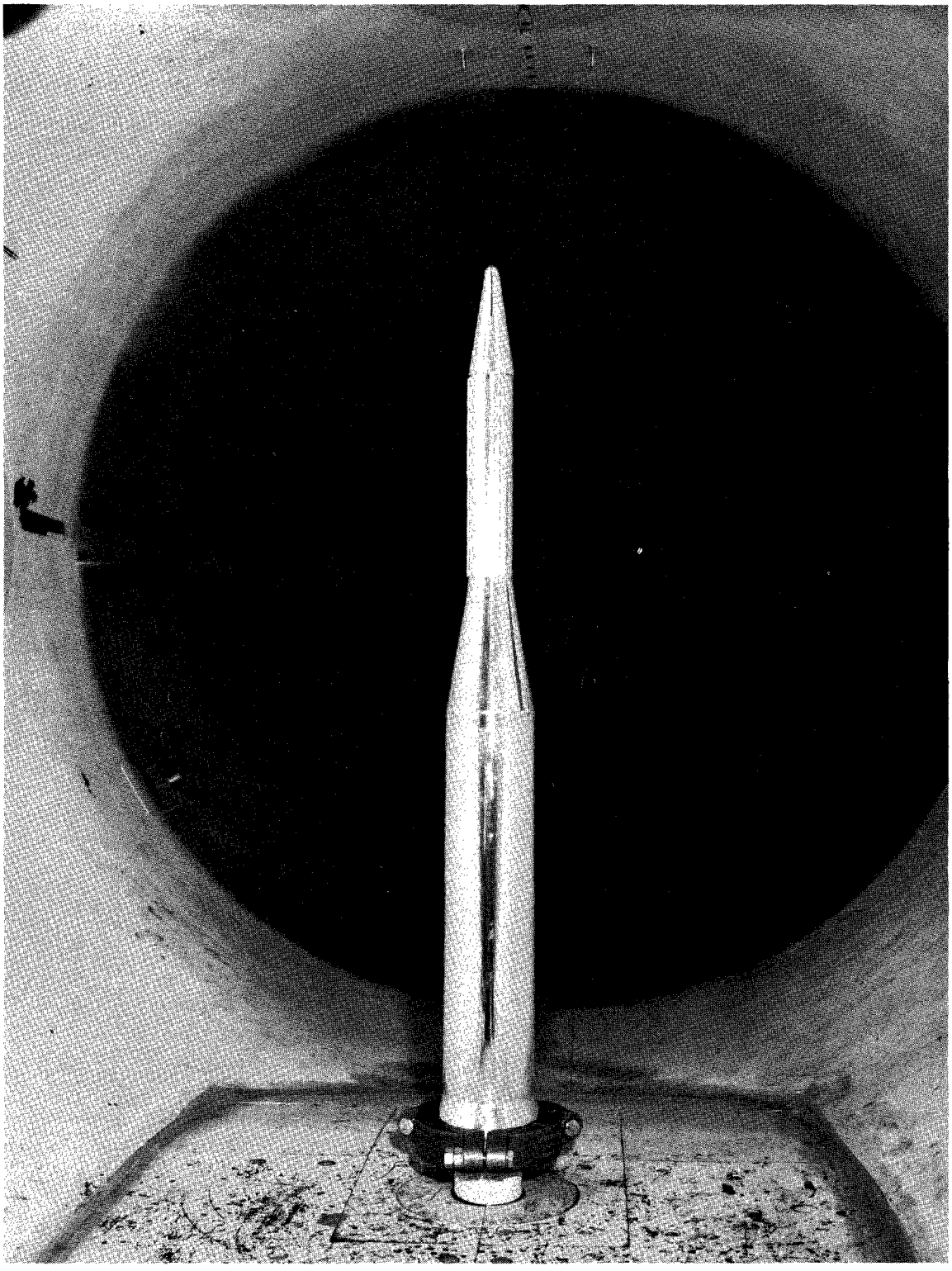

A-30564

(a) Two-diameter model with two conduits on the upper stage.

Figure 2.- Photographs of the simplified models.

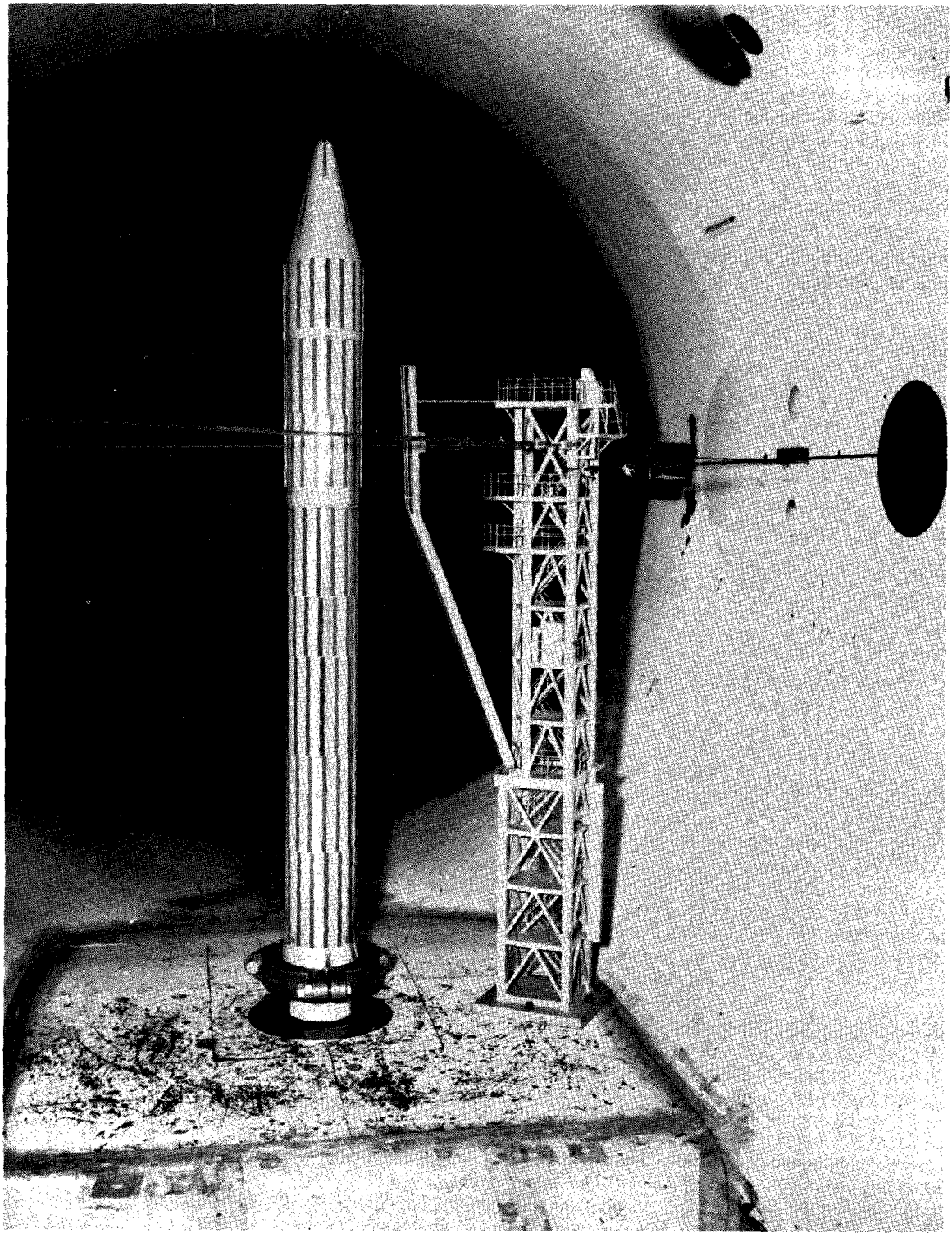

A-30670

(b) Constant-diameter model with staggered tapes, two conduits on the upper stage, and nearby umbilical tower.

Figure 2.- Concluded.

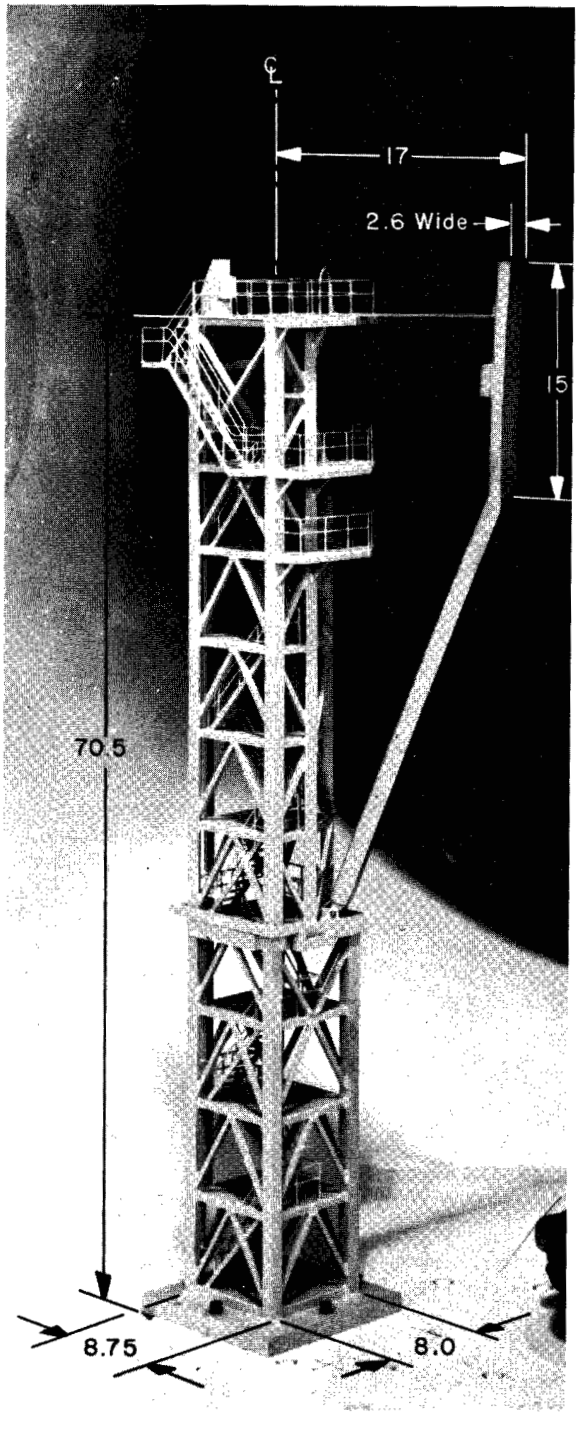

(a) Tower 1. A-29430.2

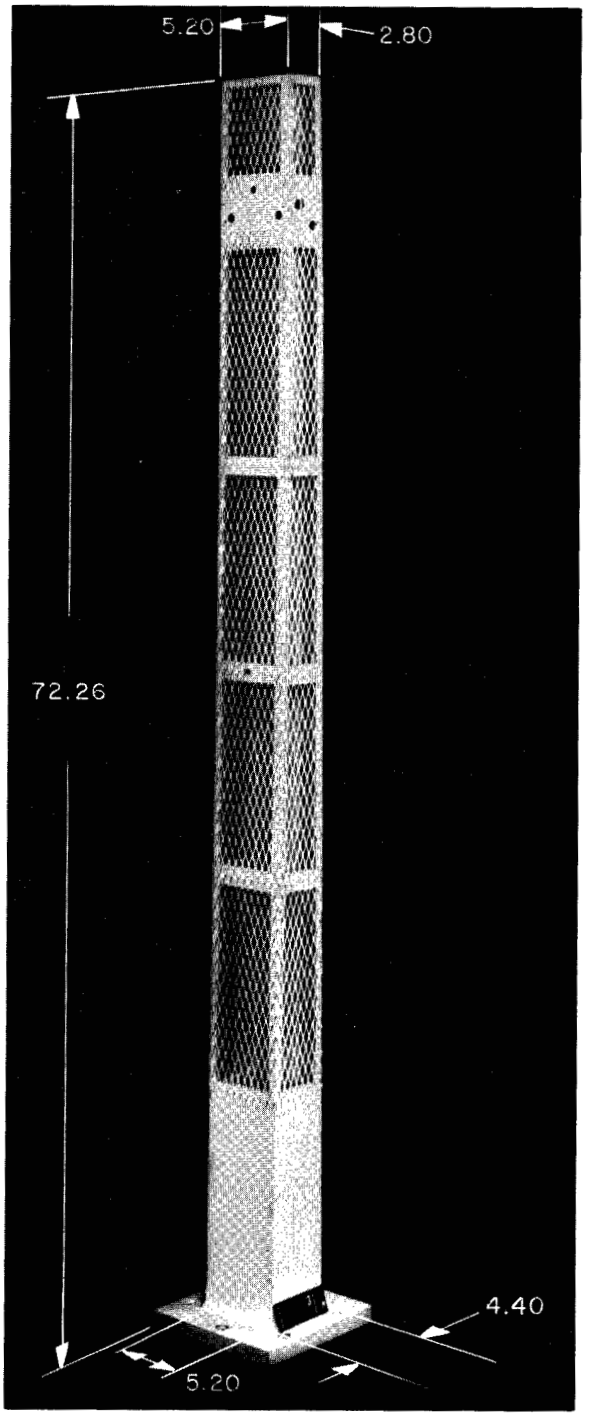

(b) Tower 2. A-29050.1

Figure 3.- Photographs of the umbilical towers. Dimensions in inches.

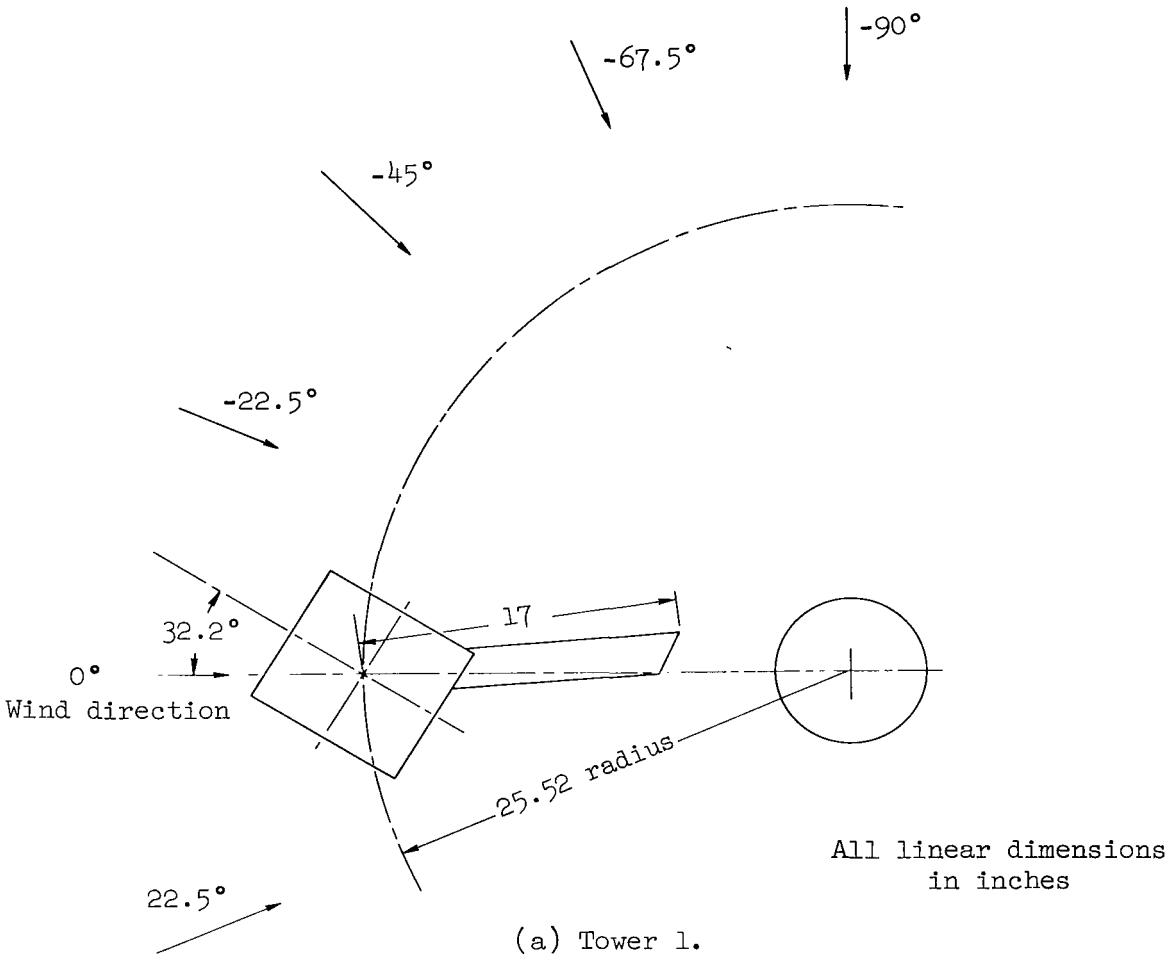

(a) Tower 1.

(b) Tower 2.

Figure 4.- Geometric relationships of towers and models.

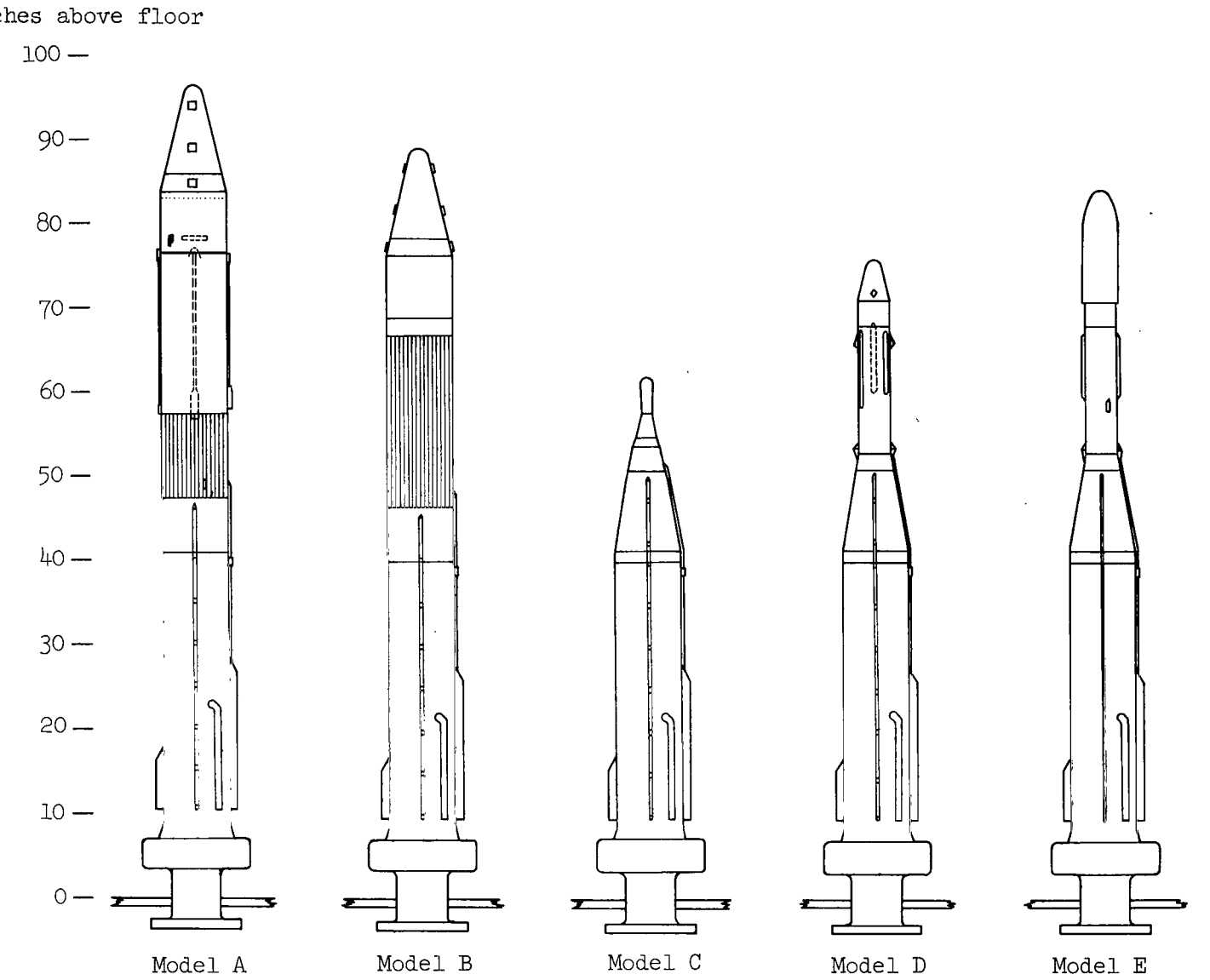

(a) Assembled models.

Figure 5.- Sketches of the models of specific vehicles.

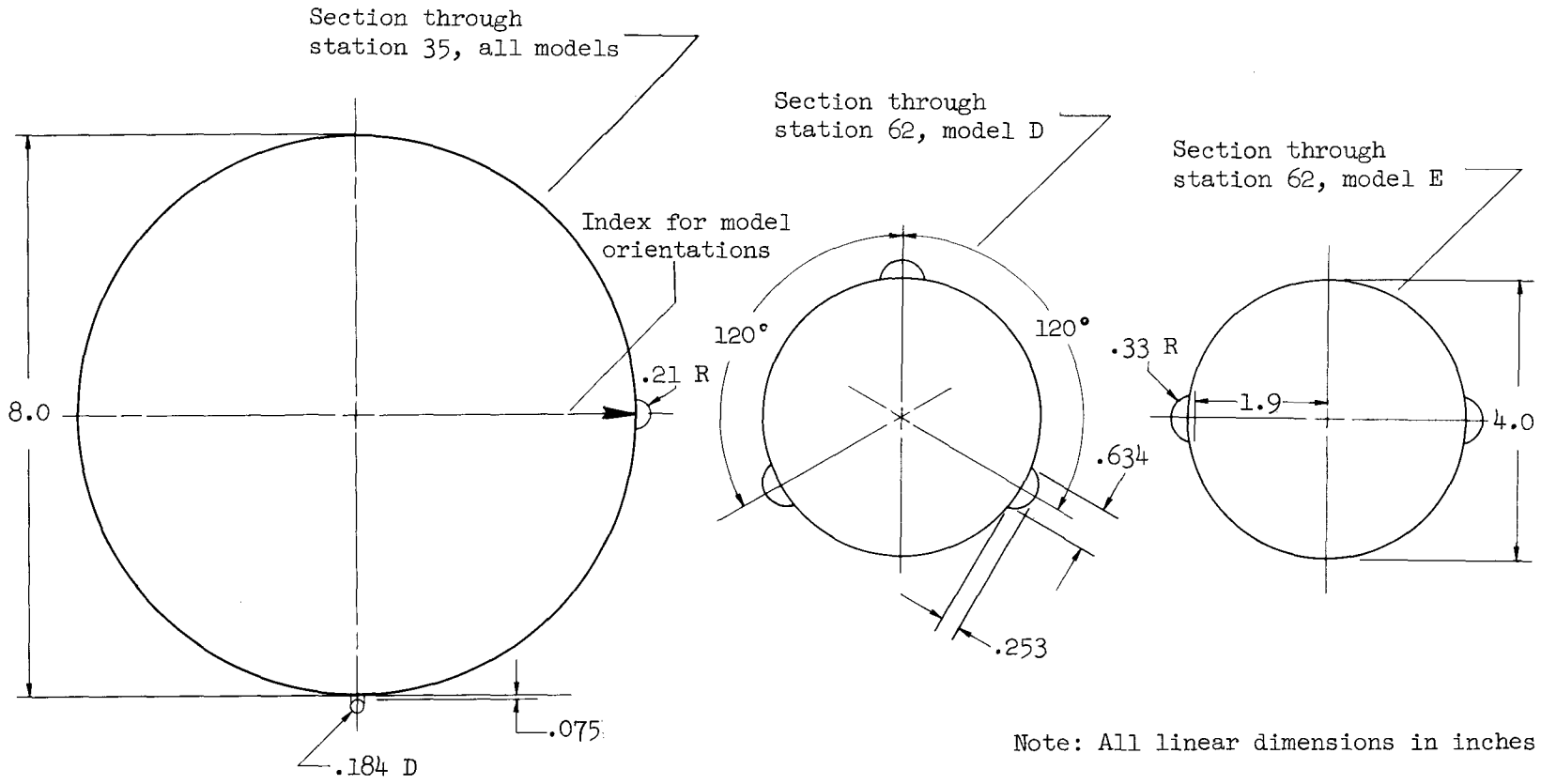

Note: All linear dimensions in inches

(b) Prominent conduits.

Figure 5.- Concluded.

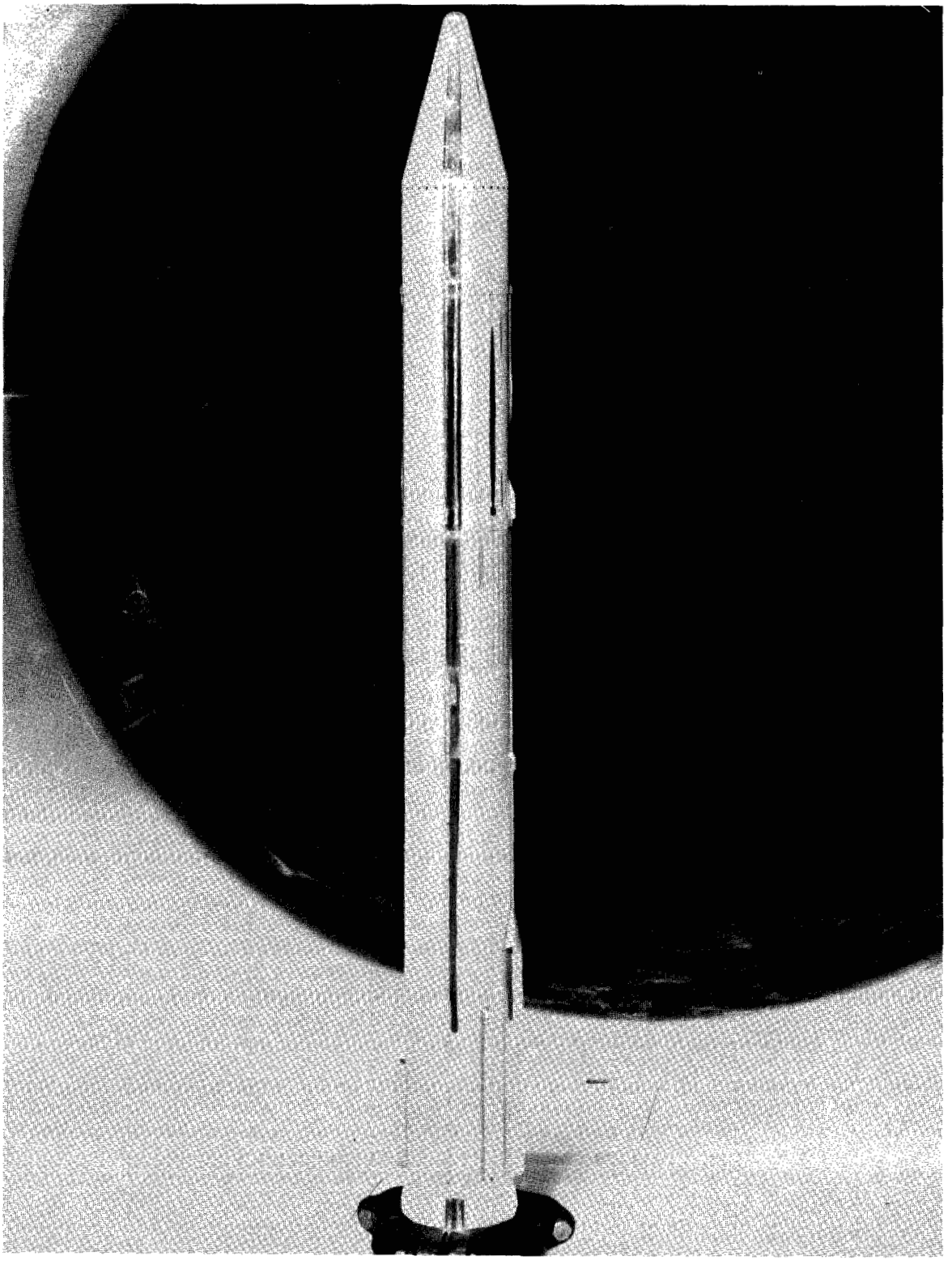

A-29431

(a) Model A.

Figure 6.- Photographs of the models of specific vehicles.

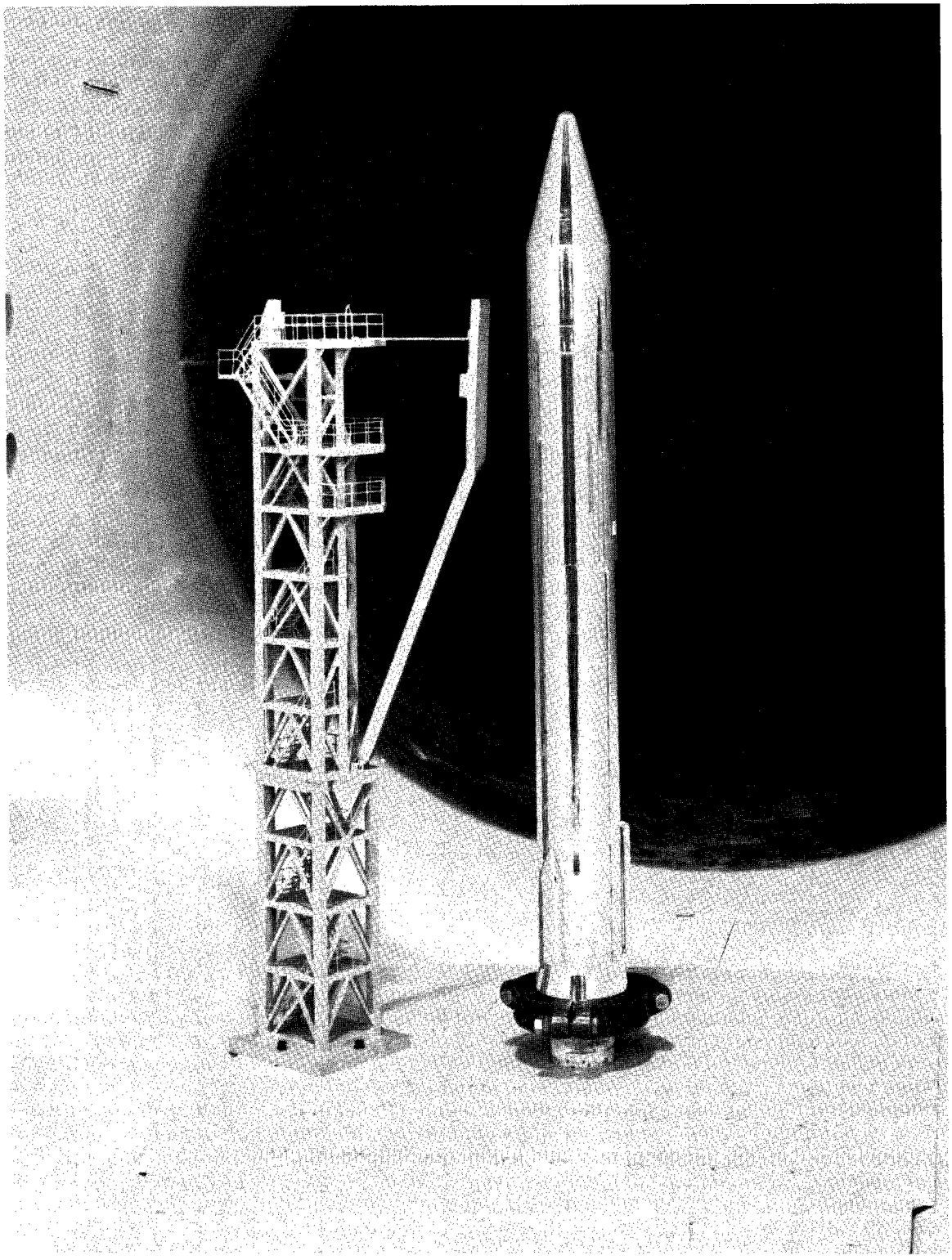

A-29437

(b) Model B and tower 1.

Figure 6.- Continued.

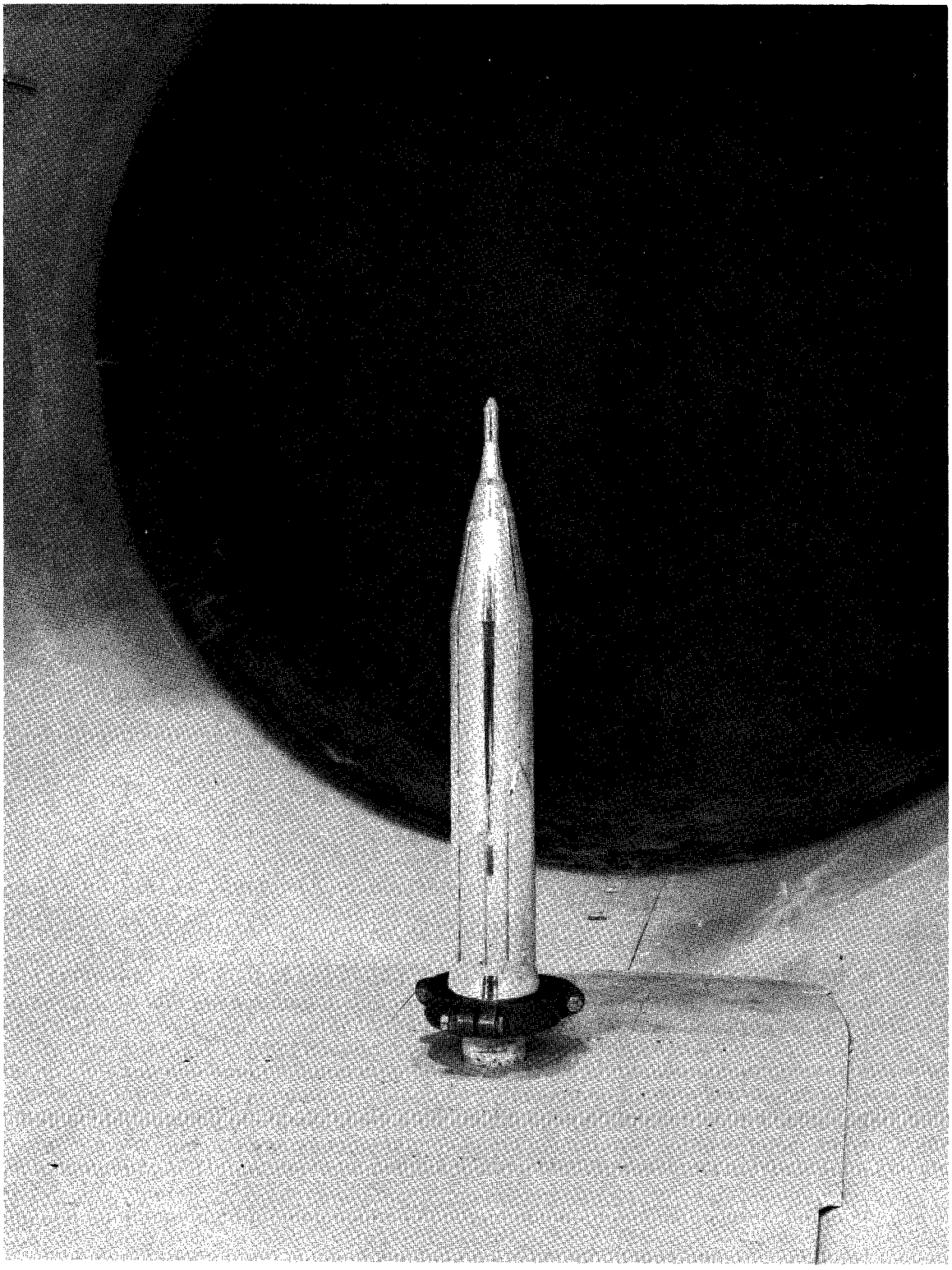

(c) Model C.

A-29435

Figure 6.- Continued.

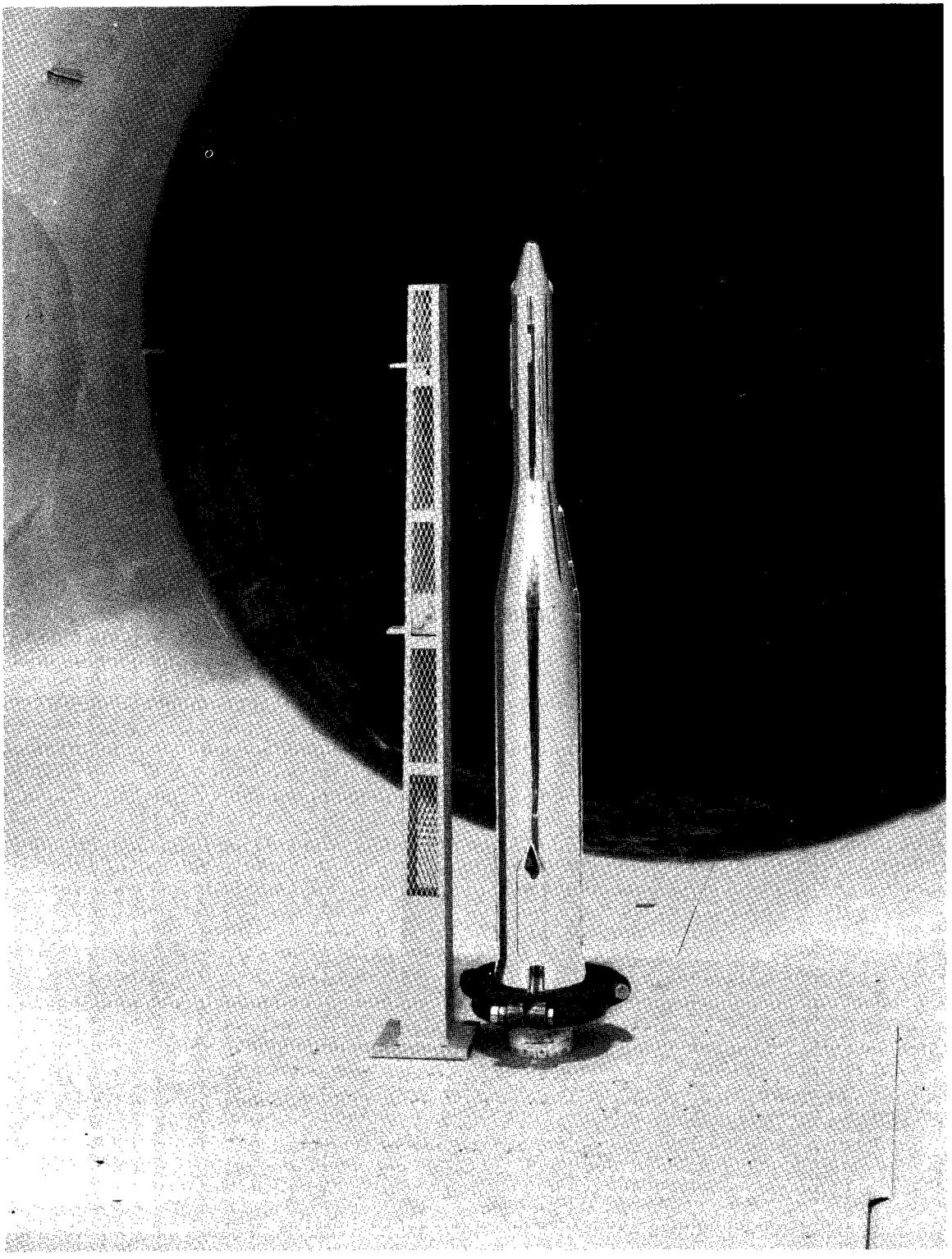

A-29442

(d) Model D and tower 2.

Figure 6.- Continued.

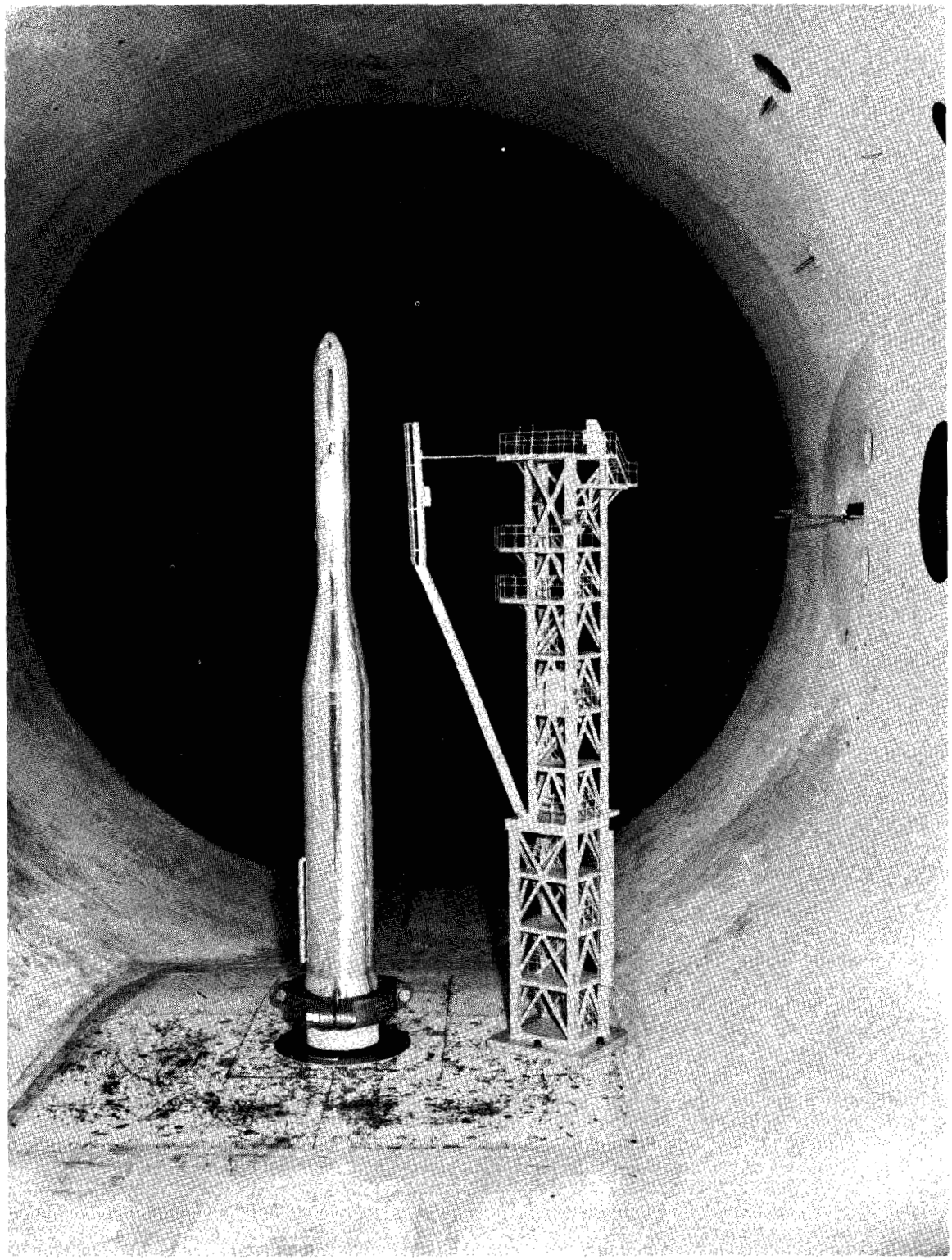

A-31650

(e) Model E and tower 1. Damping compound applied to pedestal.

Figure 6.- Continued.

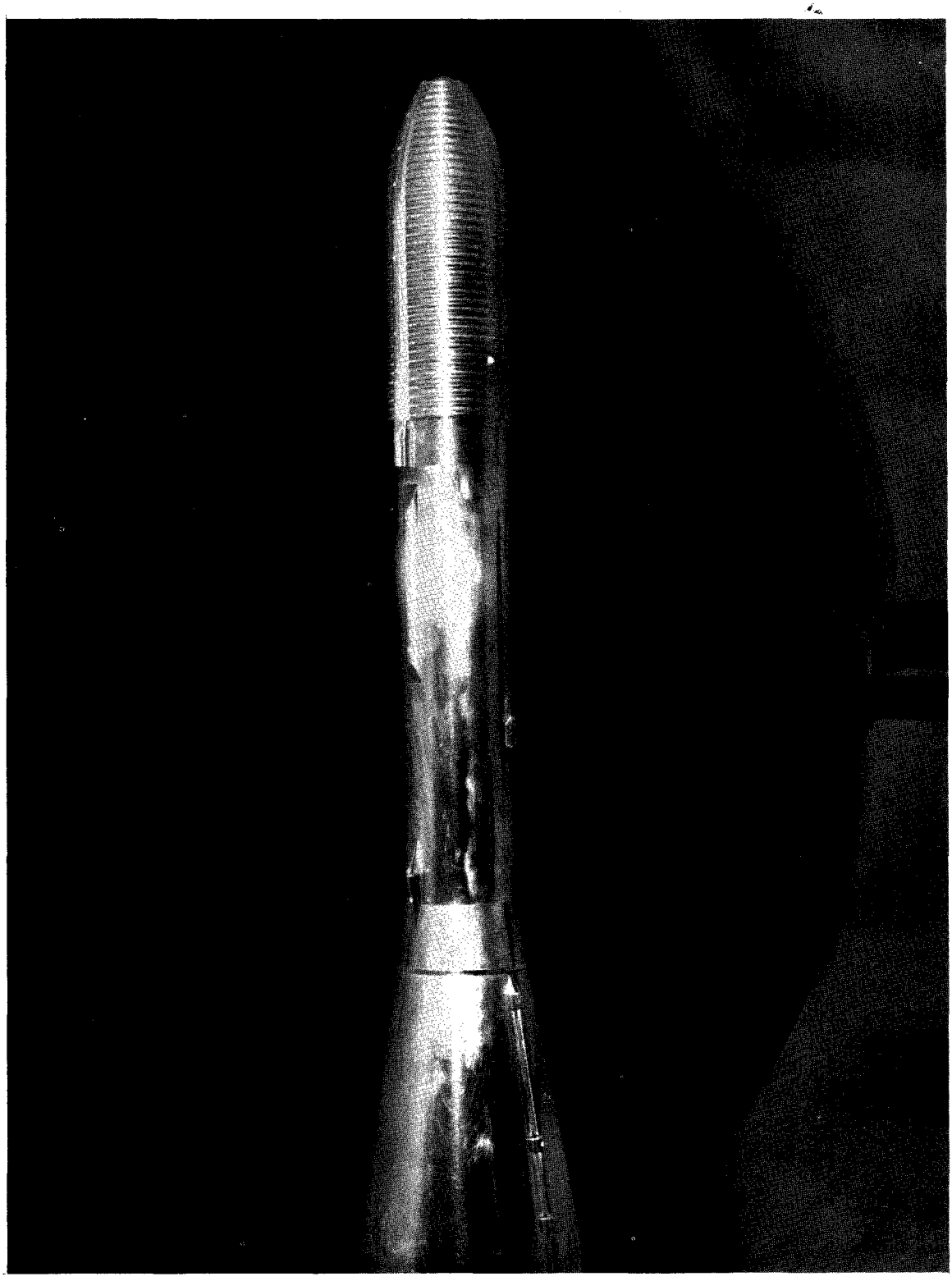

A-30447

(f) Model E with payload insulation blanket simulation.

Figure 6.- Concluded.

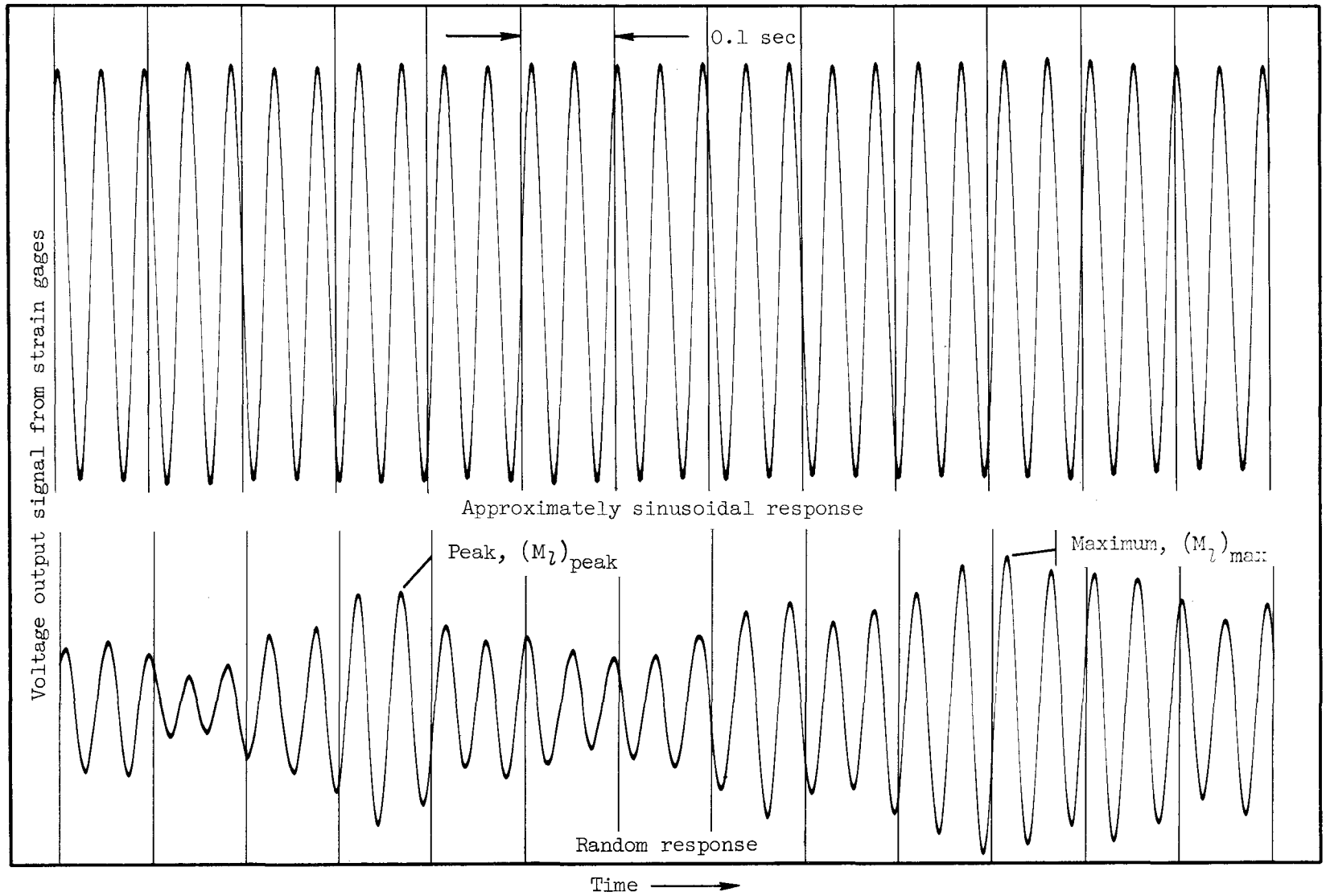

Figure 7.- Samples of typical response records.

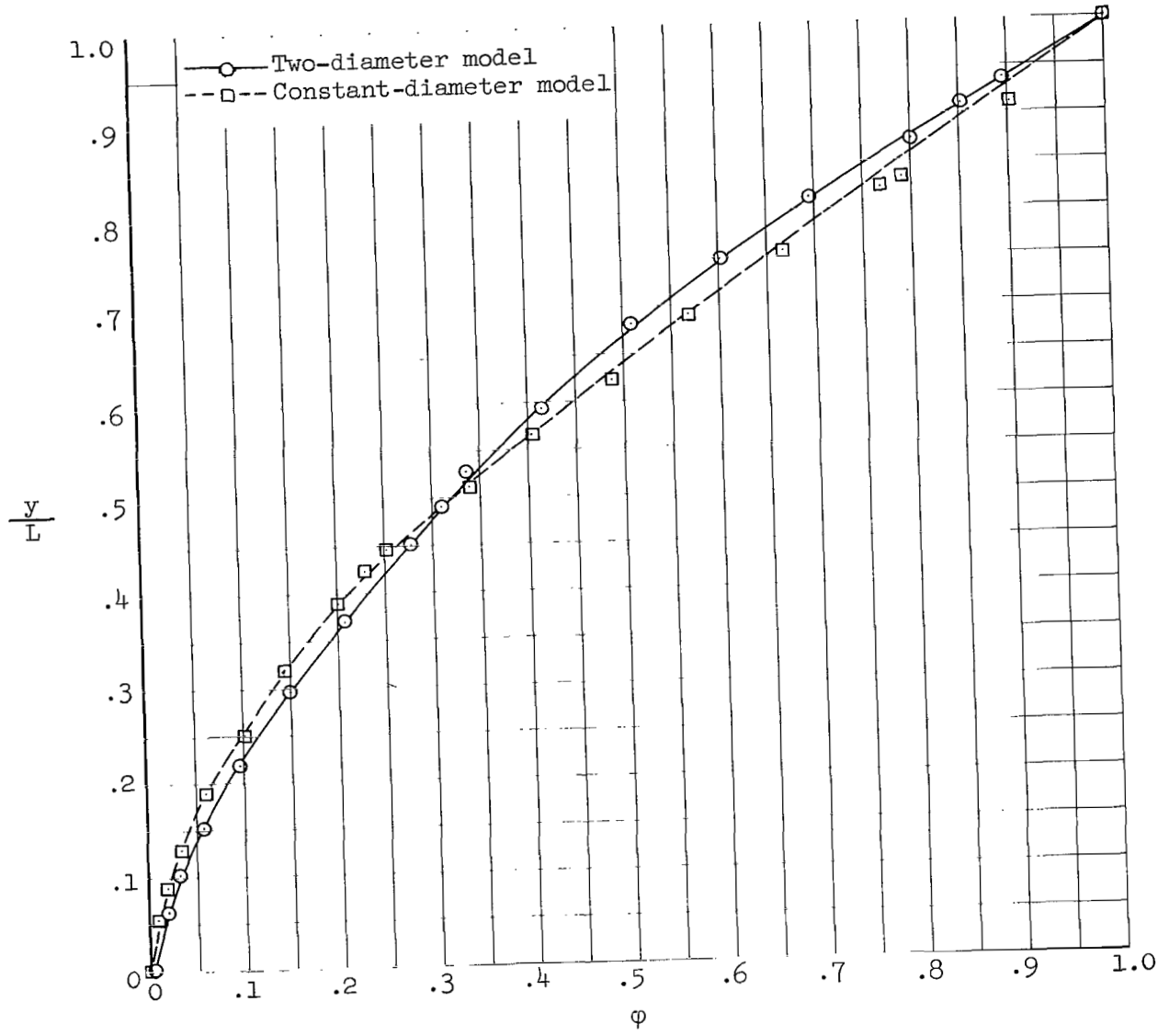

Figure 8.- First cantilever mode shapes of the simplified models in the lateral plane.

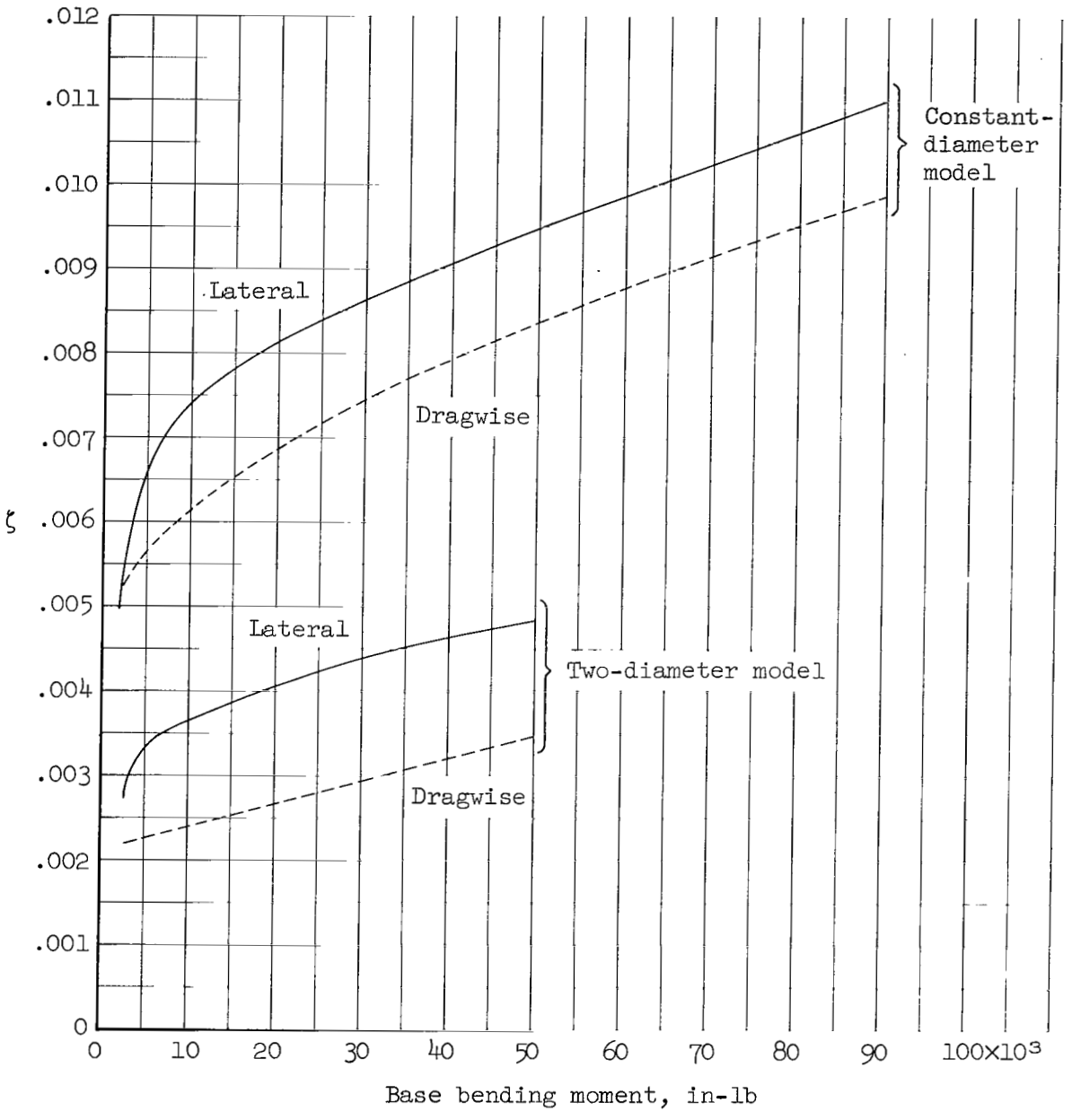

Figure 9.- Typical values of first-mode damping.

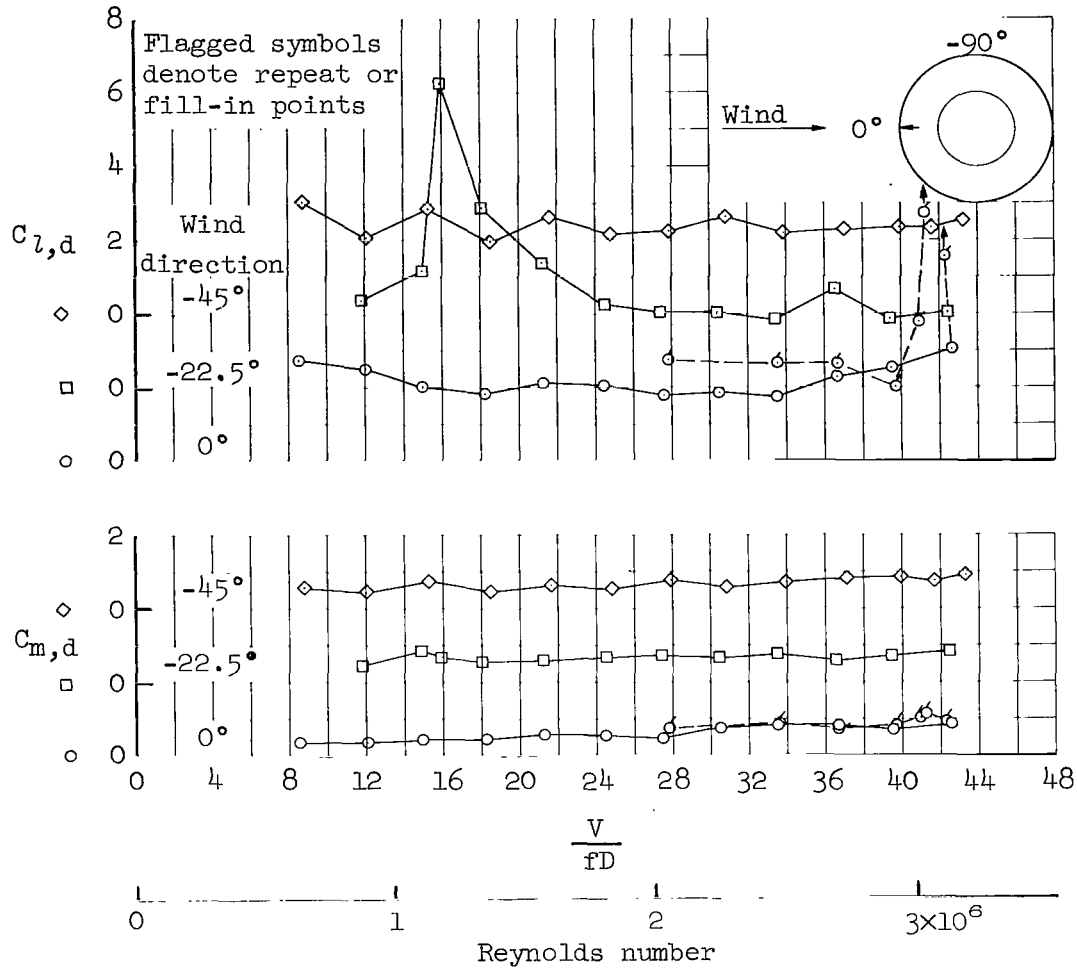

(a) Dynamic data.

Figure 10.- Data for the basic two-diameter model; $(\zeta_l)_{max} \approx 0.004$ to 0.005; $\rho \approx 0.011$.

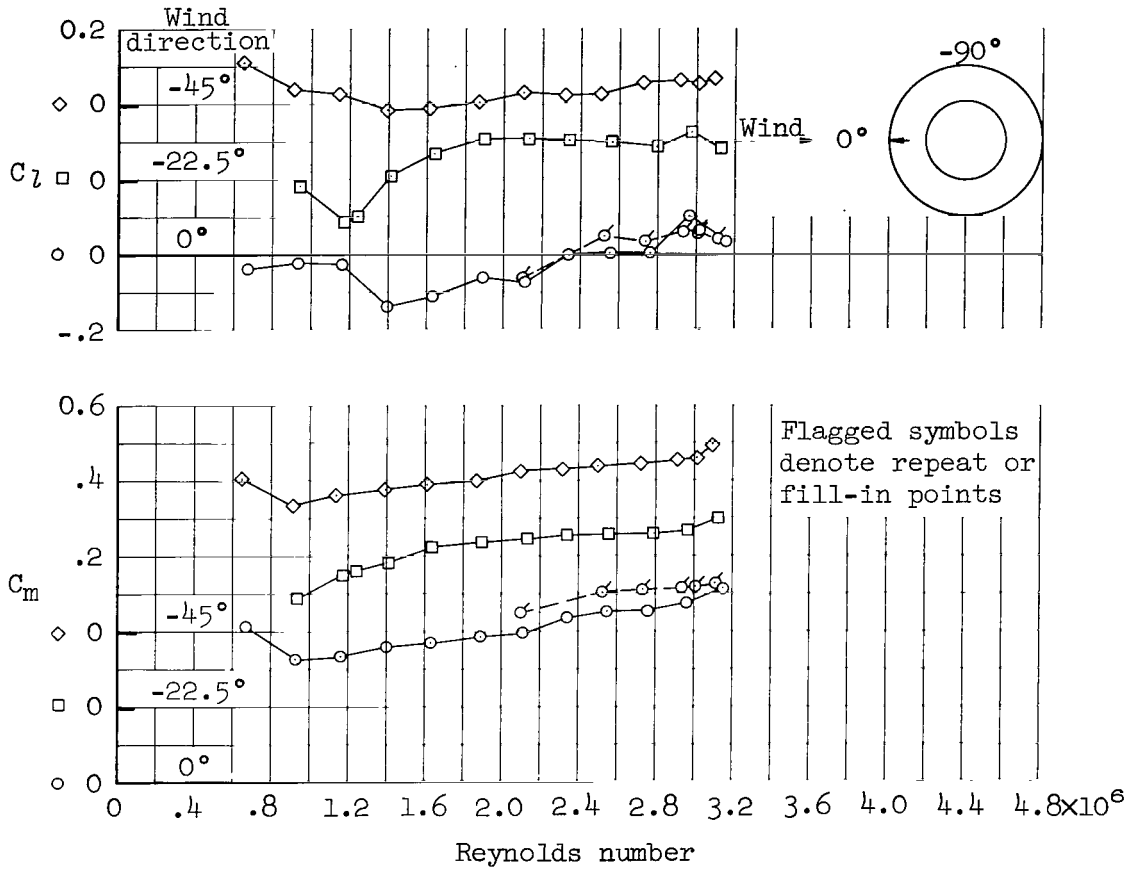

(b) Steady-state data.

Figure 10.- Concluded.

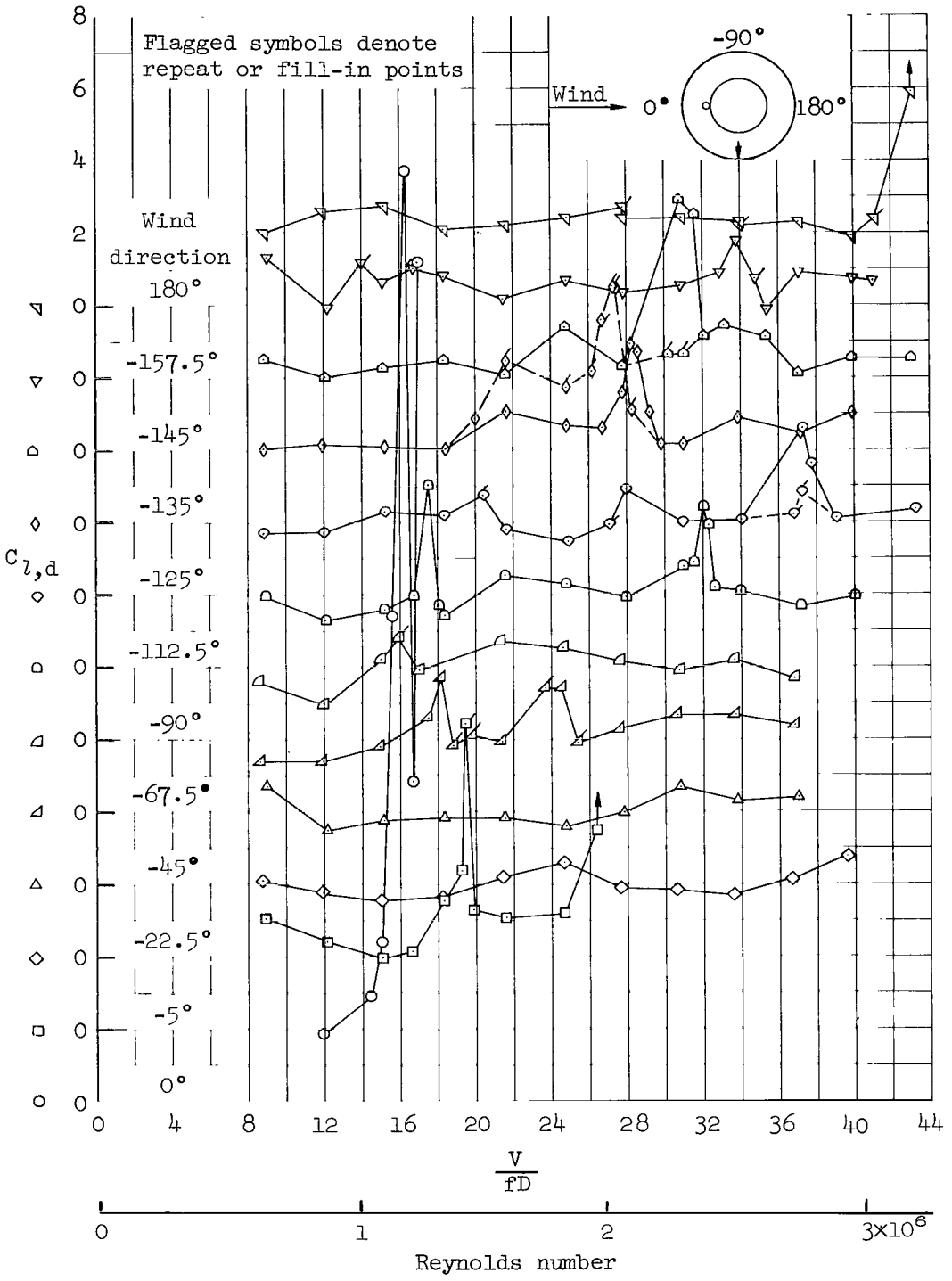

(a) $\rho \approx 0.011$

Figure 11.- Lateral dynamic response of the two-diameter model with one conduit on the upper stage; $(\zeta_l)_{max} \approx 0.004$ to 0.005; conduit diameter 0.06D.

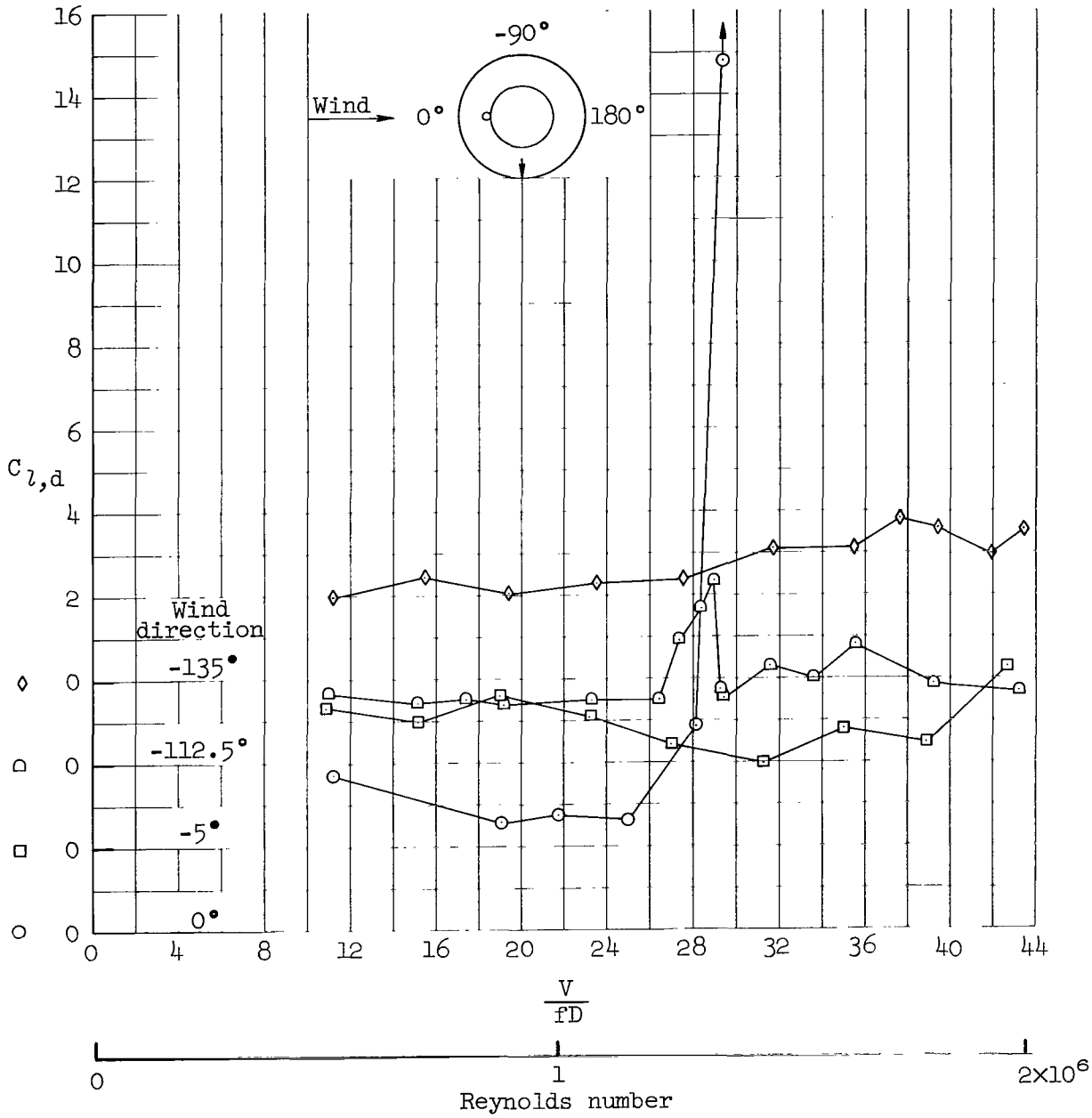

(b) $\rho \approx 0.007$

Figure 11.- Concluded.

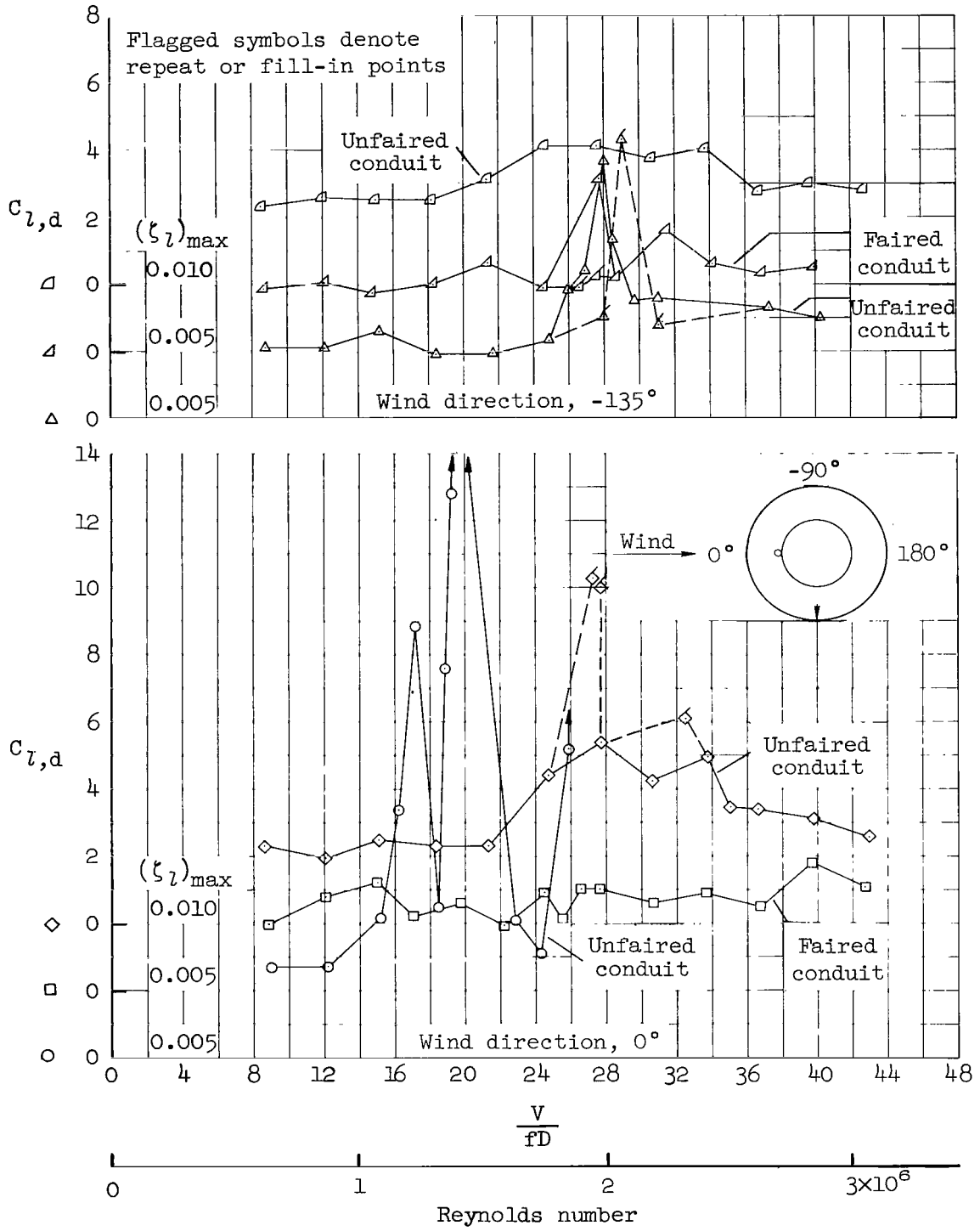

Figure 12.- Effect of fairing conduit on the lateral dynamic response of the two-diameter model with one conduit on the upper stage and a circular plate under the nose concentric with the upper stage and twice its diameter; $\rho \approx 0.011$; conduit diameter 0.06D.

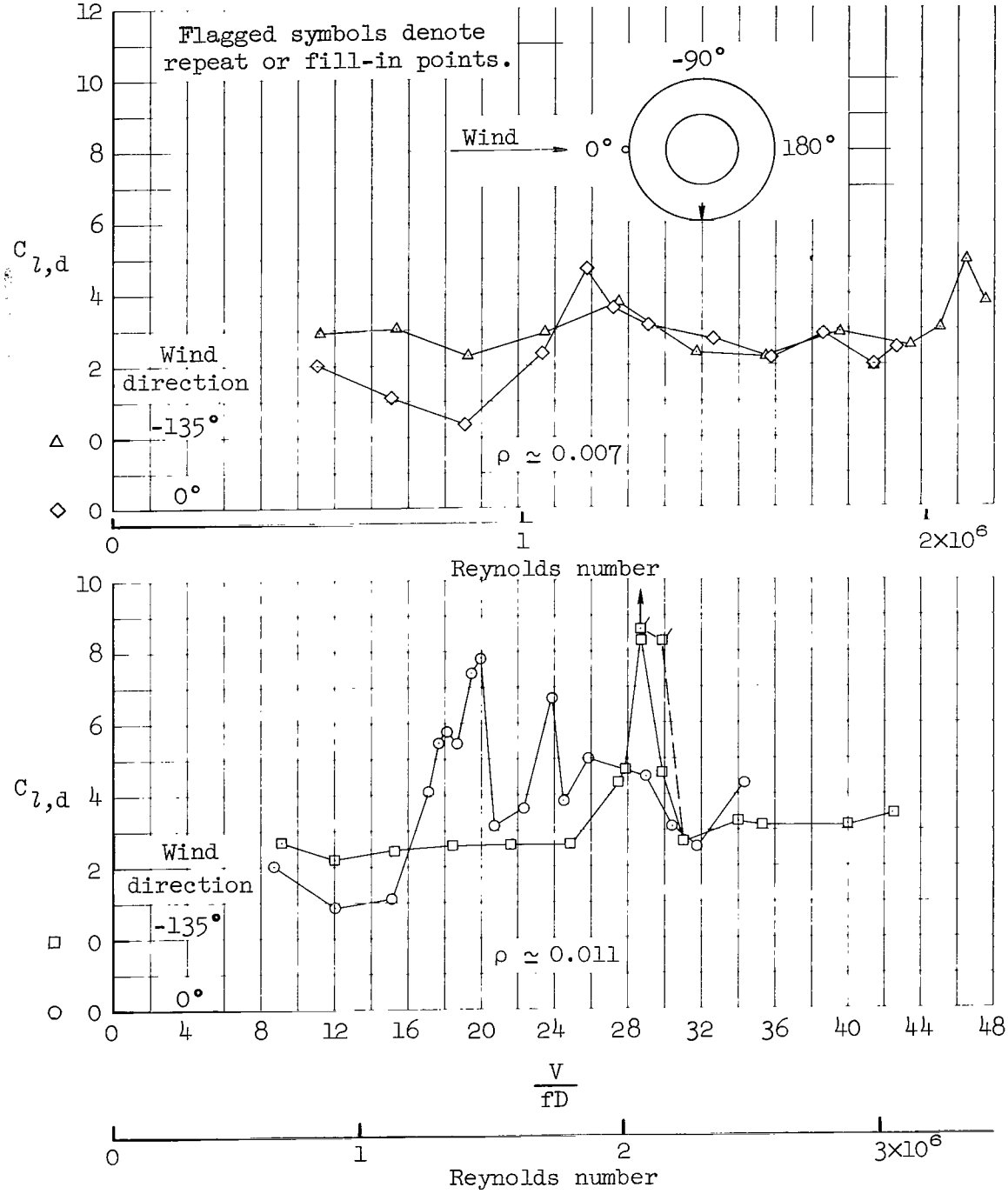

Figure 13.- Lateral dynamic response of the two-diameter model with one conduit on the lower stage; $(\zeta_l)_{max} \simeq 0.005$; conduit diameter 0.03 of the lower stage diameter.

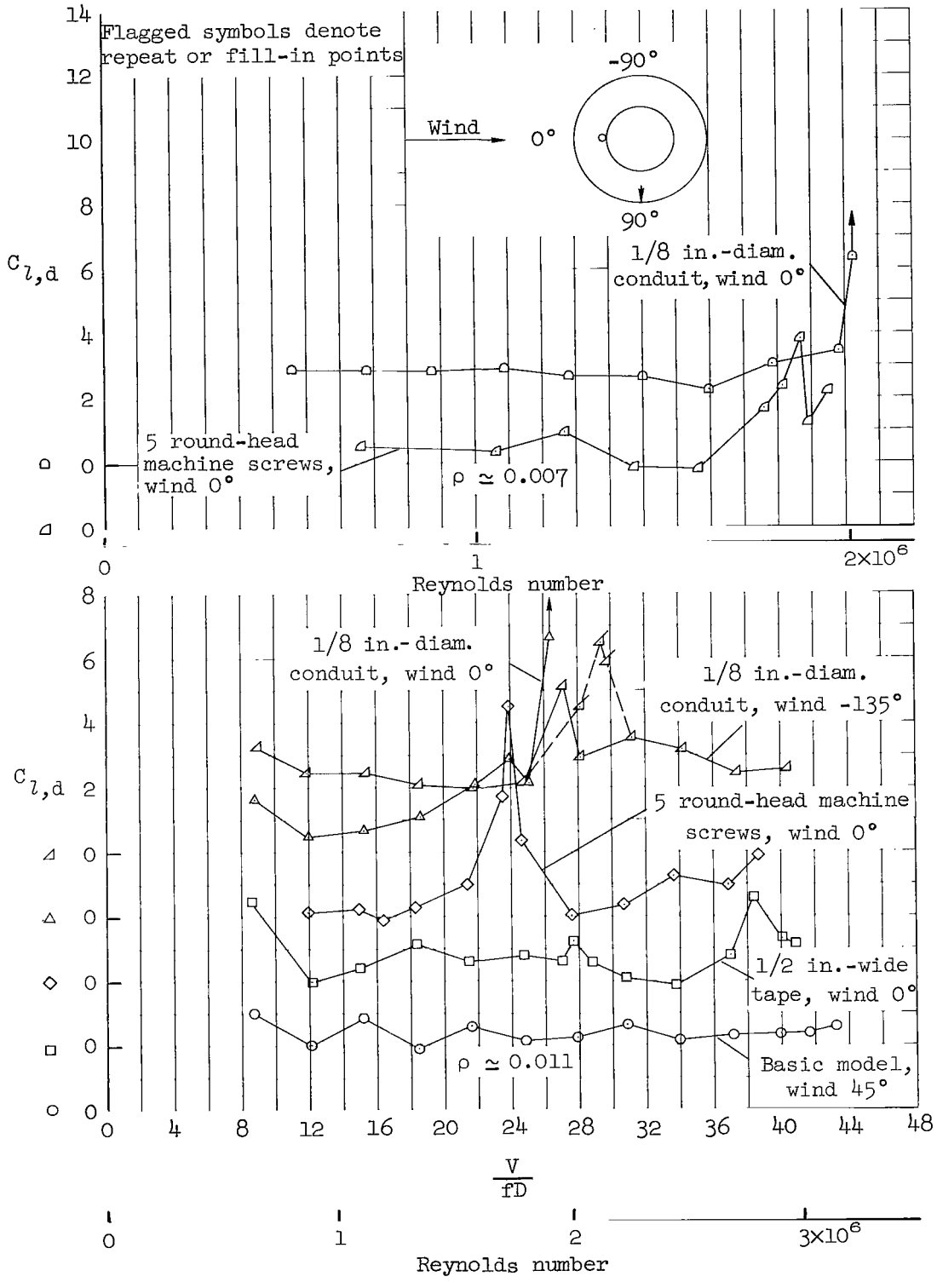

Figure 14.- Effect of small protuberances on the lateral dynamic response of the two-diameter model; $(\zeta_l)_{max} \simeq 0.004$ to 0.005; D = 4 inches.

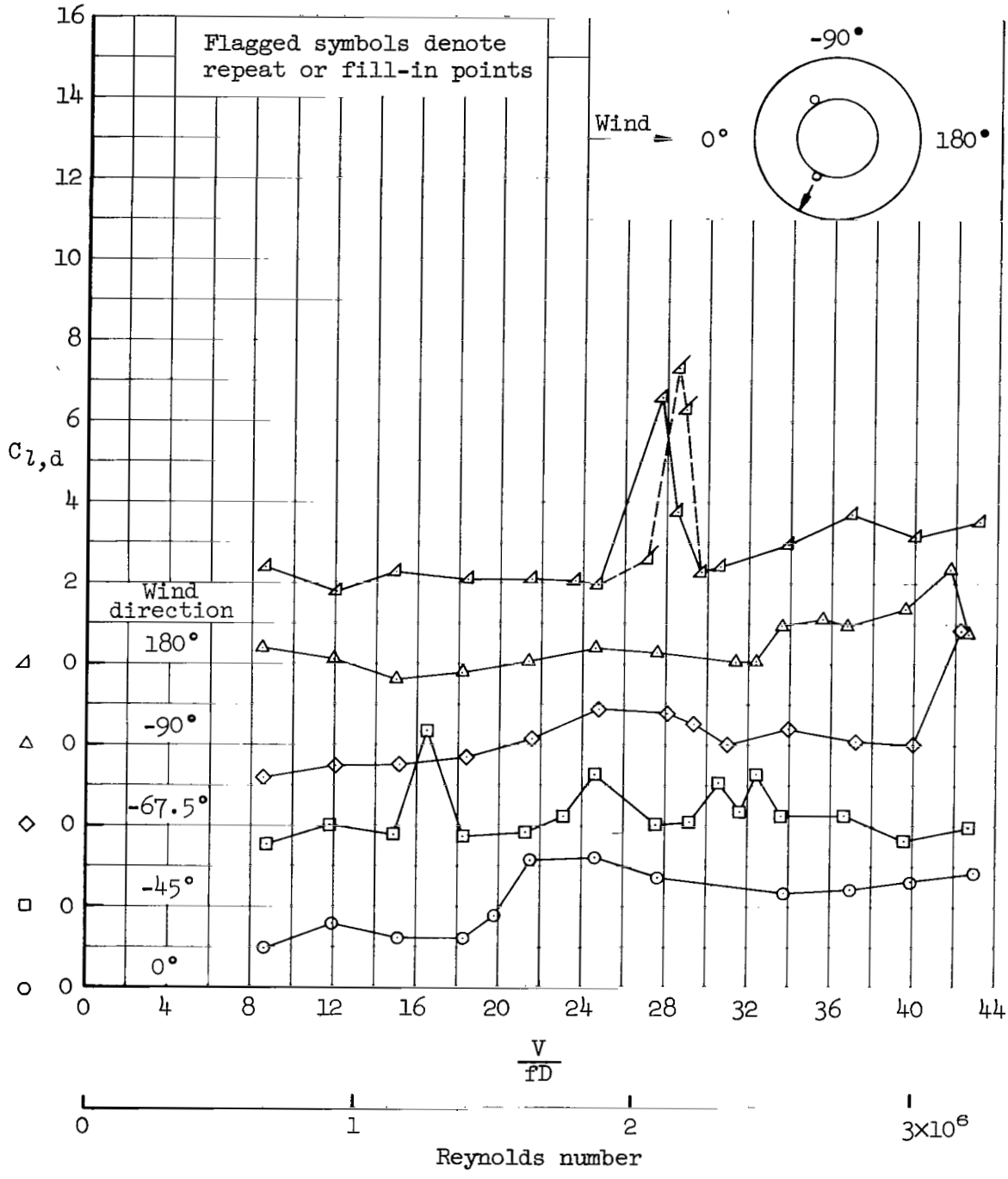

(a) Conduits at 90° interval.

Figure 15.- Lateral dynamic response of the two-diameter model with two conduits on the upper stage; $(\zeta_l)_{max} \approx 0.004$ to 0.005; $\rho \approx 0.011$; conduit diameter 0.06D.

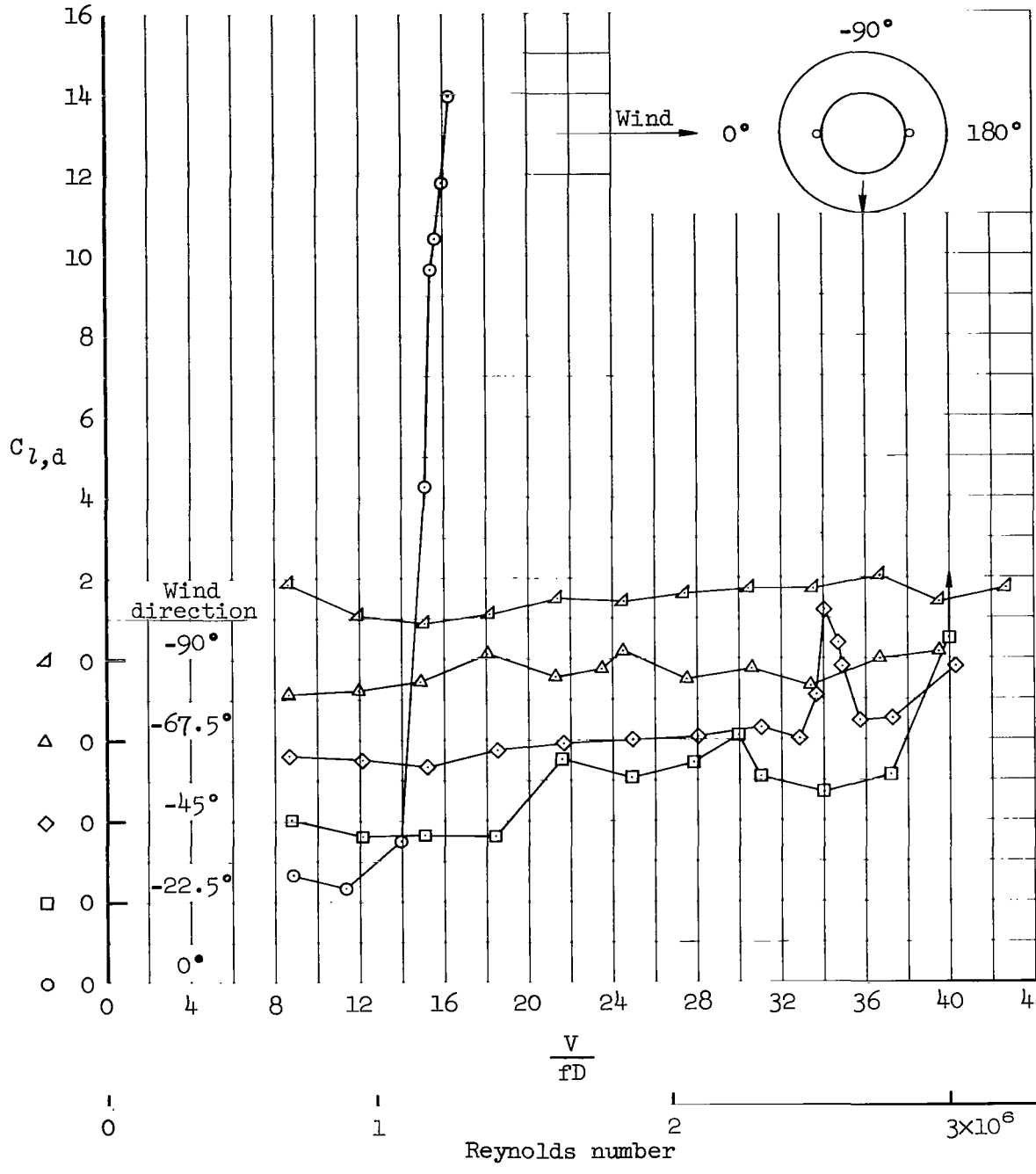

(b) Conduits at 180° interval.

Figure 15.- Concluded.

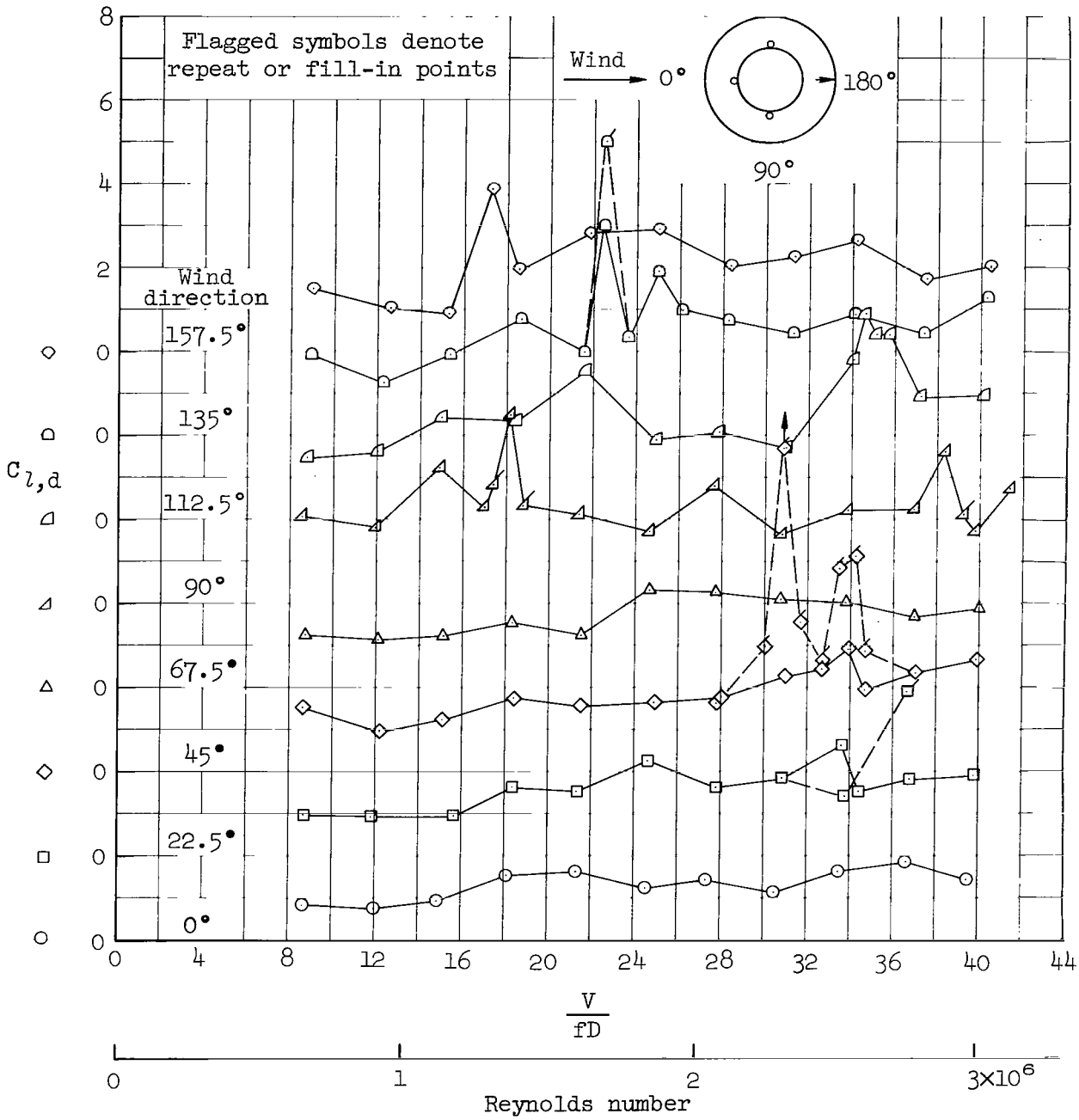

Figure 16.- Lateral dynamic response of the two-diameter model with three conduits on the upper stage; conduits at 90° intervals; $(\zeta_l)_{max} \approx 0.004$ to 0.005; $\rho \approx 0.011$; conduit diameter 0.06D.

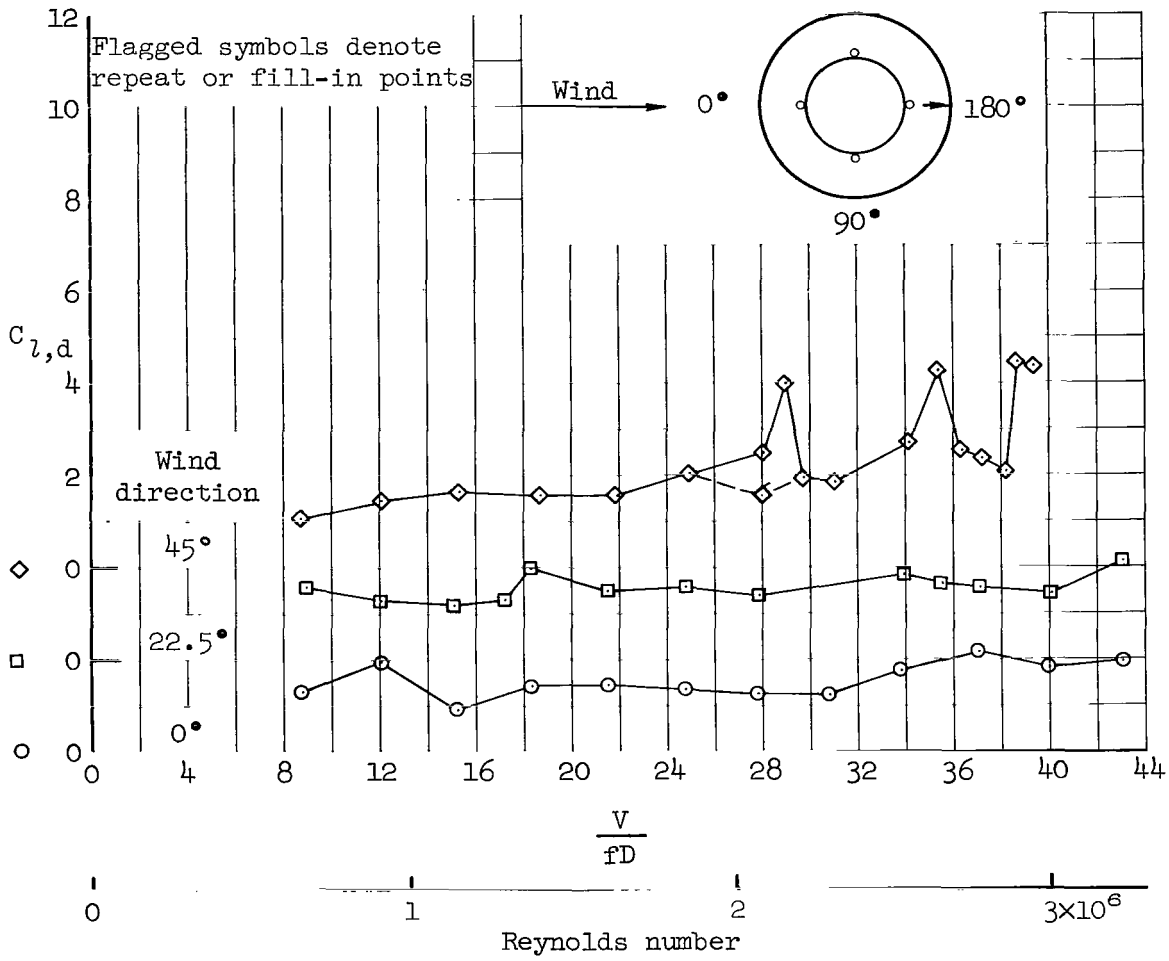

Figure 17.- Lateral dynamic response of the two-diameter model with four conduits on the upper stage; conduits at 90° intervals; $(\zeta_l)_{max} \approx 0.004$ to 0.005; $\rho \approx 0.011$; conduit diameter 0.06D.

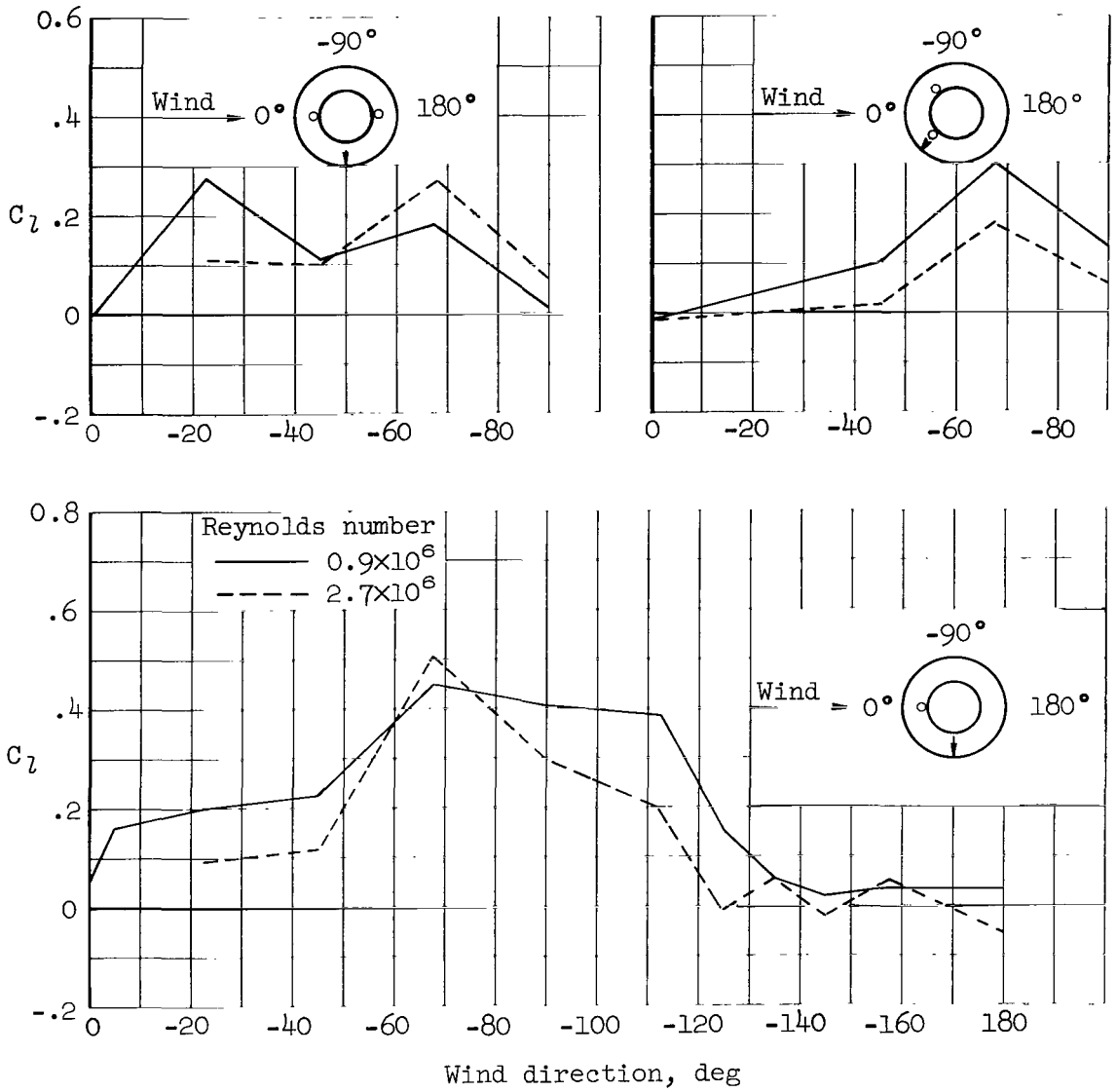

(a) One and two conduits.

Figure 18.- Steady-state lateral moment coefficients for the two-diameter model with conduits on the upper stage; conduit diameter 0.06D.

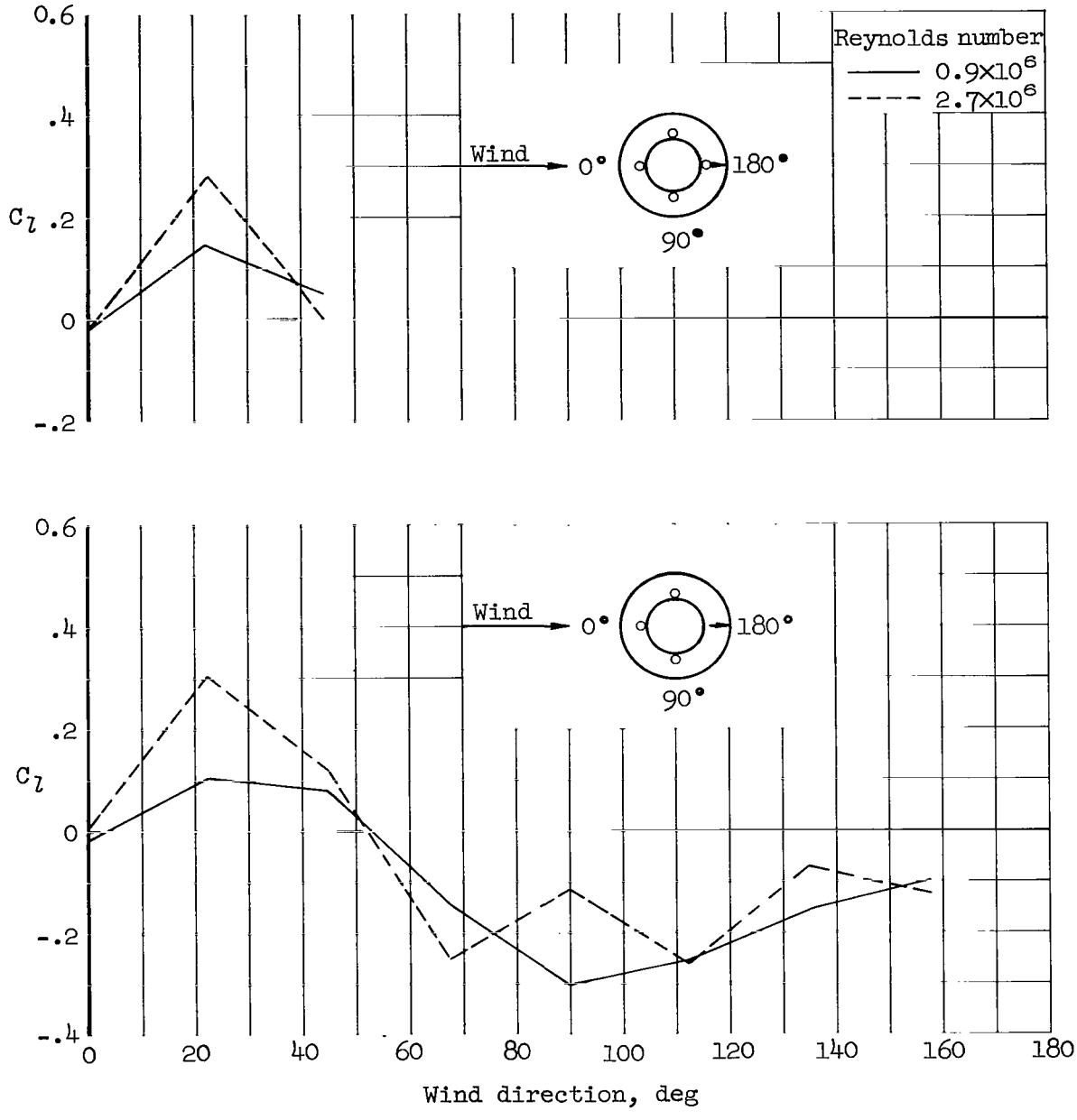

(b) Three and four conduits.

Figure 18.- Concluded.

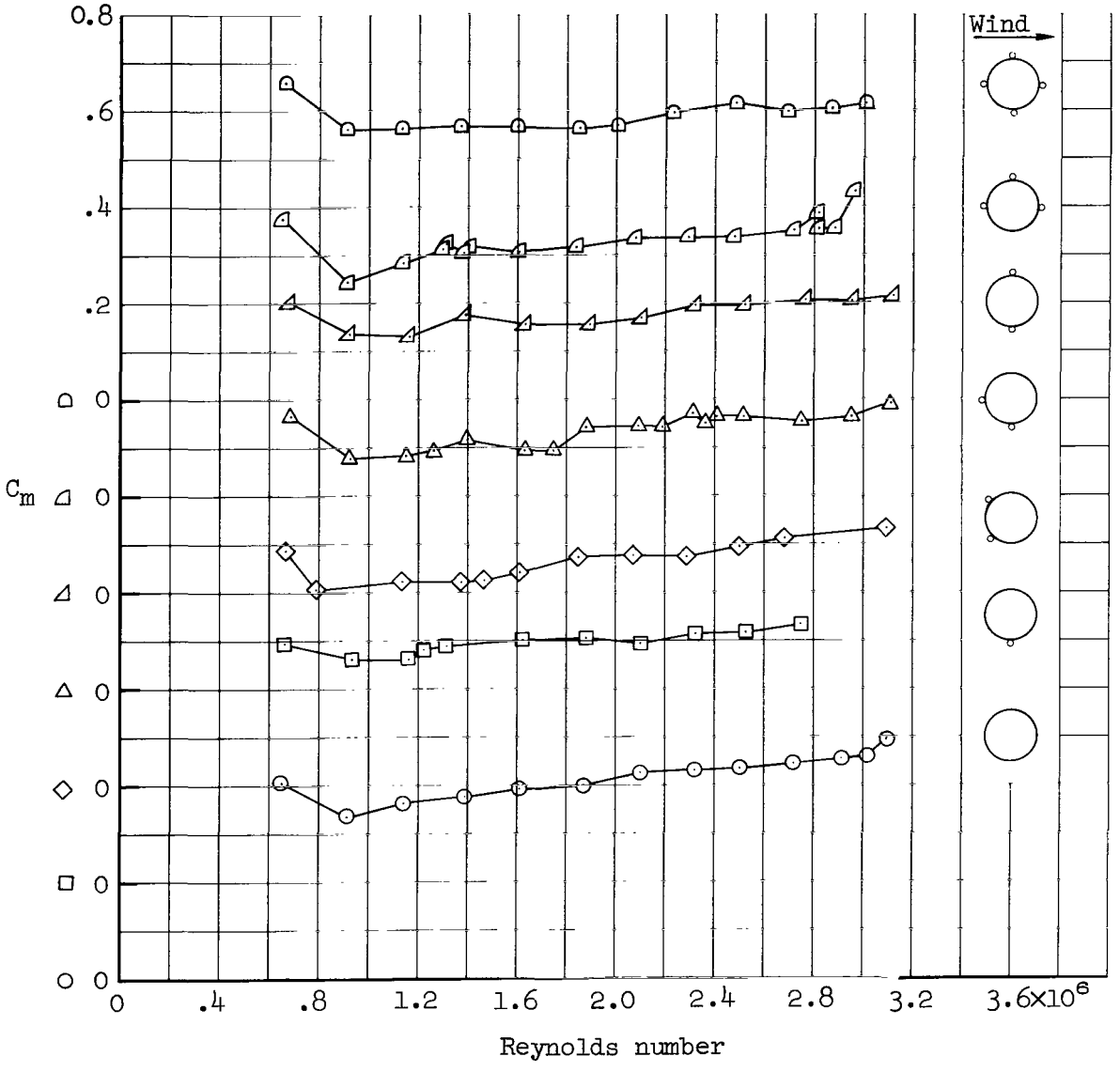

Figure 19.- Steady-state dragwise moment coefficients for the two-diameter model with conduits on the upper stage; conduit diameter 0.06D.

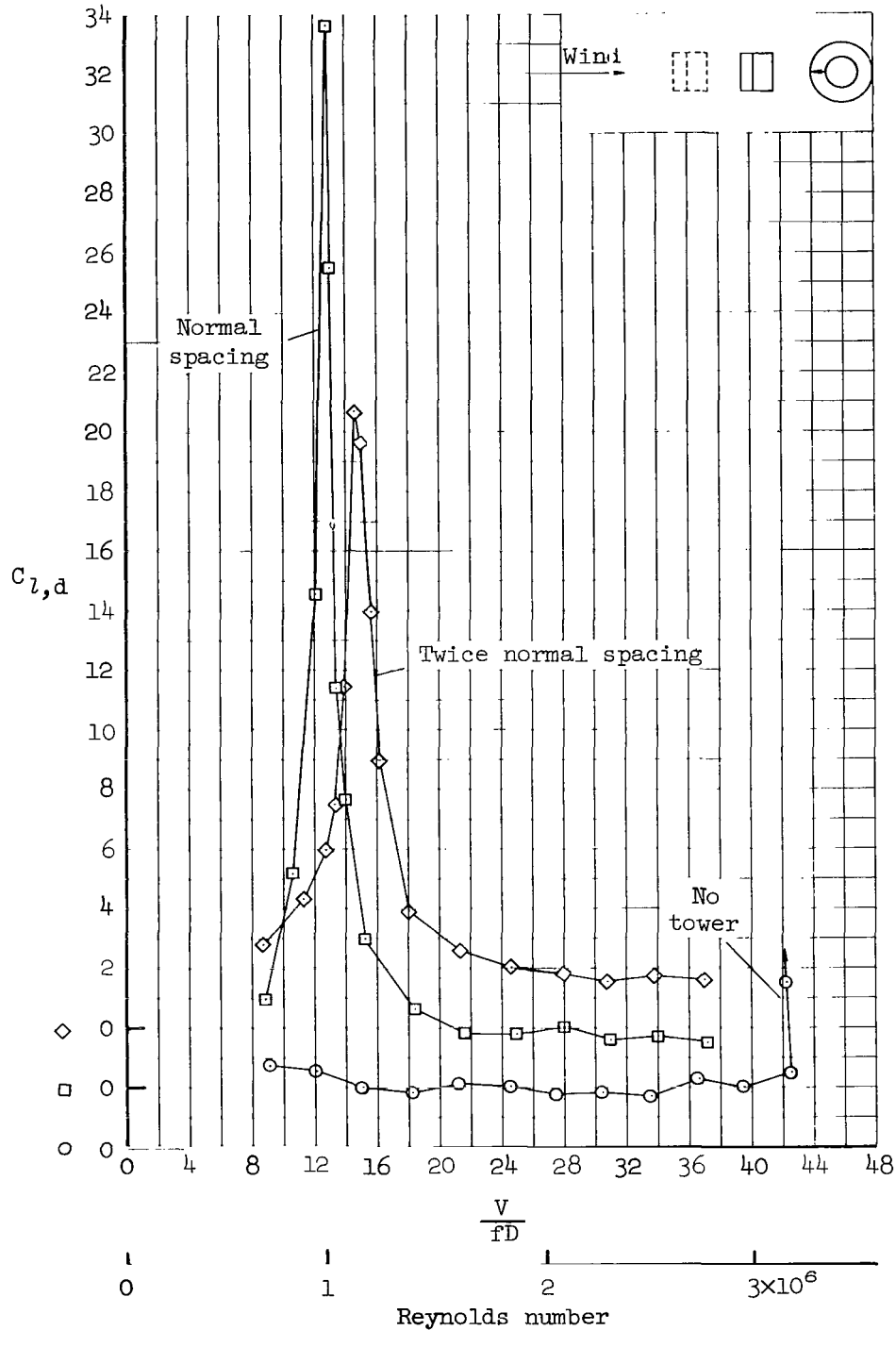

(a) Basic tower.

Figure 20.- Lateral dynamic response of the two-diameter model with tower 2 directly upstream; $(\zeta_l)_{max} \approx 0.004$ to 0.005; $\rho \approx 0.011$.

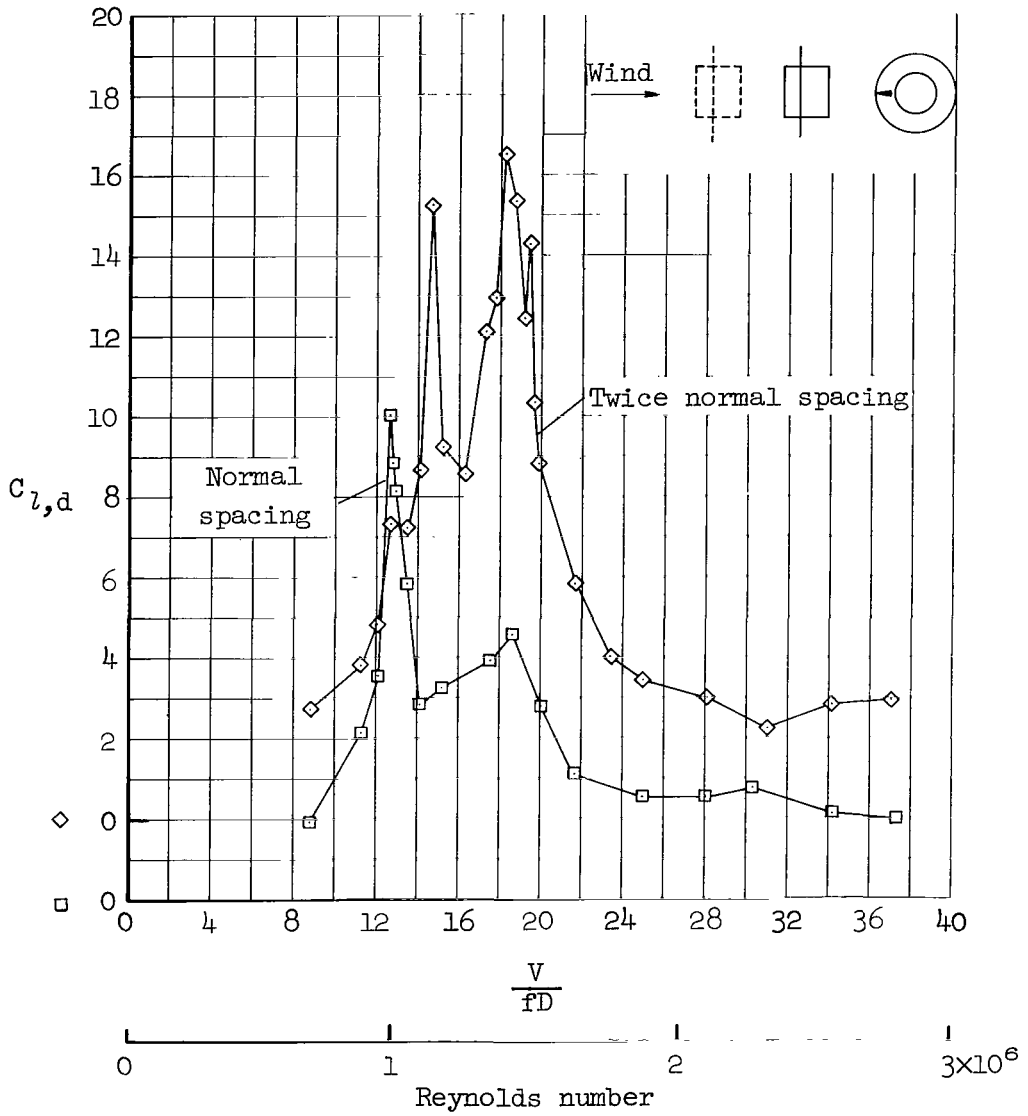

(b) With plate 2.62 D by 0.22 L attached to upstream face and flush with top of tower.

Figure 20.- Concluded.

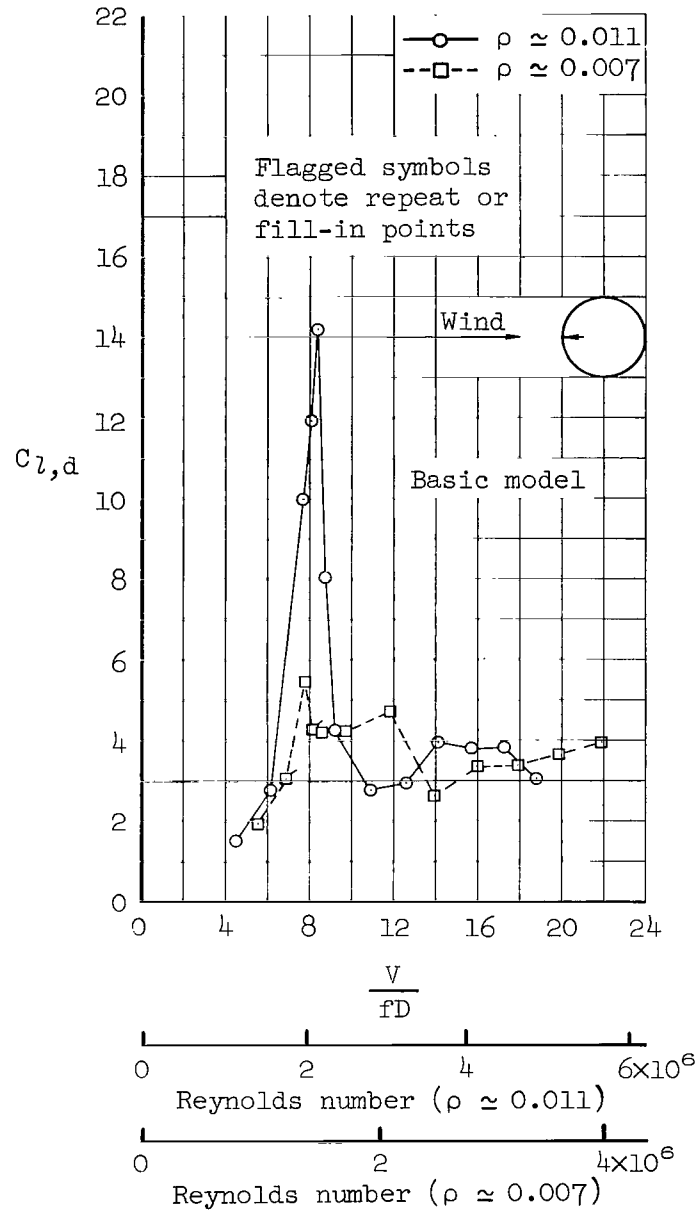

(a) Basic model.

Figure 21.- Lateral dynamic response of the constant-diameter model with vertical stiffeners on the center section; $(\zeta_l)_{max} \simeq 0.010$.

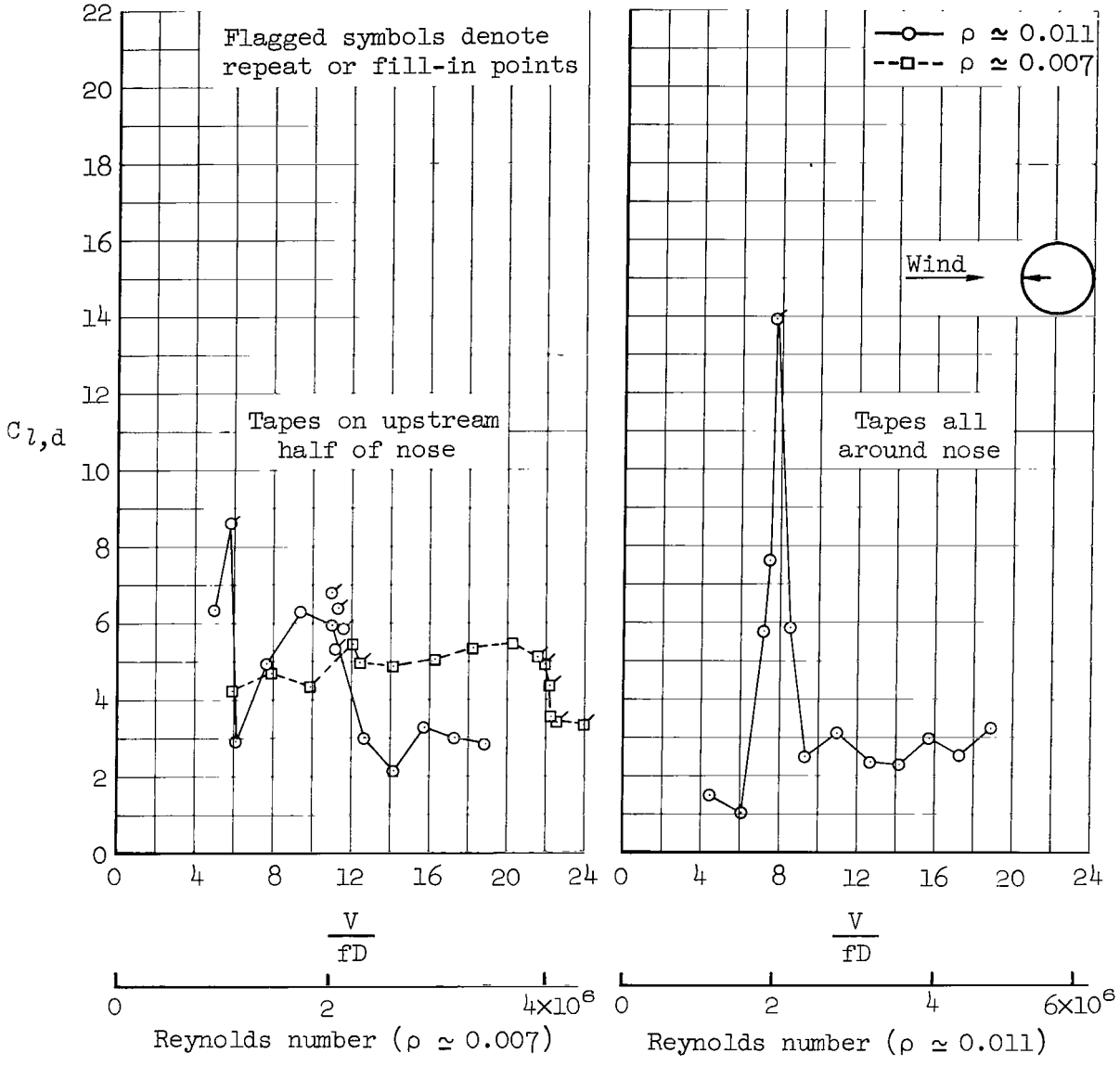

(b) Tapes on nose.

Figure 21.- Continued.

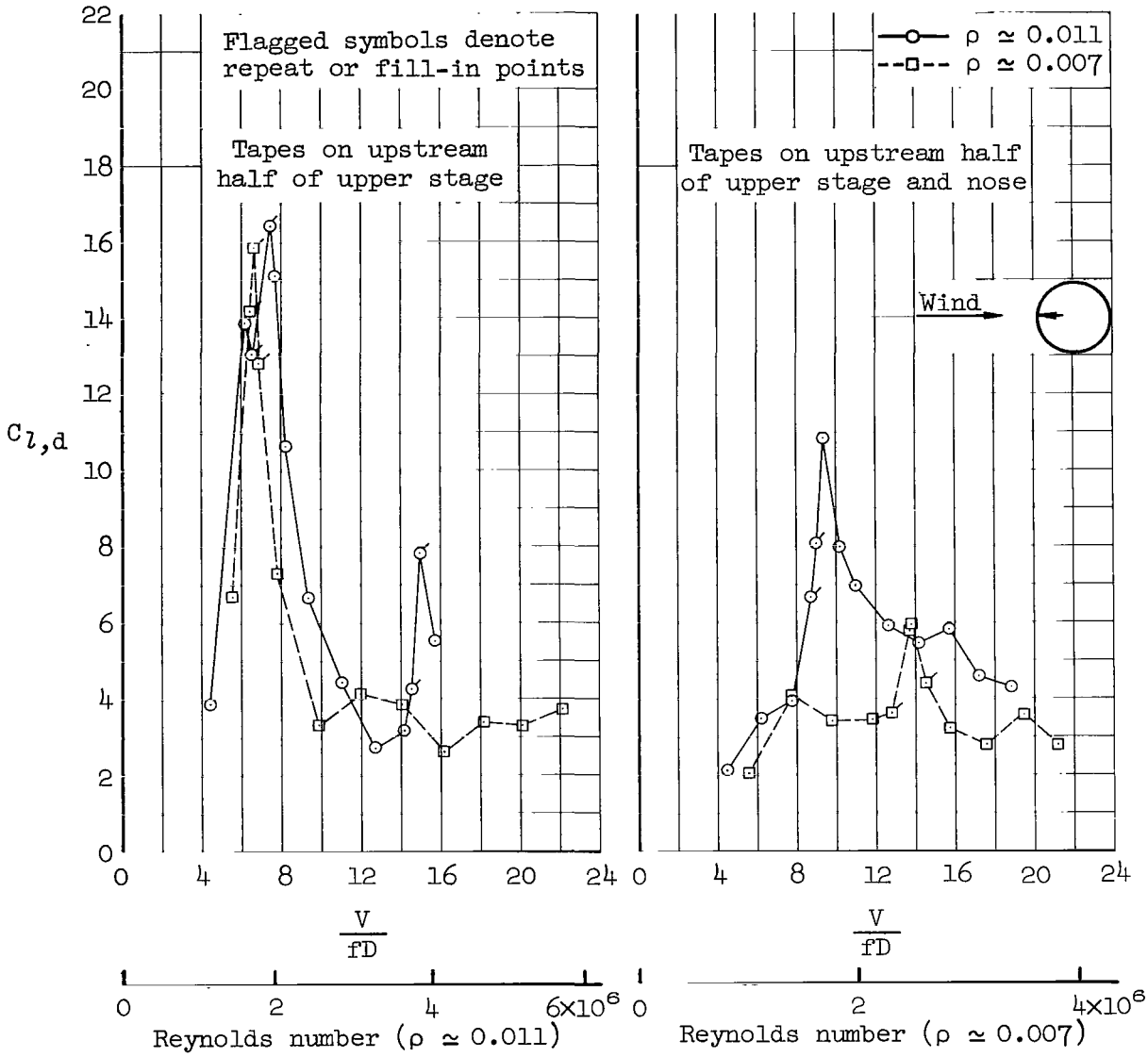

(c) Tapes on upper stage and nose.

Figure 21.- Concluded.

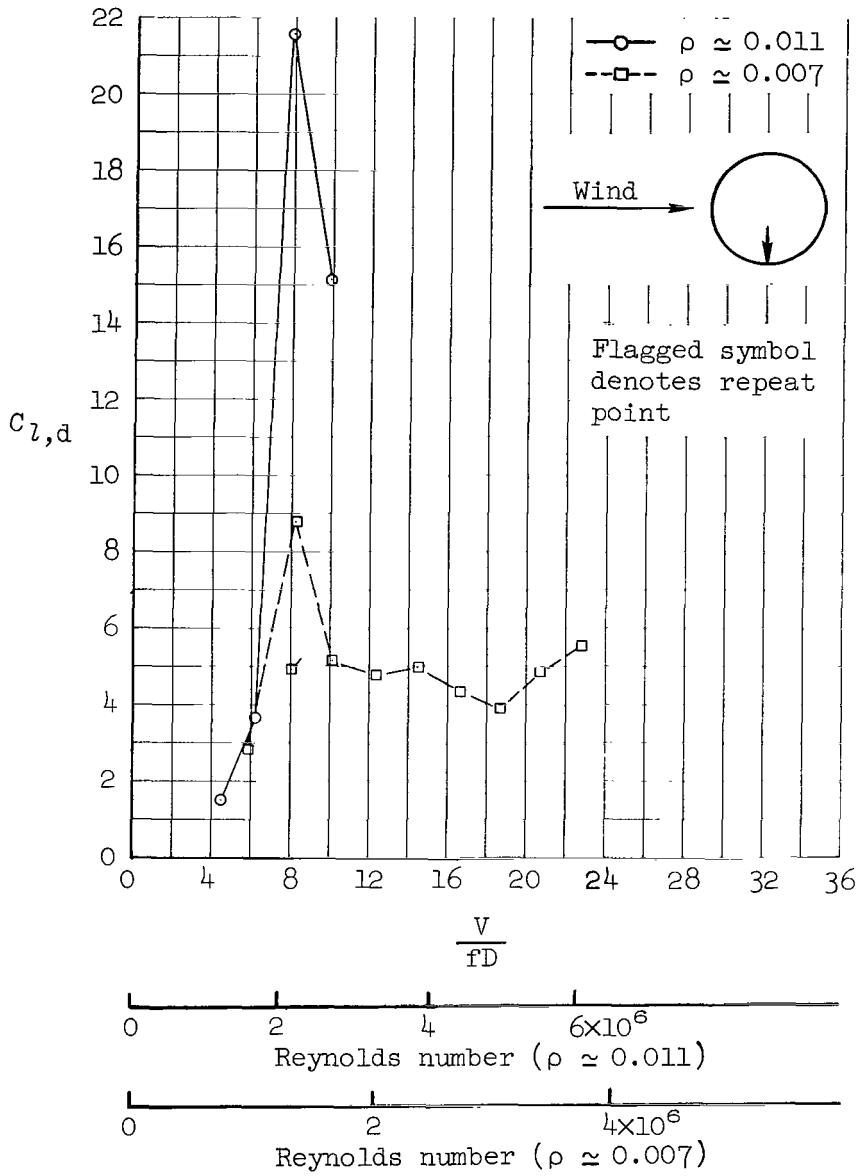

Figure 22.- Lateral dynamic response of the clean constant-diameter model; $(\zeta_l)_{max} \simeq 0.009$ to 0.010.

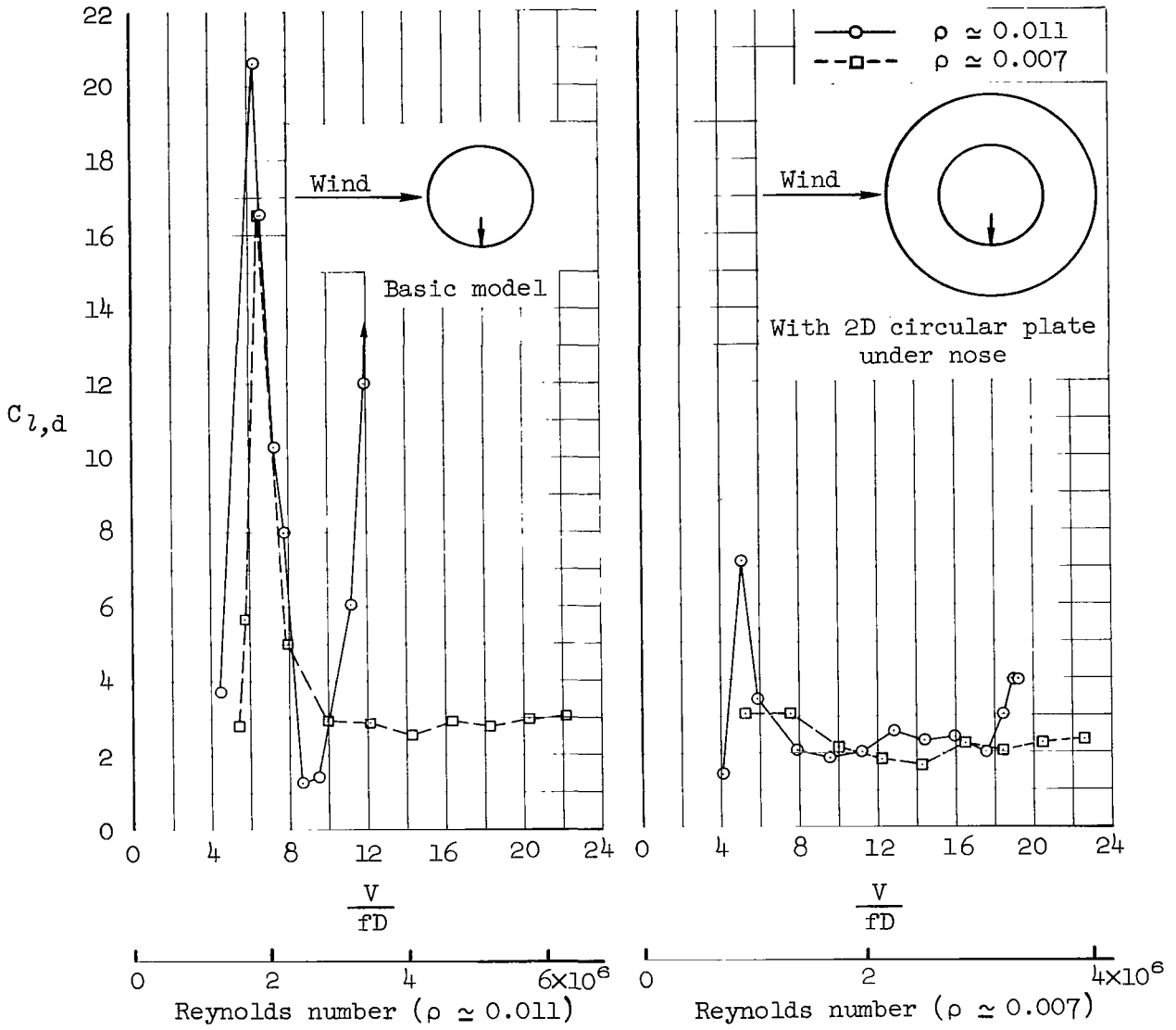

Figure 23.- Lateral dynamic response of the constant-diameter model with tapes staggered vertically (fig. 2(b)); $(\zeta_l)_{max} \simeq 0.006$ to 0.008.

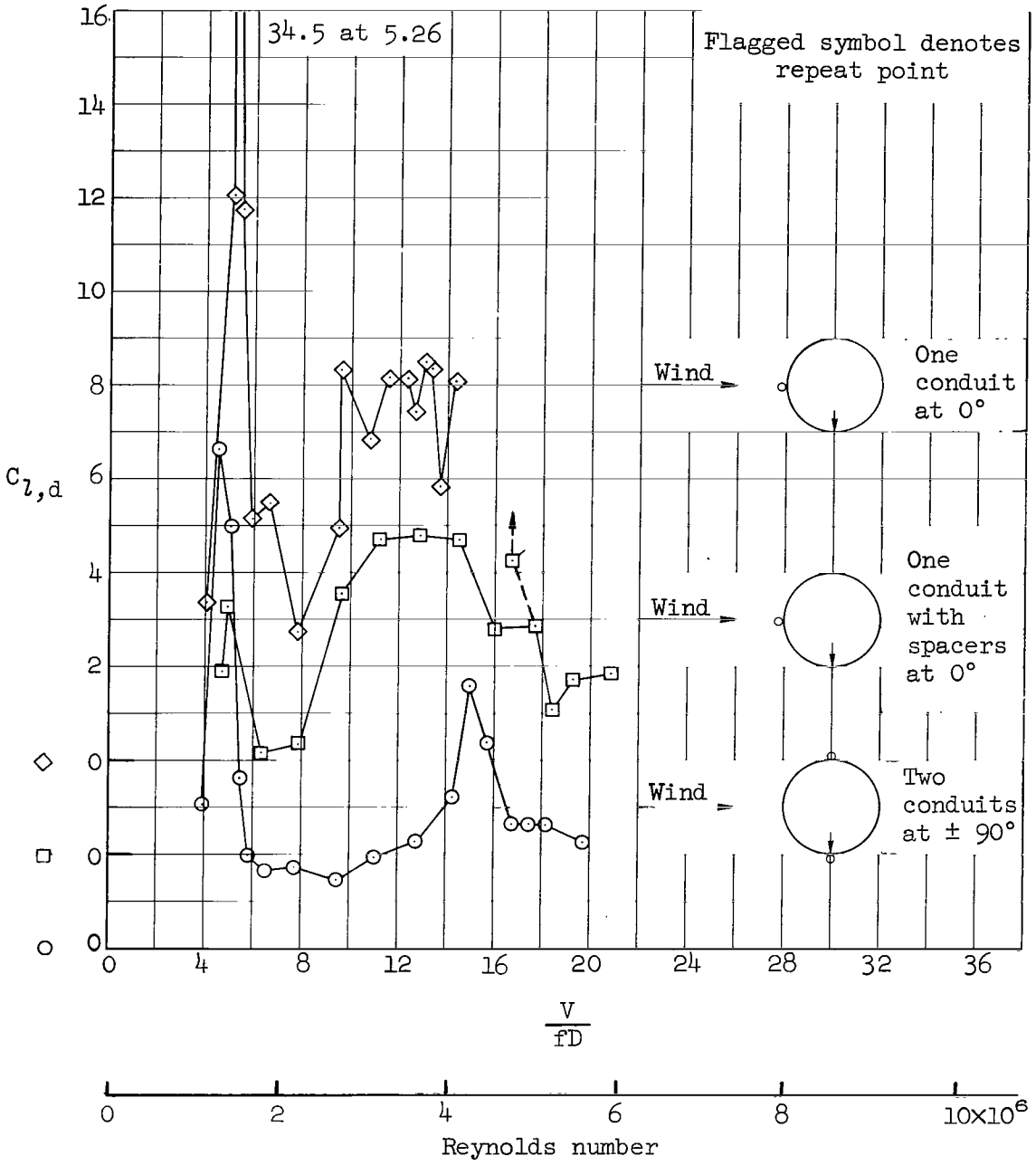

Figure 24.- Lateral dynamic response of the constant-diameter model with conduits below the nose (fig. 2(b)); $(\zeta_l)_{max} \approx 0.007$; $\rho \approx 0.011$; conduit diameter 0.03D.

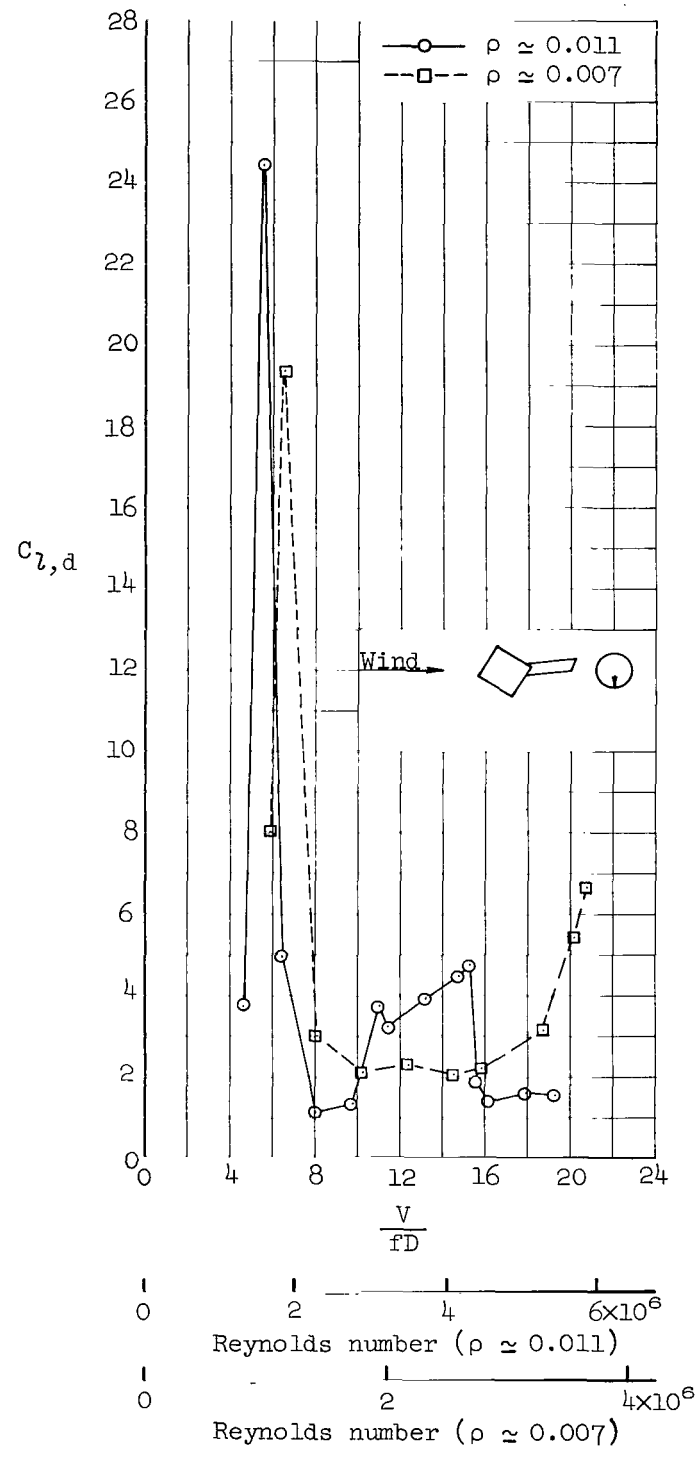

(a) Wind direction, 0°.

Figure 25.- Lateral dynamic response of the constant-diameter model with tower 1 (fig. 2(b)); $(\zeta_l)_{max} \simeq 0.006$ to 0.007.

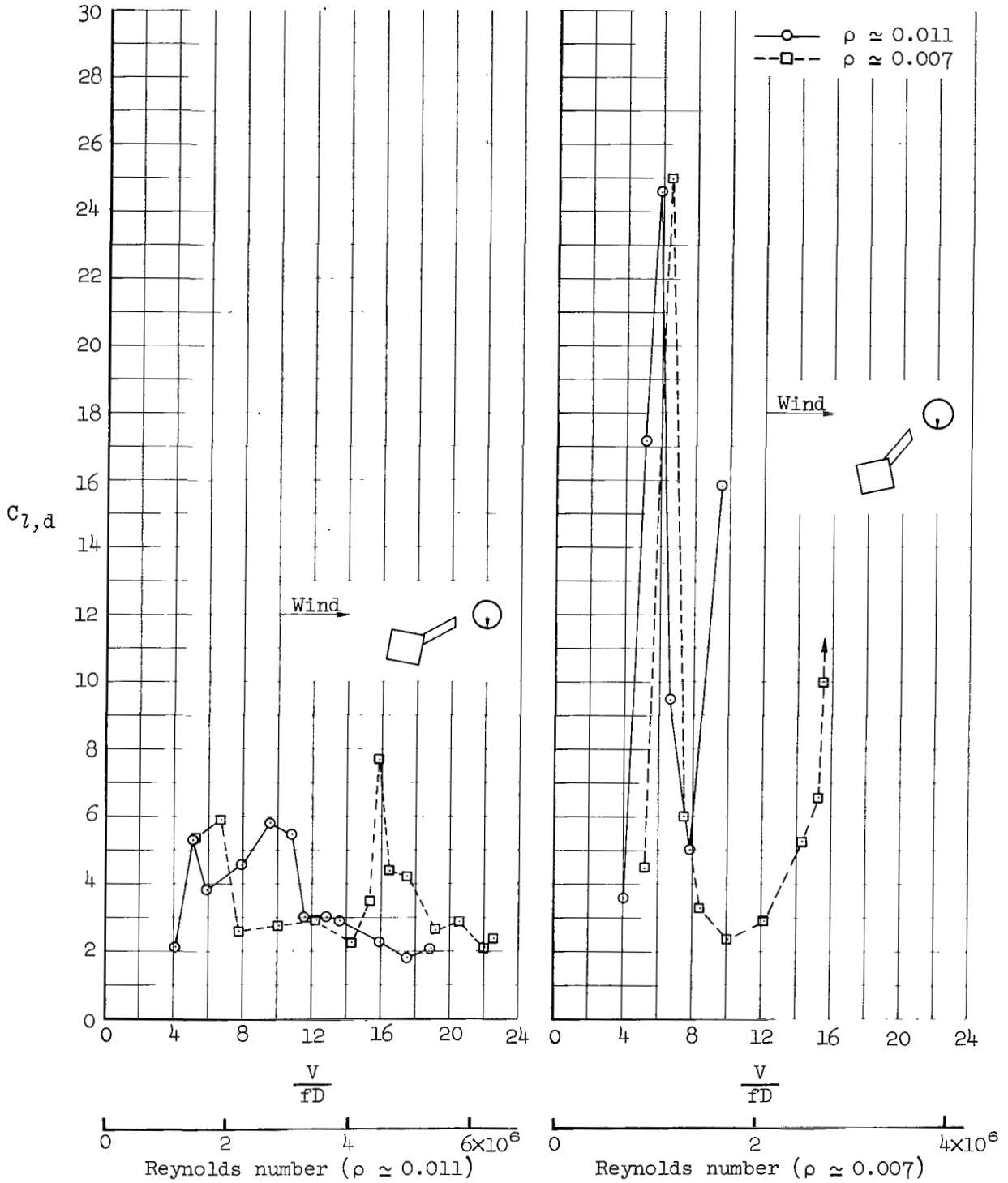

(b) Wind direction, -22.5°.

(c) Wind direction, -45°.

Figure 25.- Continued.

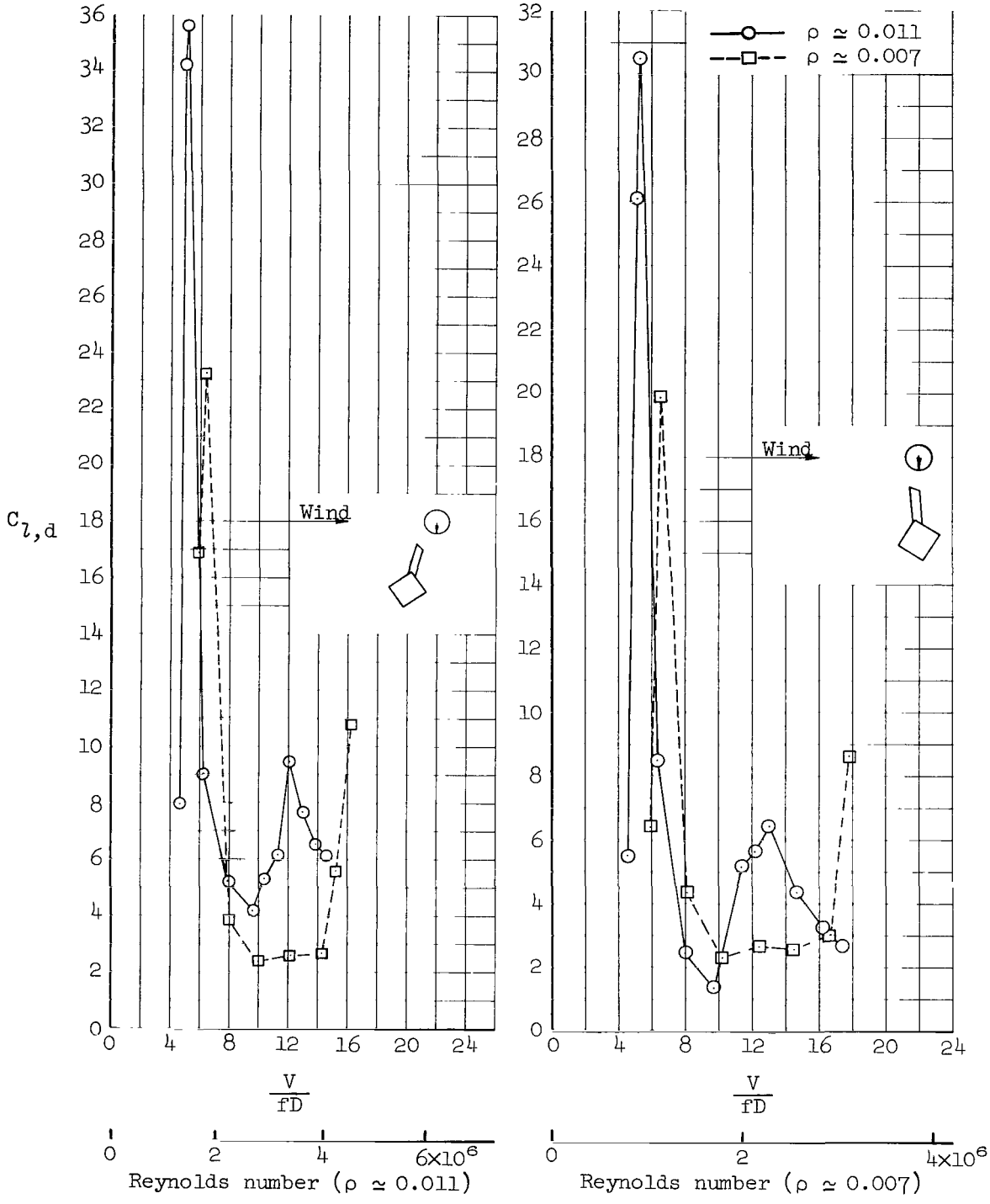

(d) Wind direction, -67.5°.

(e) Wind direction, -90°.

Figure 25.- Concluded.

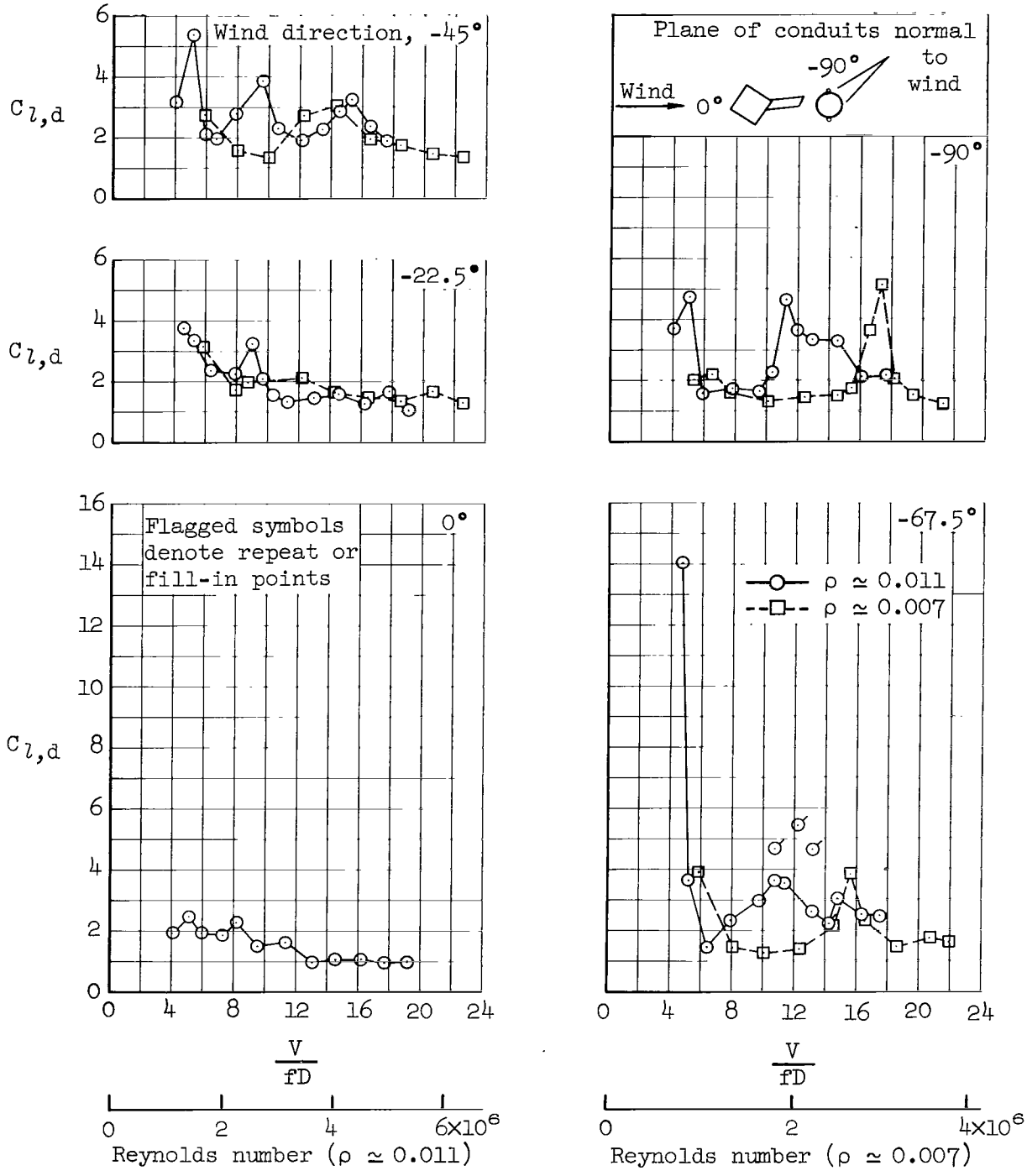

Figure 26.- Lateral dynamic response of the constant-diameter model with two conduits below the nose at an interval of 180° in the lateral plane and with tower 1 (fig. 2(b)); $(\zeta_l)_{max} \simeq 0.006$ to 0.007; conduit diameter 0.03D.

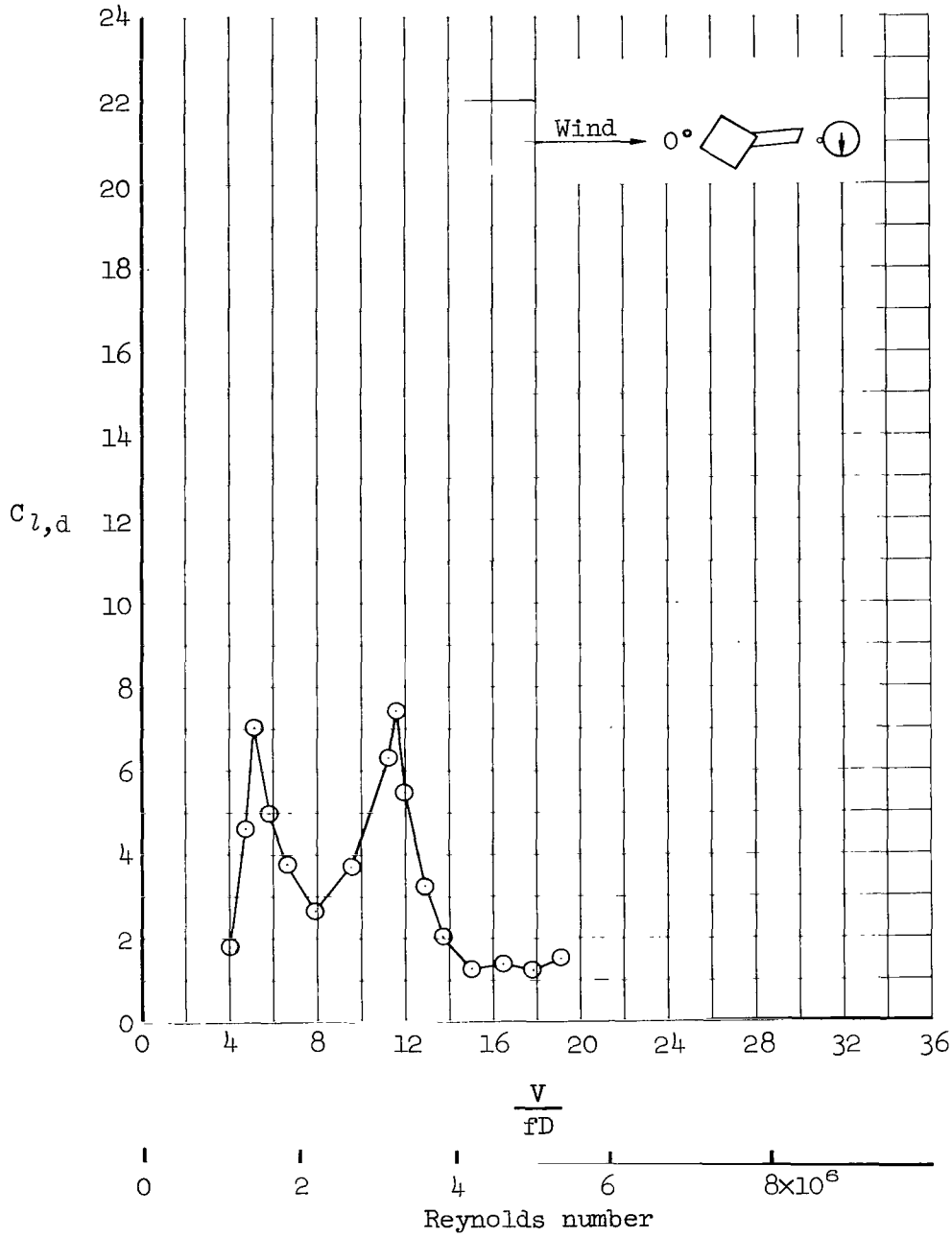

Figure 27.- Lateral dynamic response of the constant-diameter model with one conduit below the nose on the upstream stagnation line and with tower 1 directly upstream (fig. 2(b)); $(\zeta_l)_{max} \approx 0.007$; $\rho \approx 0.011$; conduit diameter 0.03D.

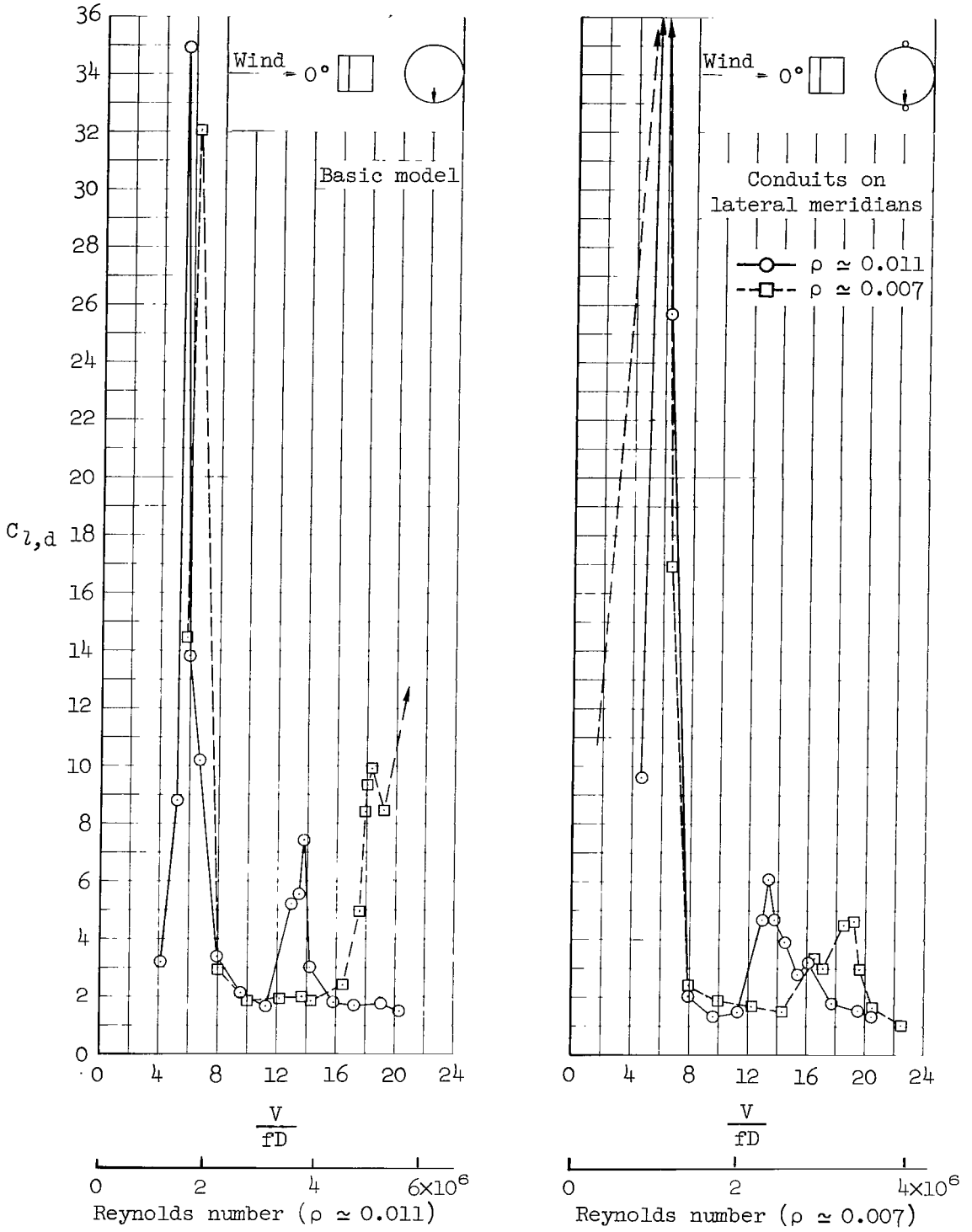

Figure 28.- Lateral dynamic response of the constant-diameter model with tower 2 directly upstream, with and without two conduits below the nose at an interval of 180° in the lateral plane; $(\zeta_l)_{max} \simeq 0.007$; conduit diameter 0.03D.

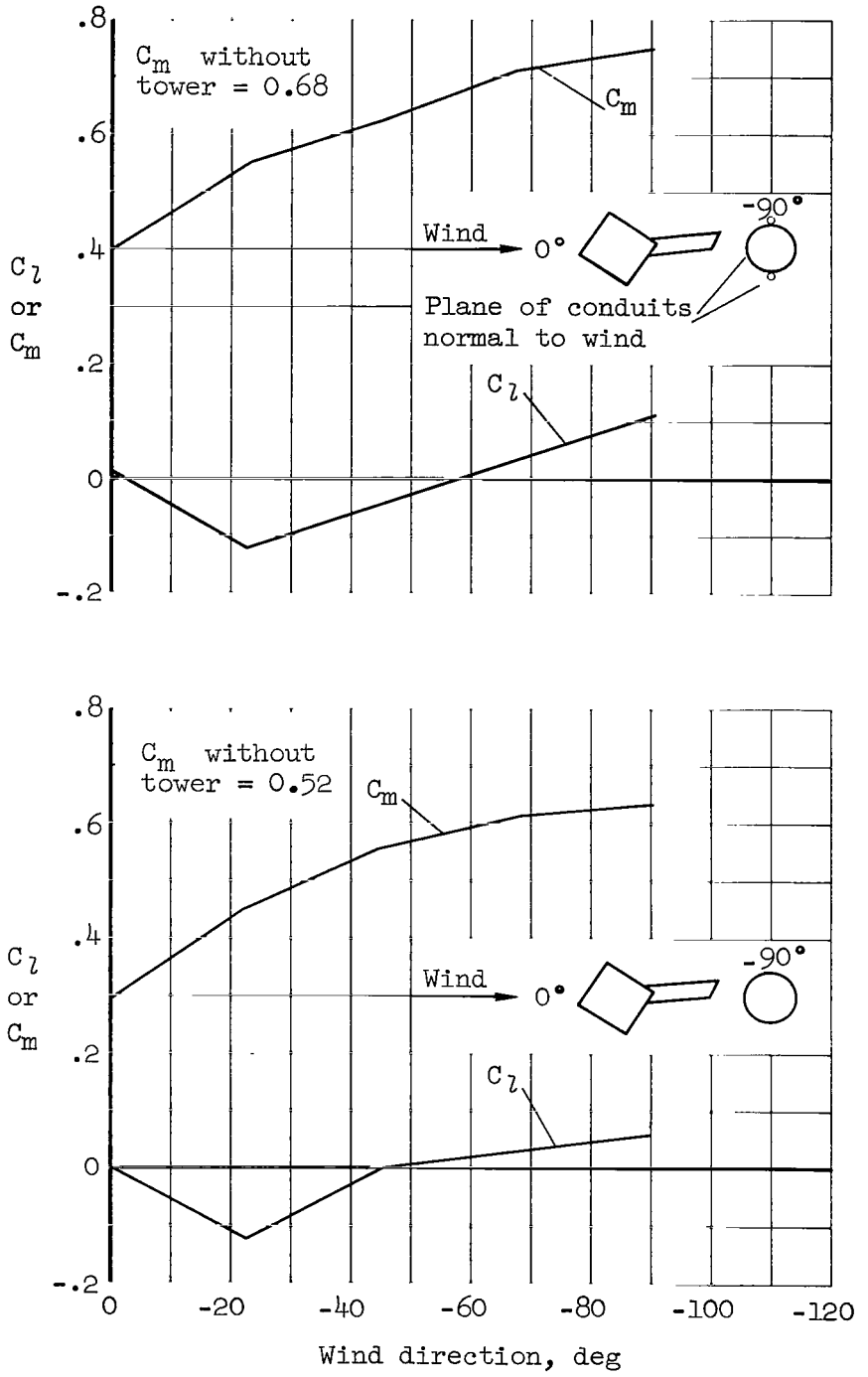

Figure 29.- Steady-state moment coefficients for the constant-diameter model with tower 1, with and without two conduits below the nose at an interval of 180° in the lateral plane (fig. 2(b)); conduit diameter 0.03D; Reynolds number approximately 3 million.

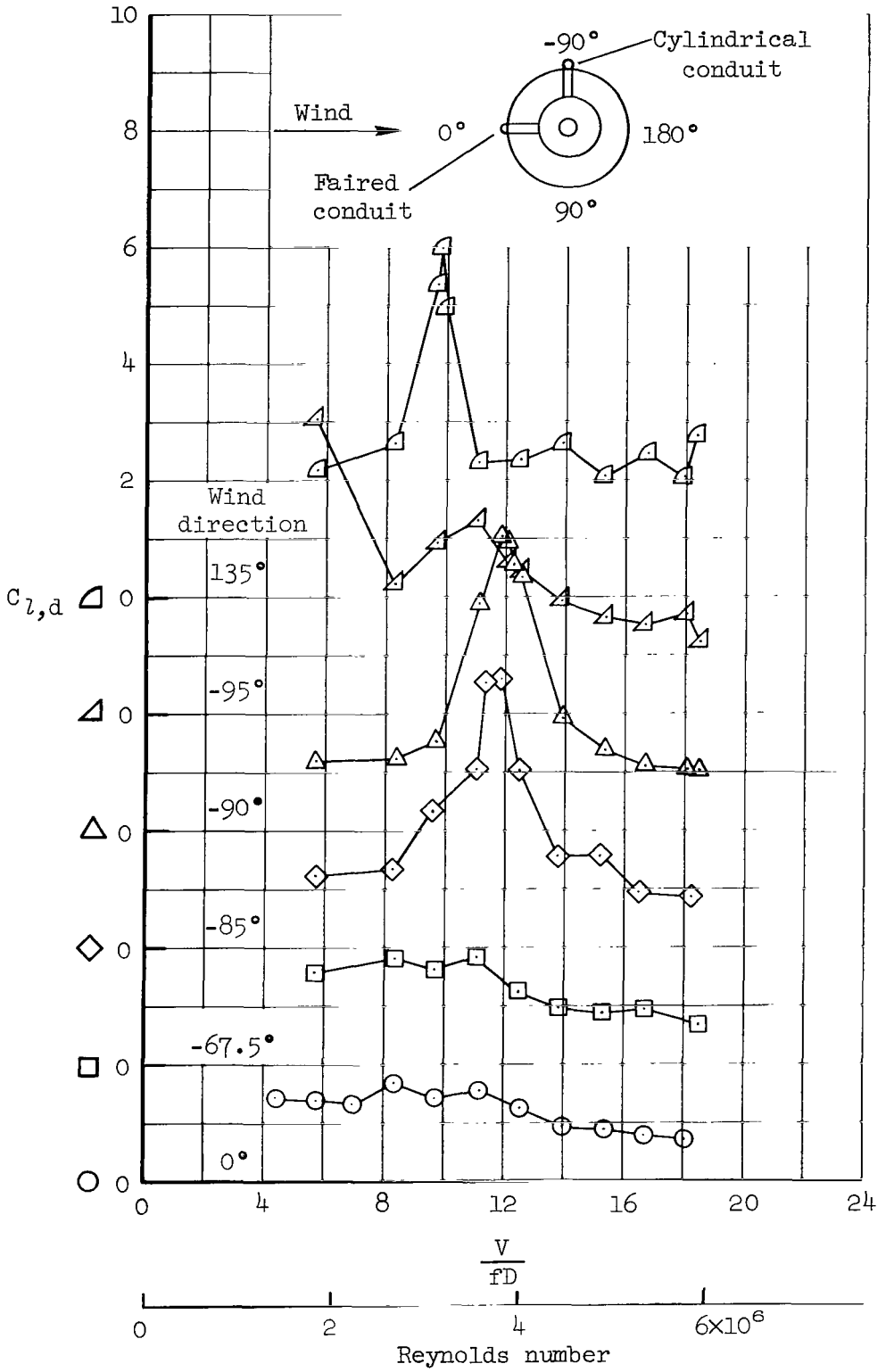

Figure 30.- Lateral dynamic response of Model C (fig. 6(c)); $(\zeta_l)_{max} \approx 0.005$ to 0.007; $\rho \approx 0.011$.

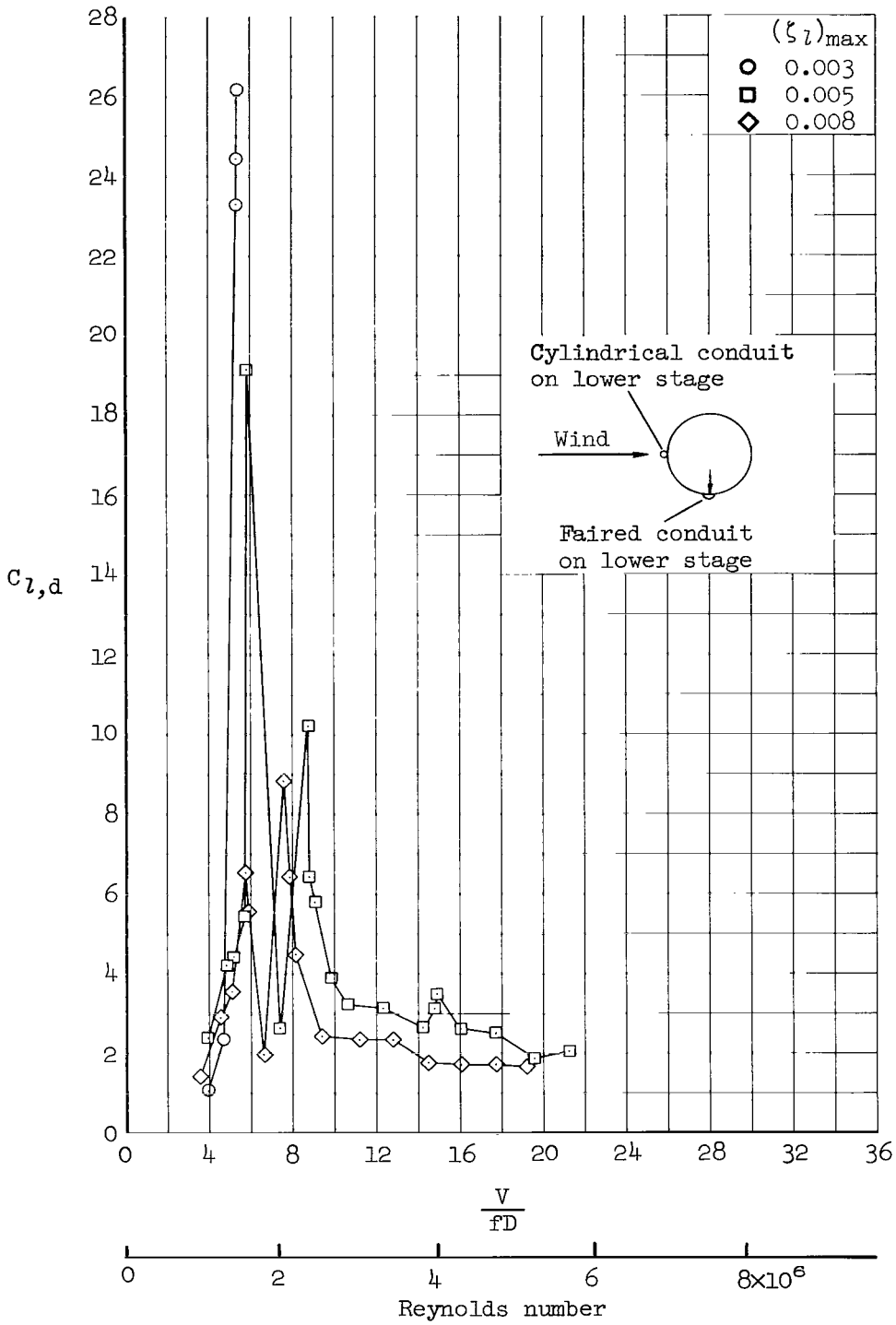

Figure 31.- Effect of increasing damping on the lateral dynamic response of Model A (fig. 6(a)); lower-stage conduit on the upstream stagnation line; $\rho \simeq 0.011$.

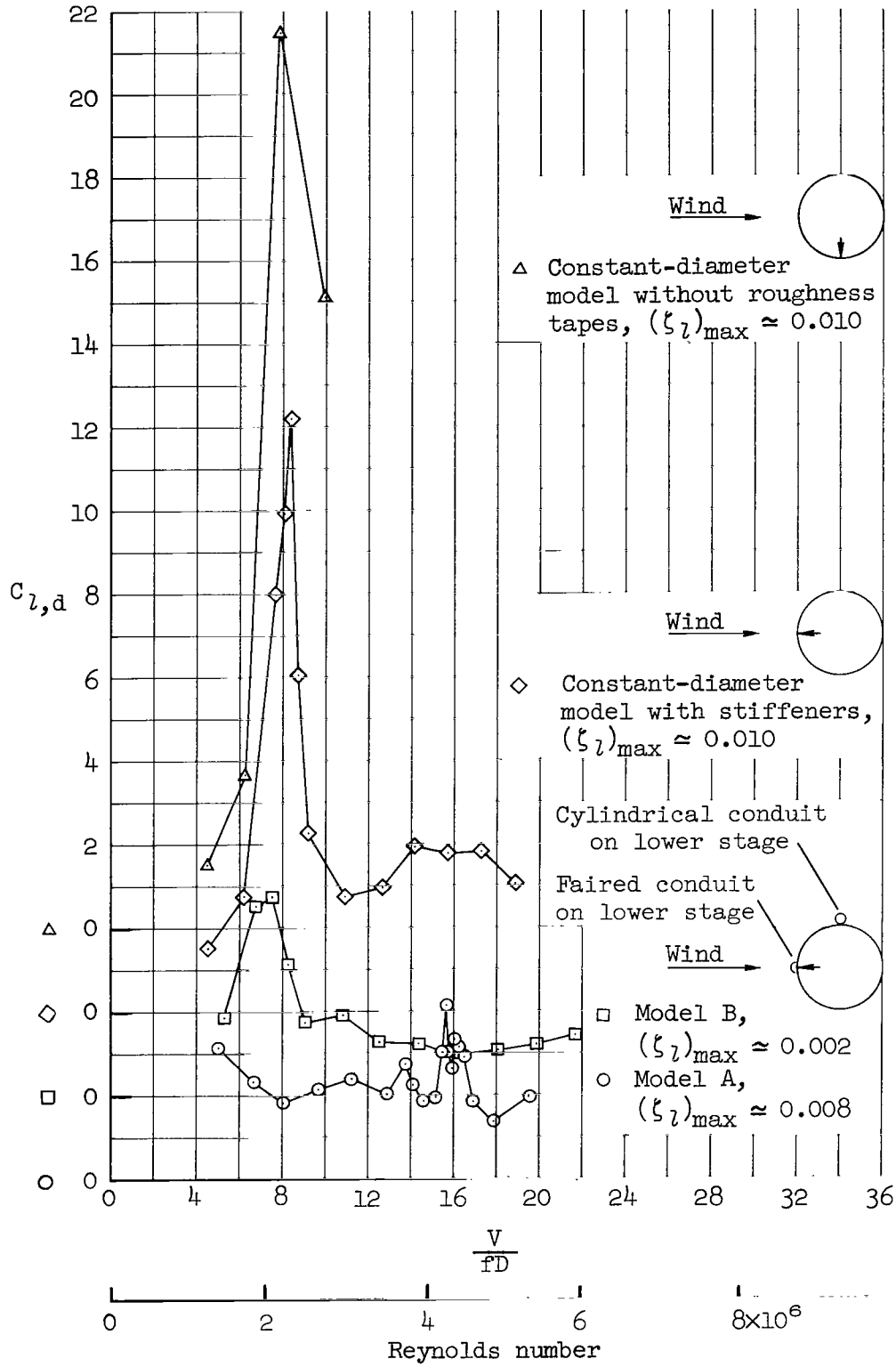

Figure 32.- Effect of increasing number of protuberances on the lateral dynamic response of the constant-diameter models; $\rho \simeq 0.011$.

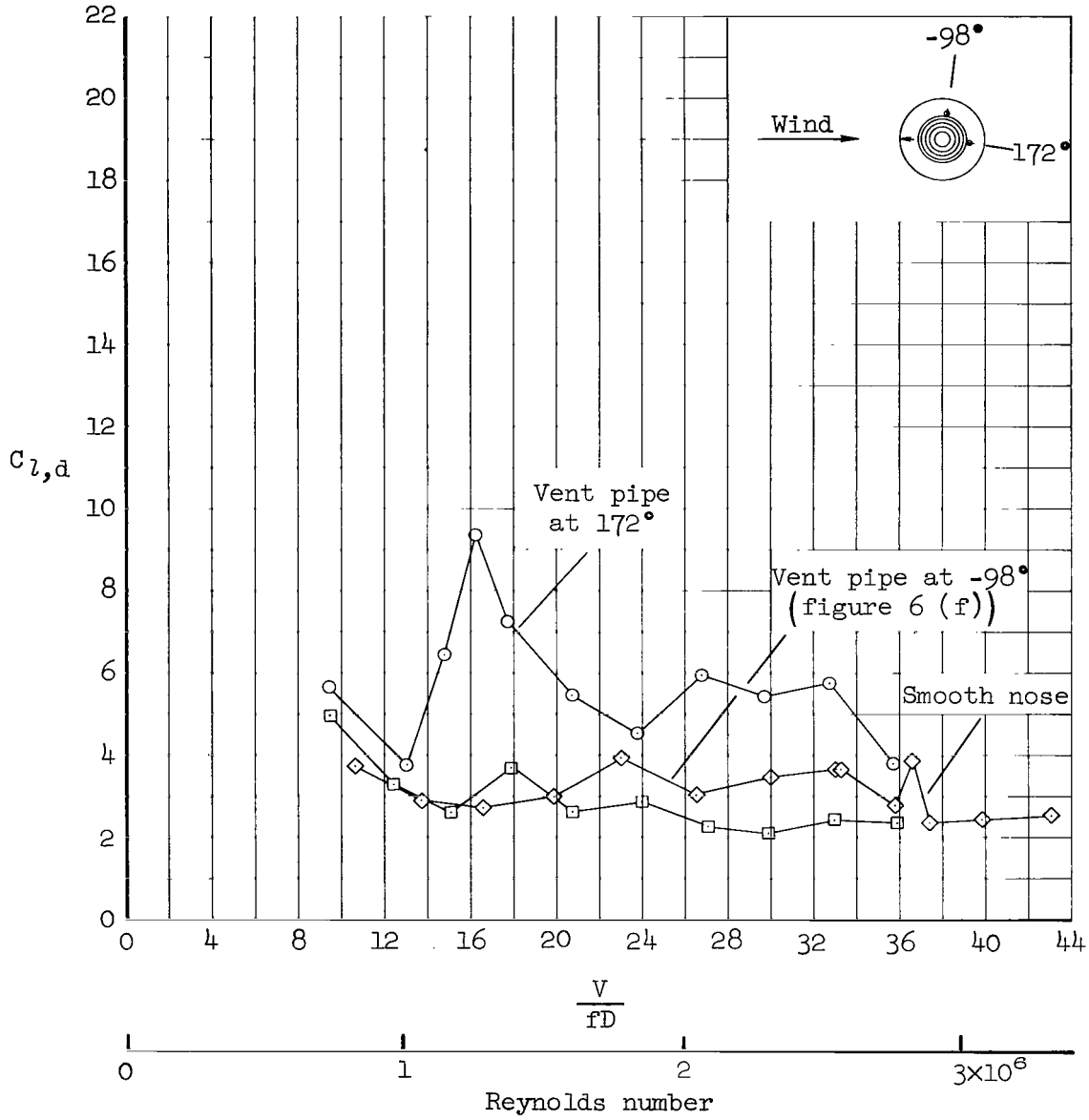

Figure 33.- Effect of payload insulation blanket on the lateral dynamic response of Model E; $(\zeta_l)_{max} \approx 0.007$ to 0.009; $\rho \approx 0.011$.

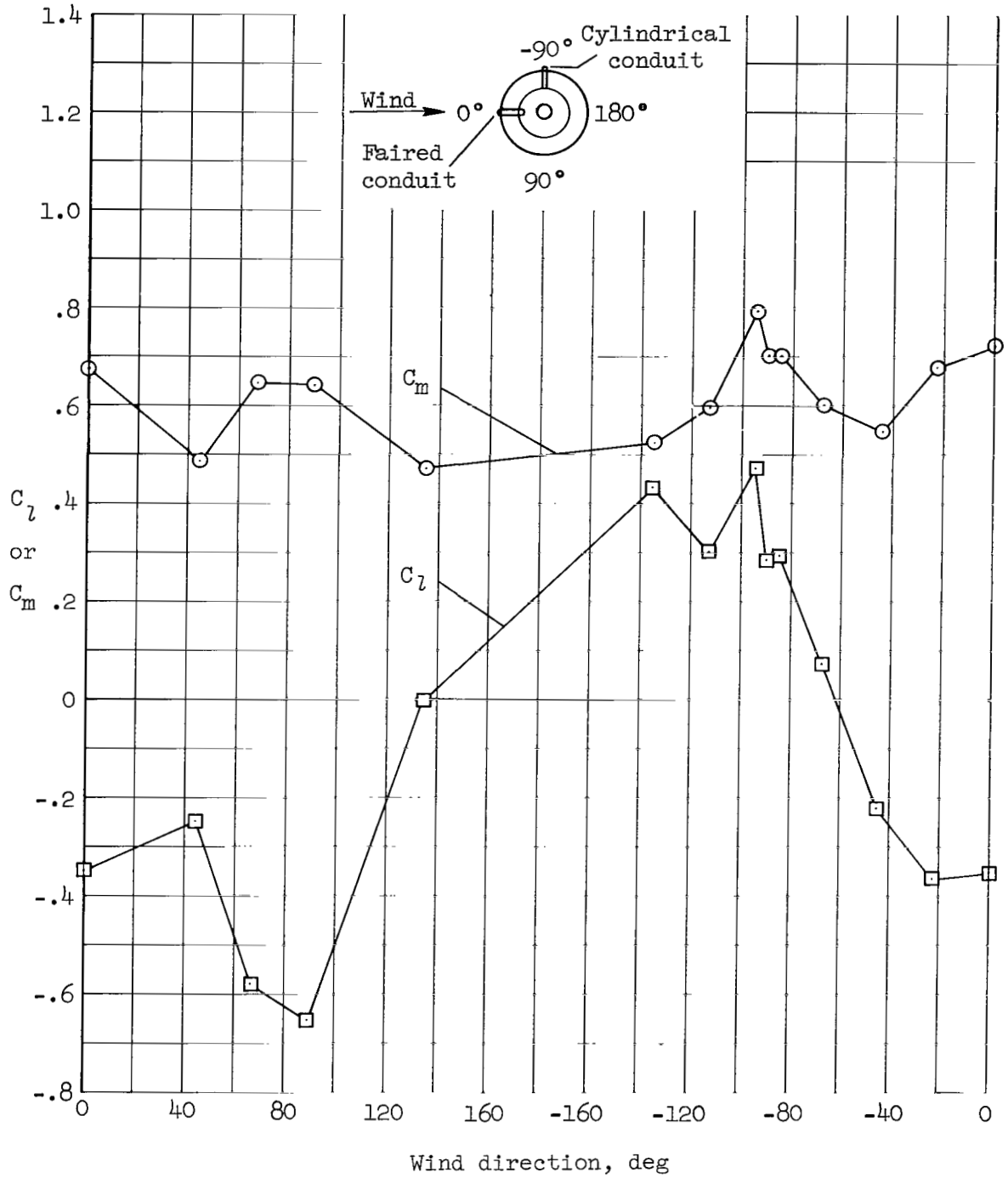

Figure 34.- Steady-state moment coefficients for Model C (fig. 6(c)); Reynolds number approximately 3.7 million.

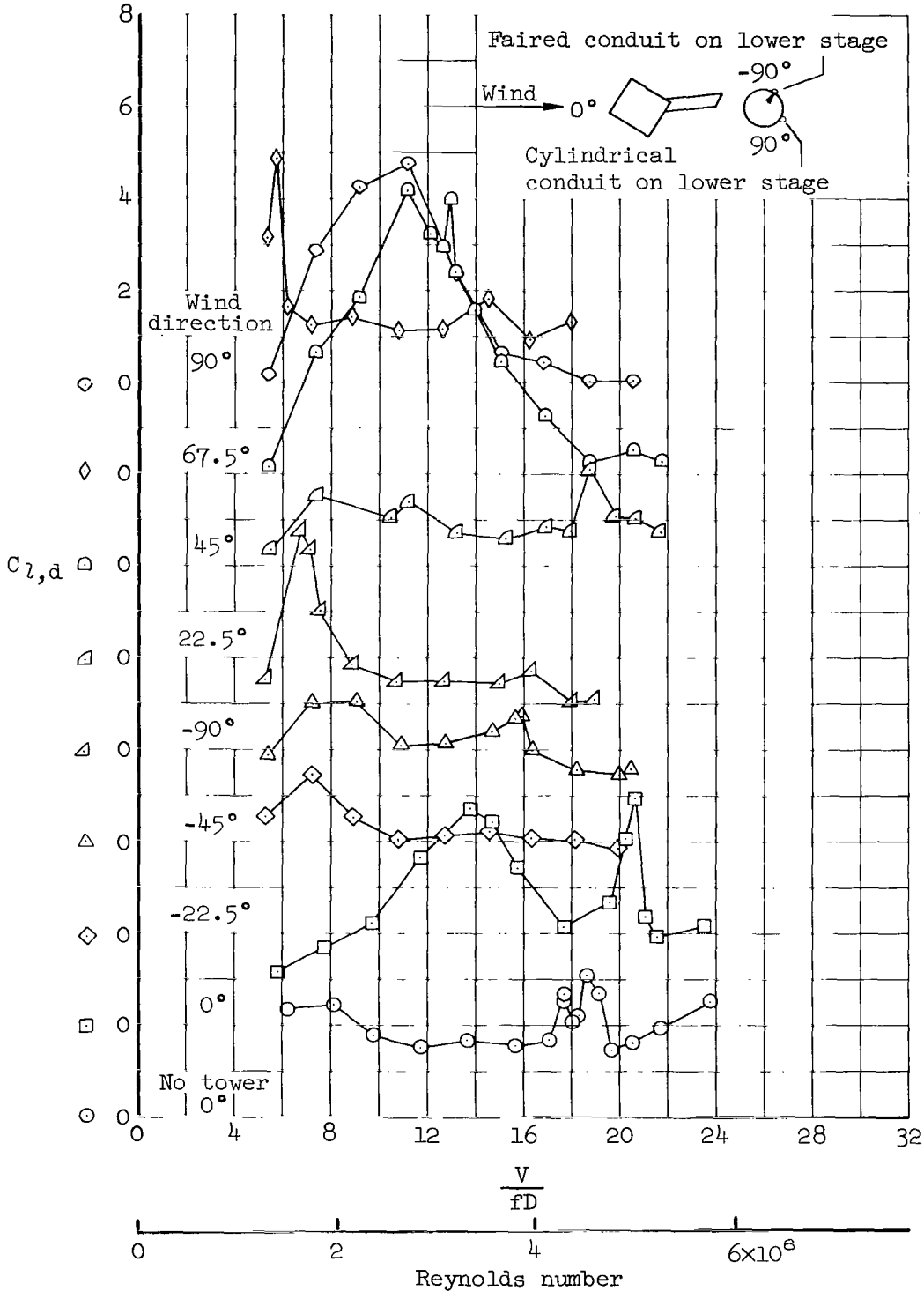

Figure 35.- Lateral dynamic response of Model B with tower 1 (fig. 6(b)); $(\zeta_l)_{max} \approx 0.003$ to 0.009; $\rho \approx 0.011$.

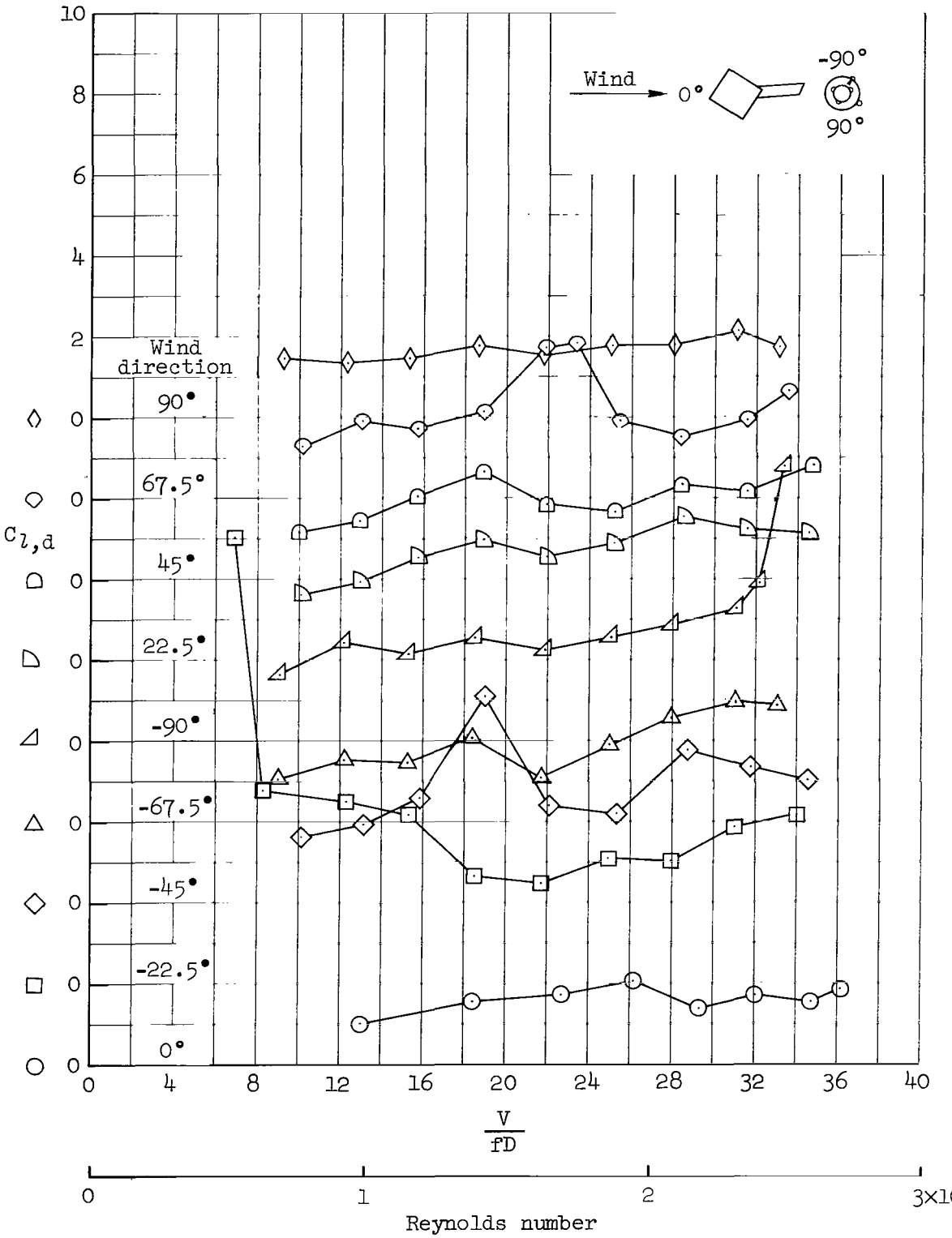

Figure 36.- Lateral dynamic response of Model D with tower 1; $(\zeta_l)_{max} \approx 0.003$ to 0.005; $\rho \approx 0.011$.

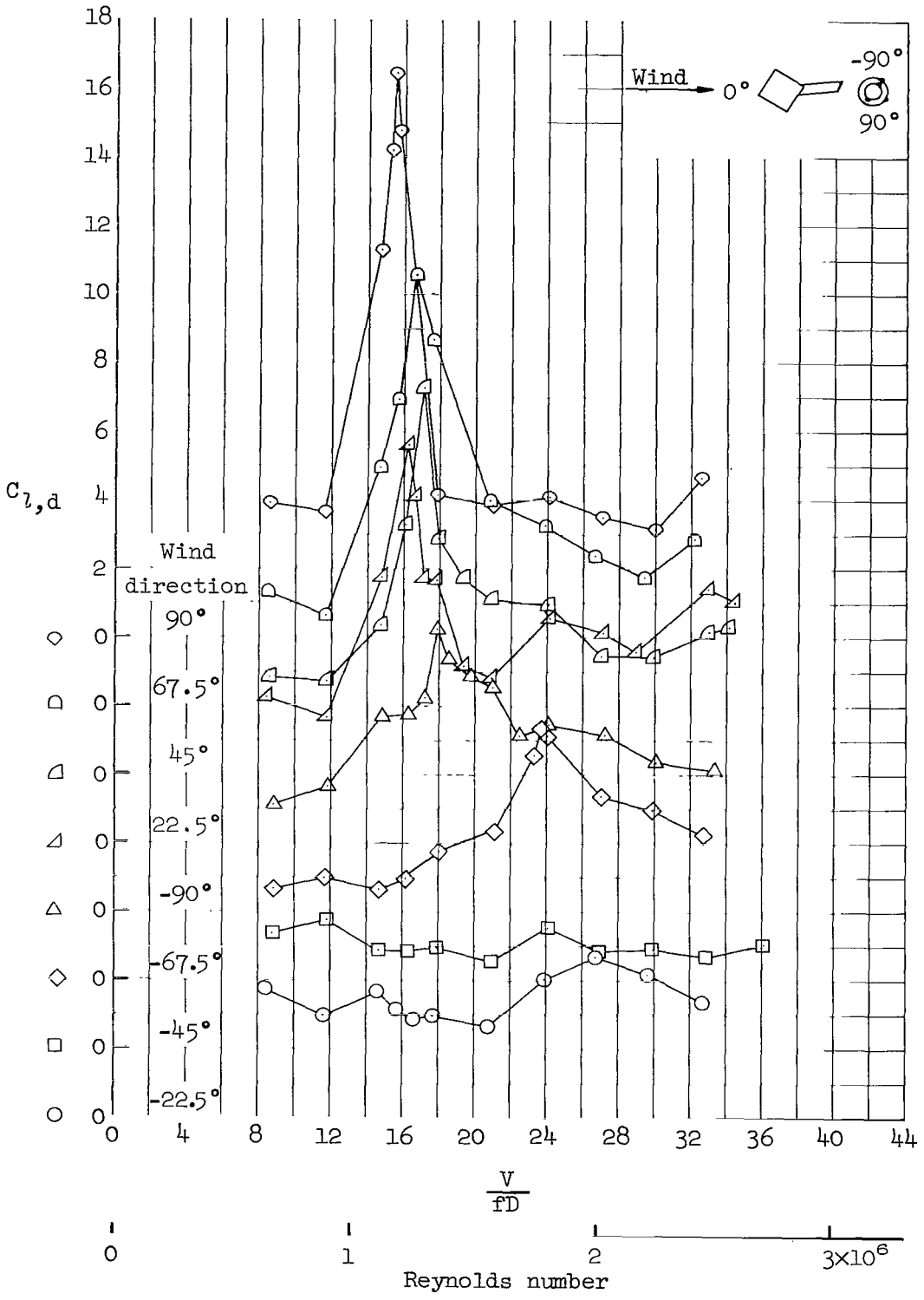

Figure 37.- Lateral dynamic response of Model E with payload insulation blanket and with tower 1; $(\zeta_l)_{max} \approx 0.009$ to 0.010; $\rho \approx 0.011$.

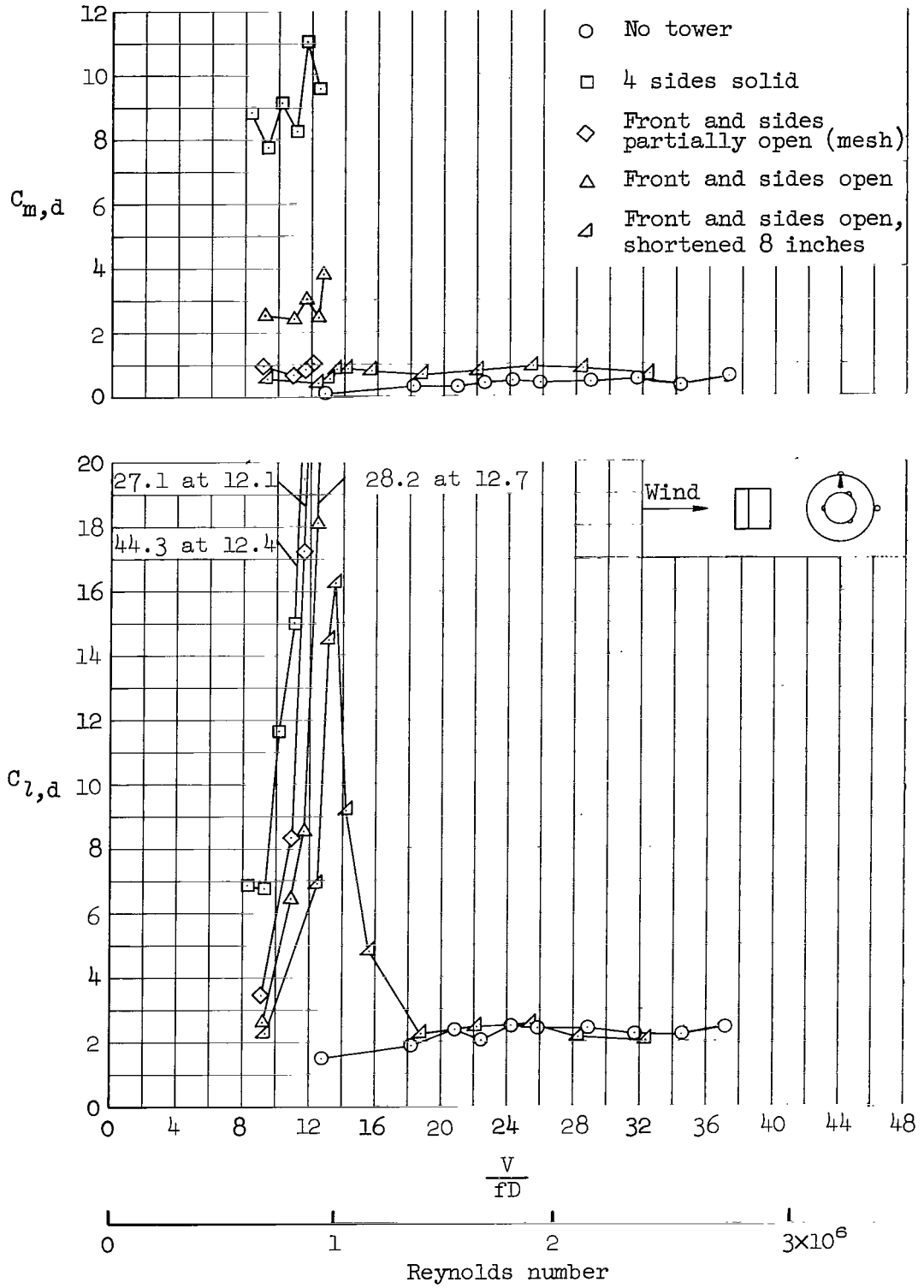

Figure 38.- Dynamic response of Model D with several tower 2 configurations directly upstream; $(\zeta_l)_{max} \approx 0.004$ to 0.005; $\rho \approx 0.011$.

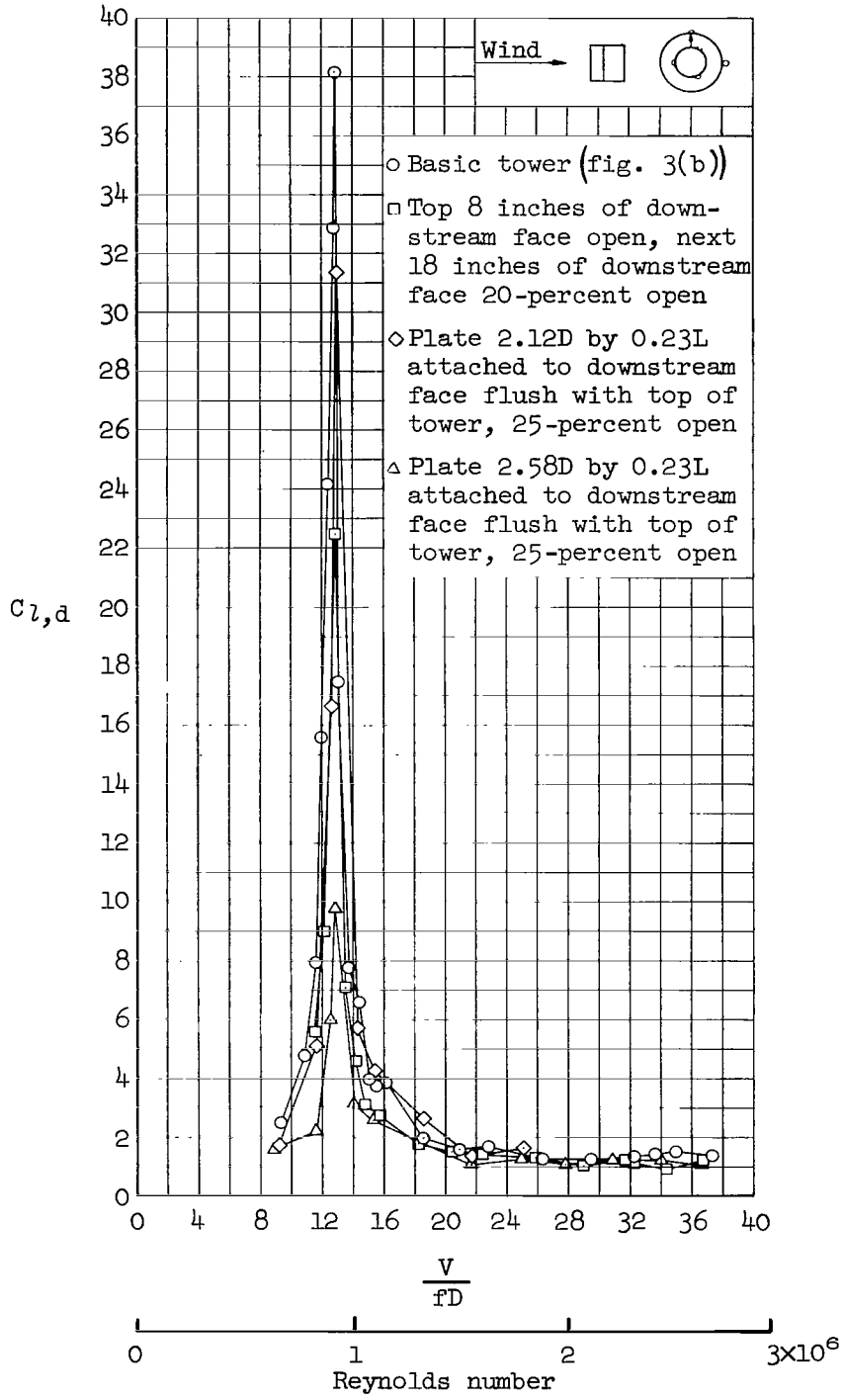

(a) Porous fixes.

Figure 39.- Effect of "fixes" applied to tower 2 on the lateral dynamic response of Model D with tower 2 directly upstream; $(\zeta_l)_{max} \approx 0.002$ to 0.009; $\rho \approx 0.011$.

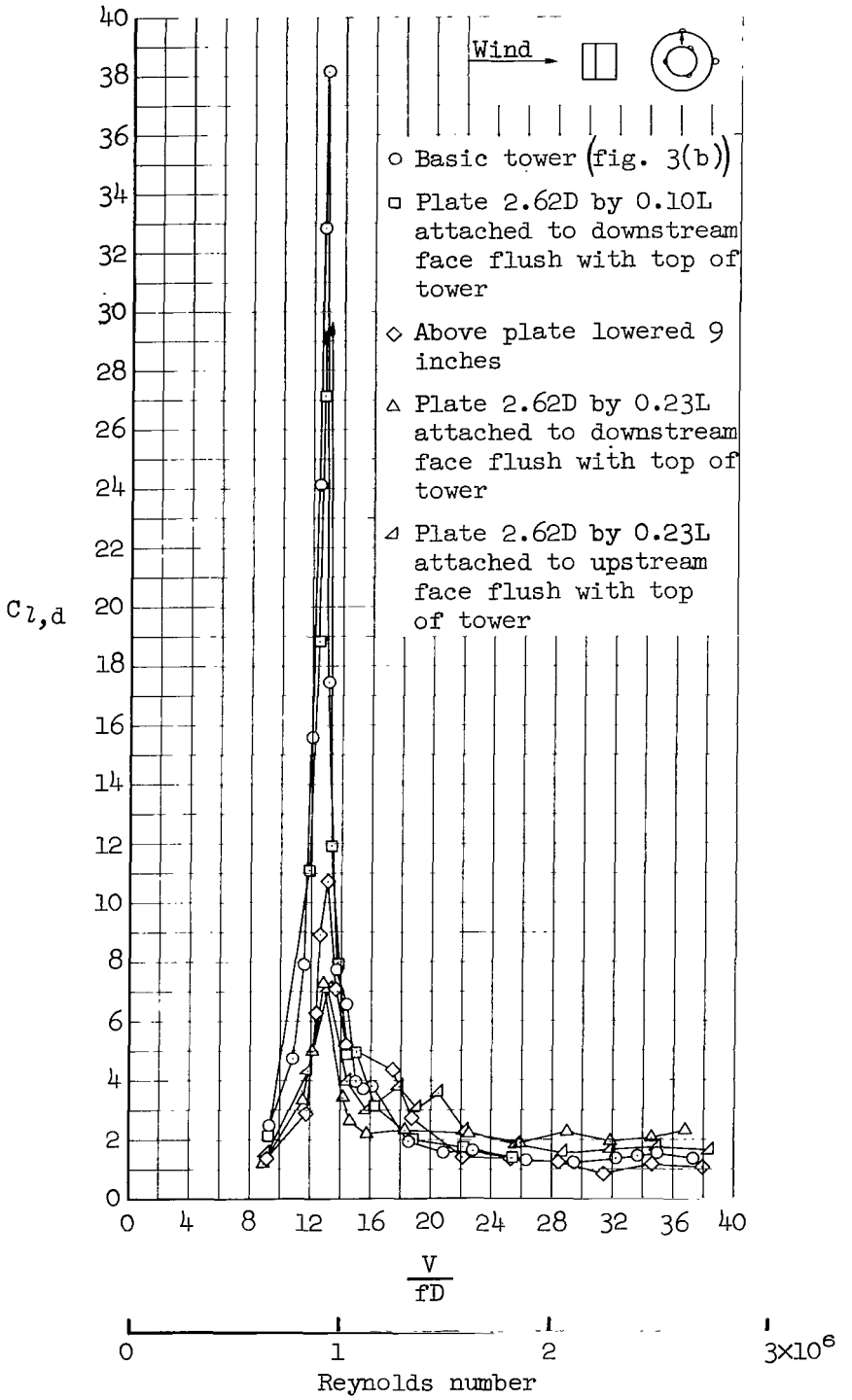

(b) Solid fixes.

Figure 39.- Concluded.

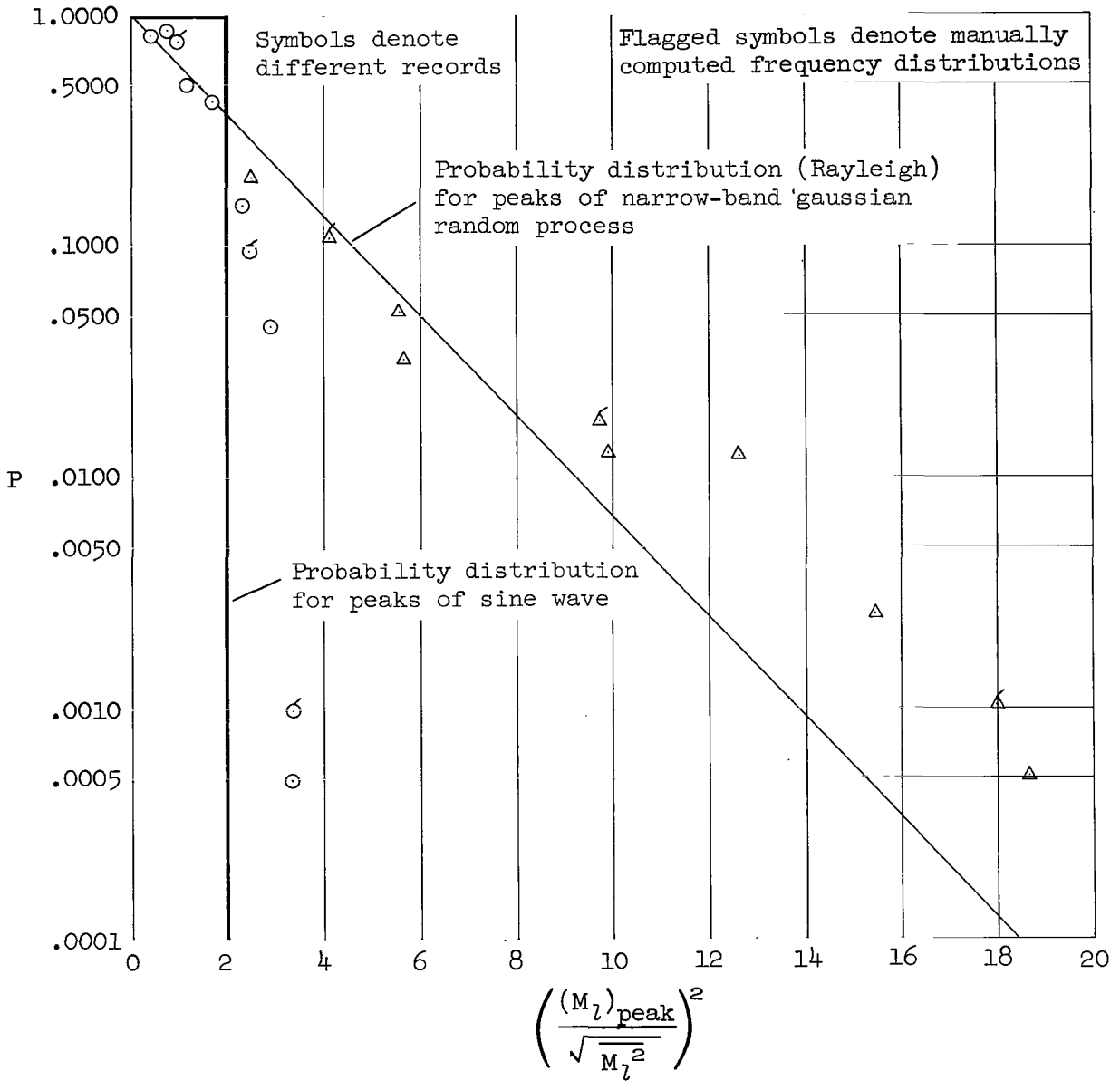

Figure 40.- Comparison of manually and electronically computed frequency distributions for two data samples.

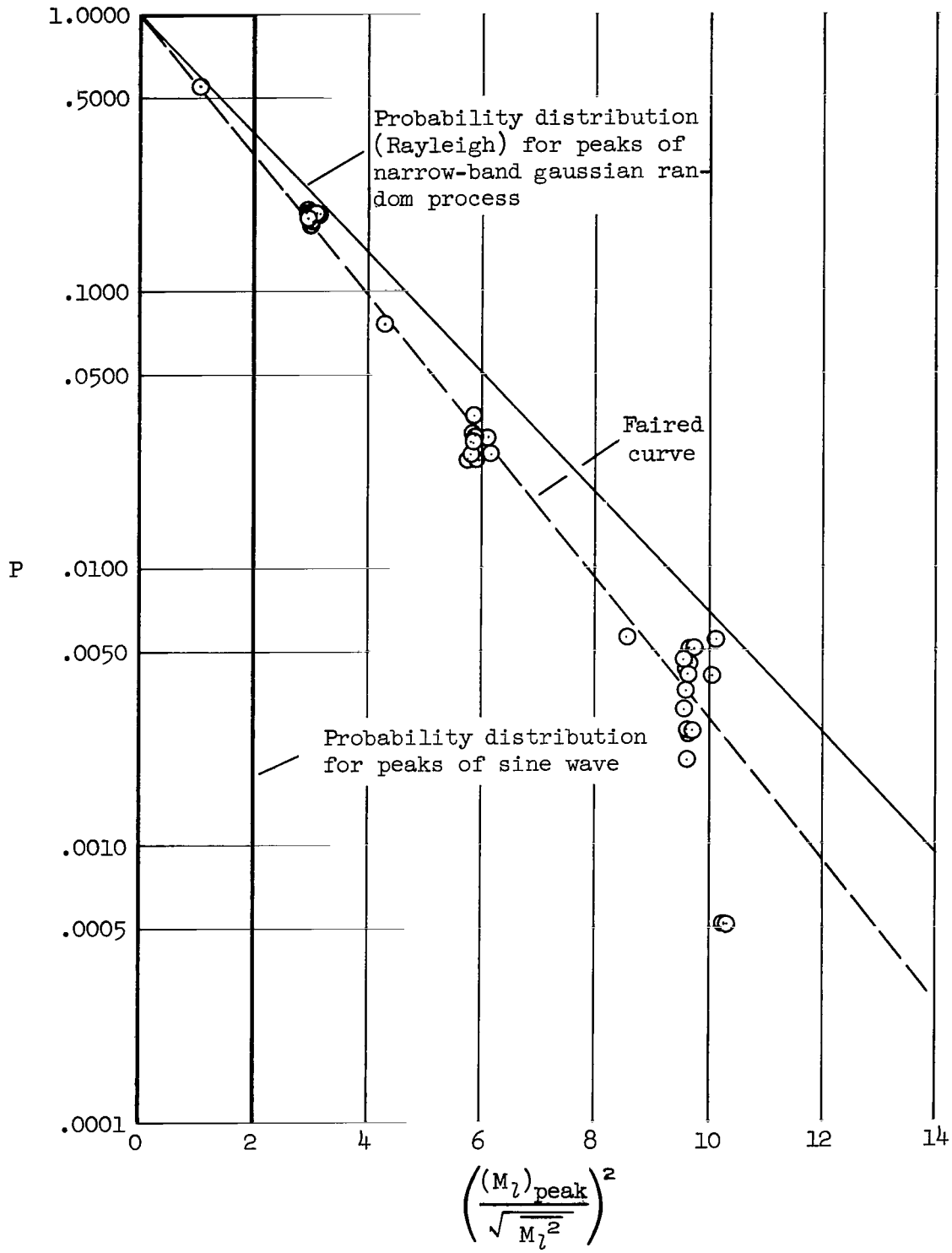

Figure 41.- Frequency distributions from 17 separate analyses of a single response record.

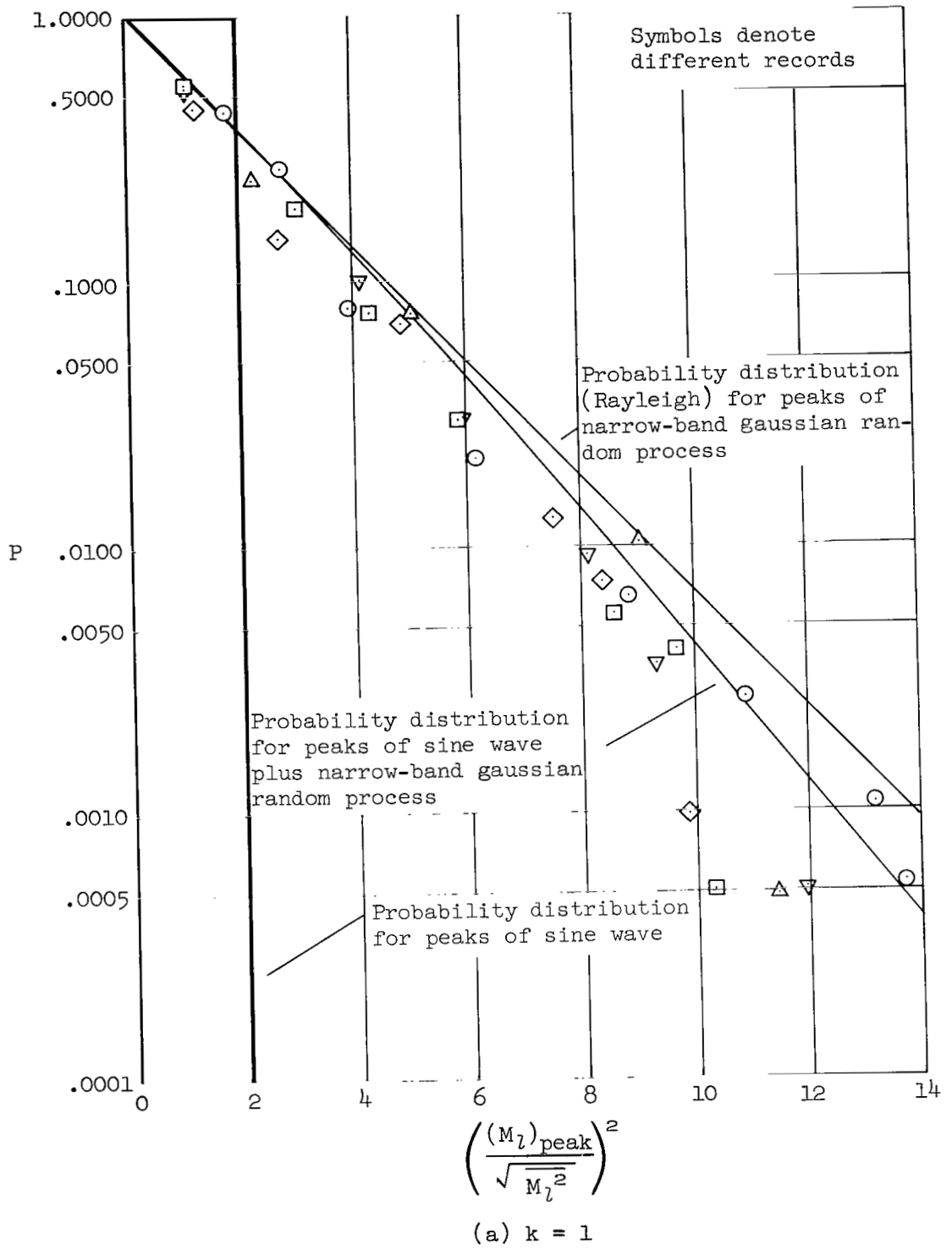

(a) k = 1

Figure 42.- Comparison of frequency distributions for selected data samples with the probability distribution of the peaks of a sine wave plus narrow-band gaussian noise for three values of the sine parameter, k.

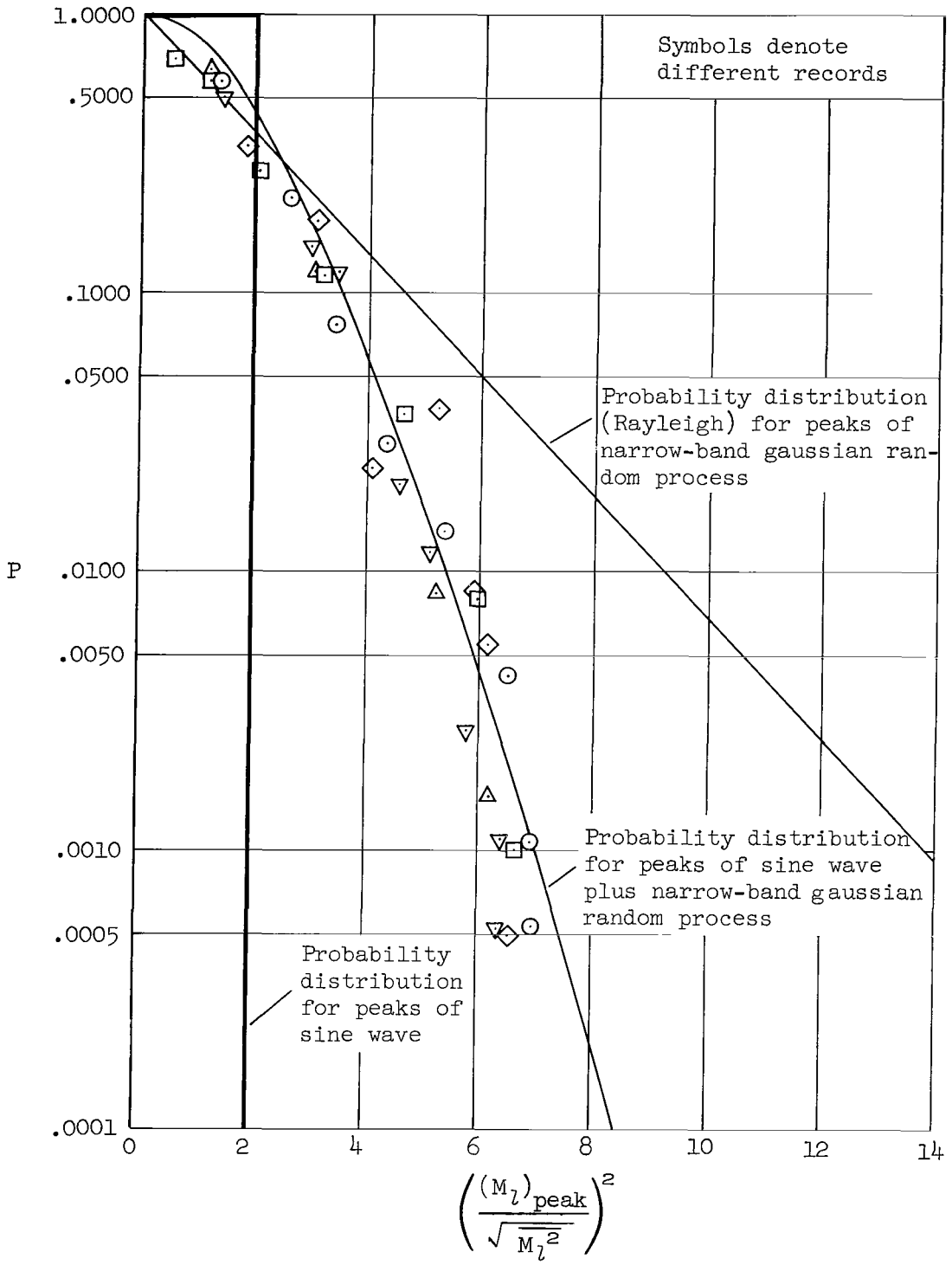

(b) k = 3

Figure 42.- Continued.

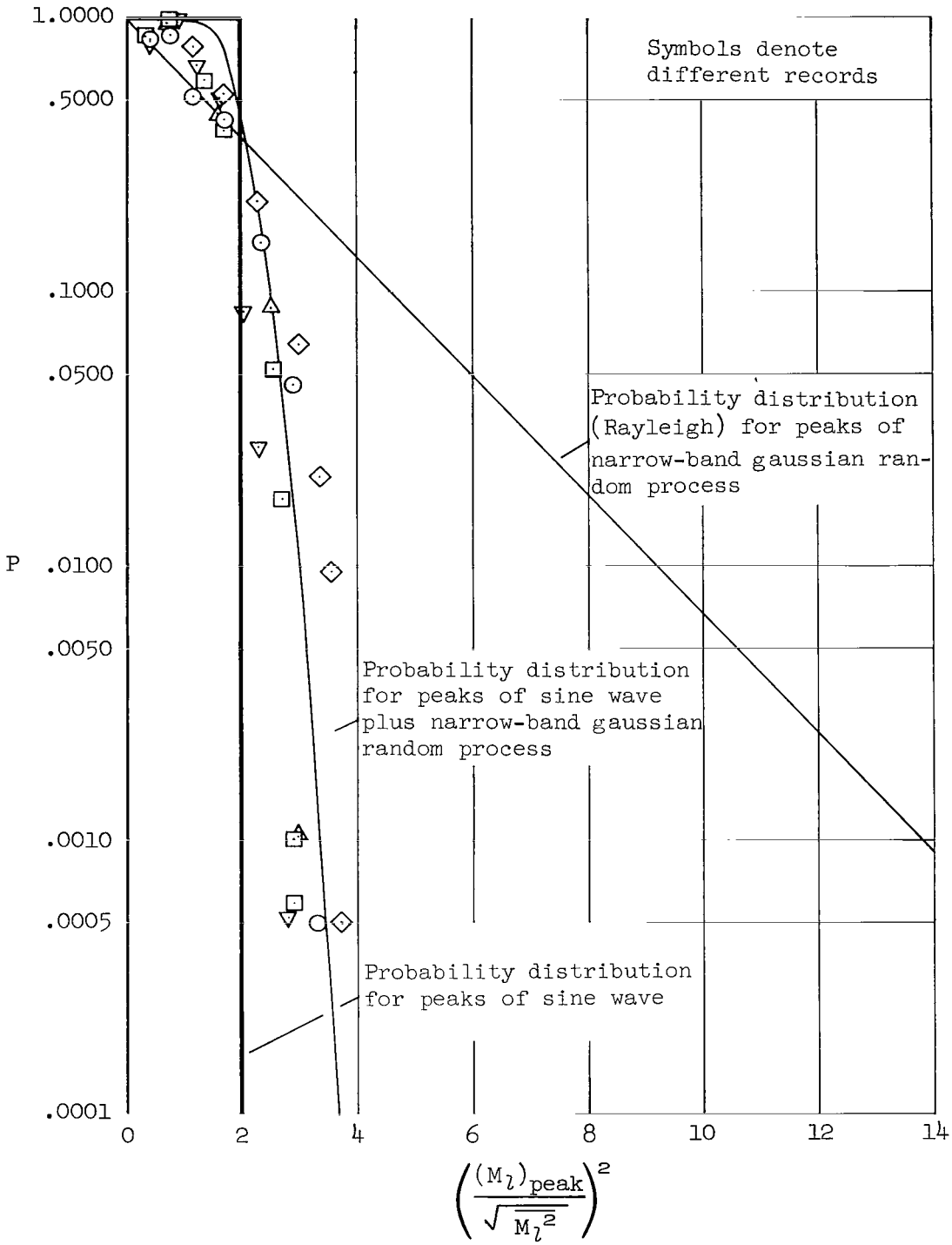

(c) k = 10

Figure 42.- Concluded.

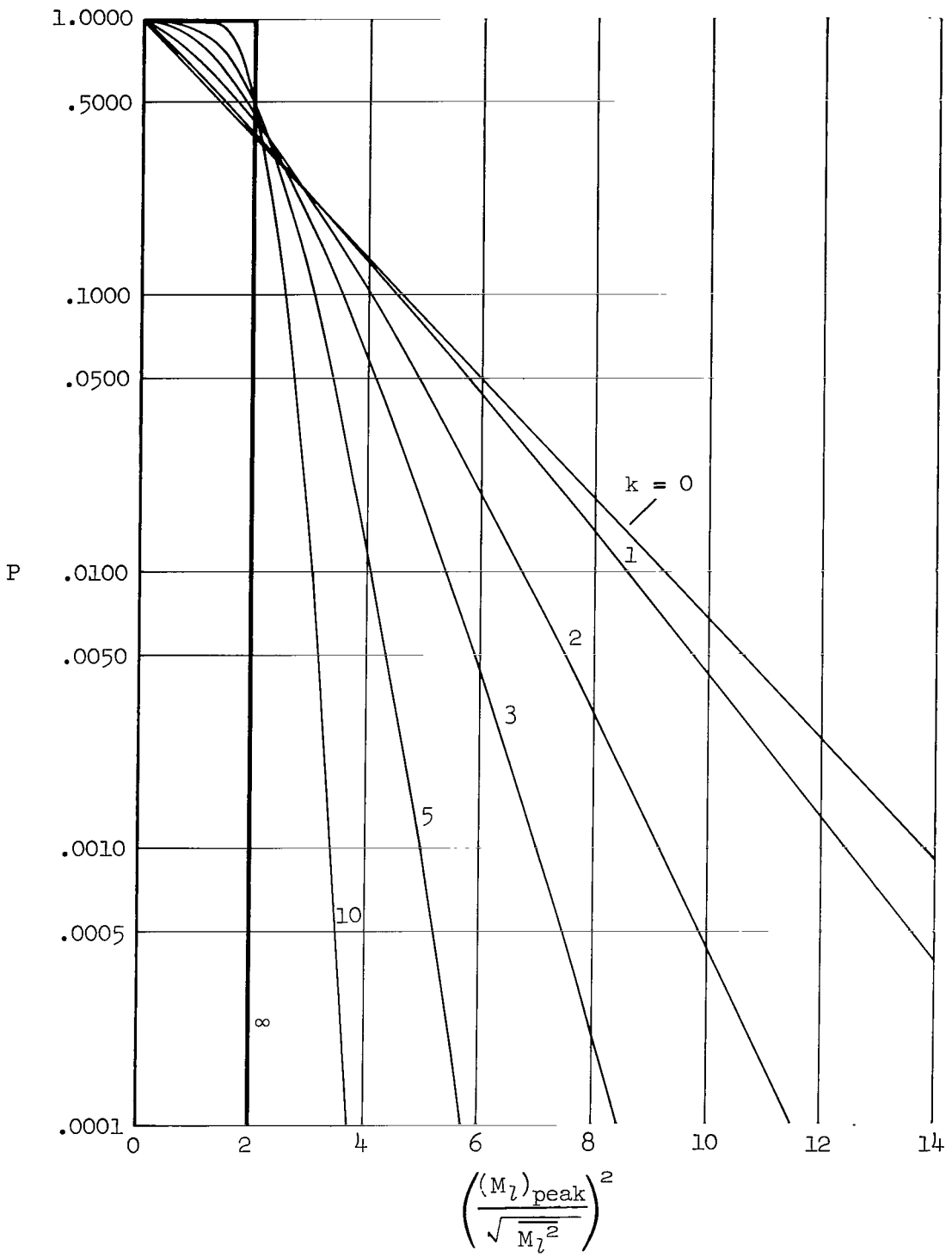

Figure 43.- Probability distribution of the envelope of a sine wave plus narrow-band gaussian noise for several values of the sine parameter, k.

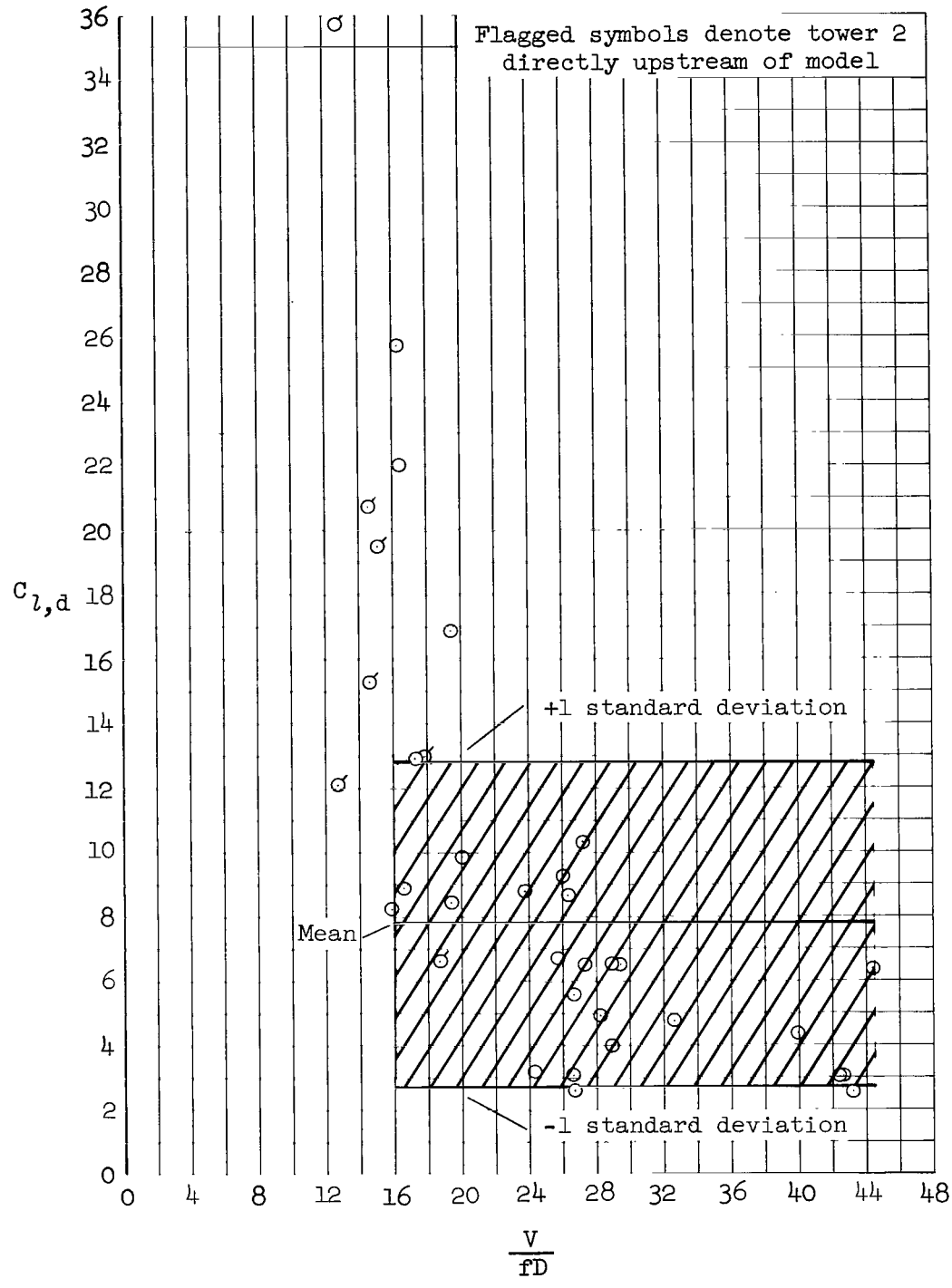

(a) Two-diameter model.

Figure 44.- Representation of selected data samples in terms of the dynamic lateral bending-moment coefficient, $C_{l,d}$.

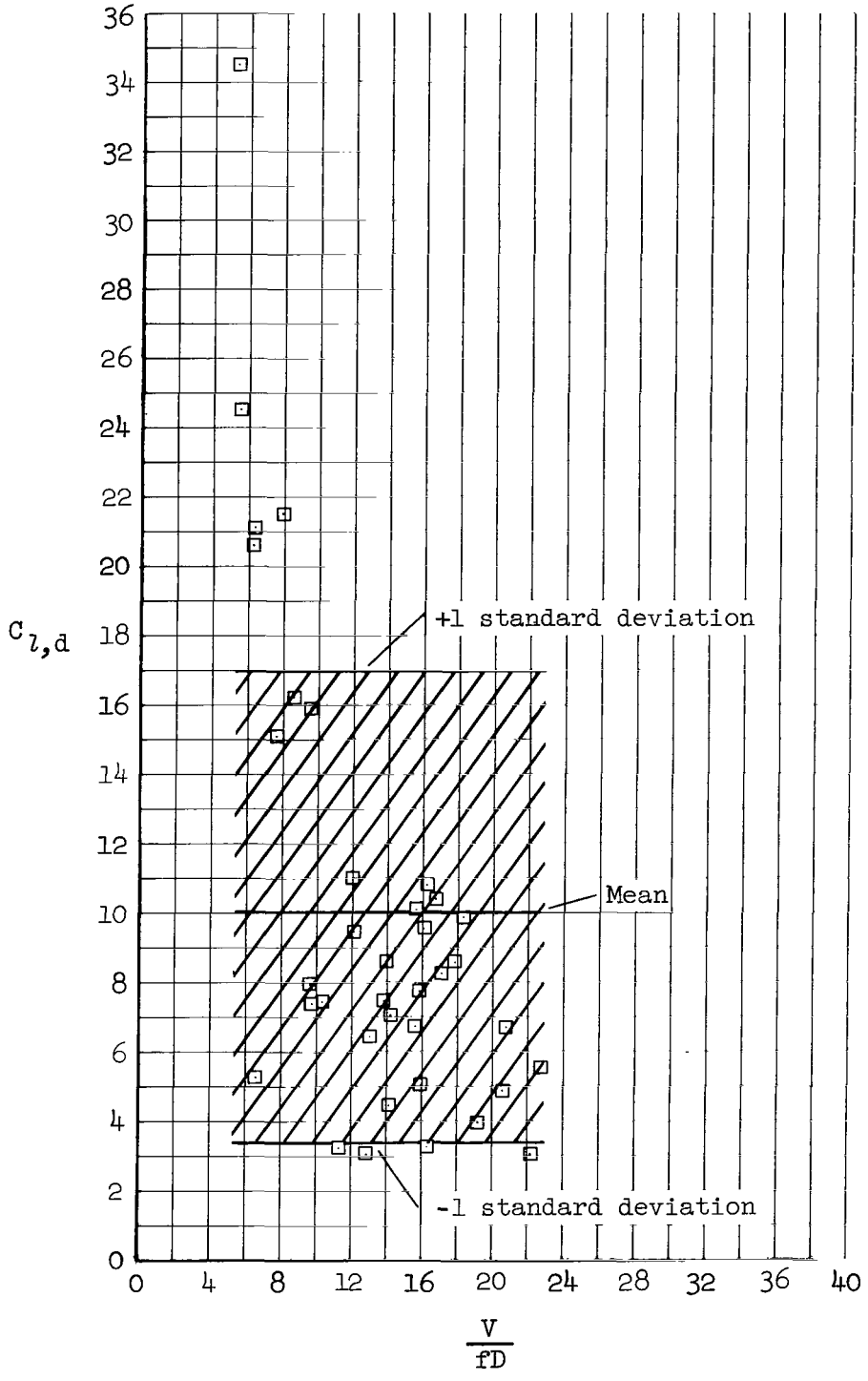

(b) Constant-diameter model.

Figure 44.- Concluded.

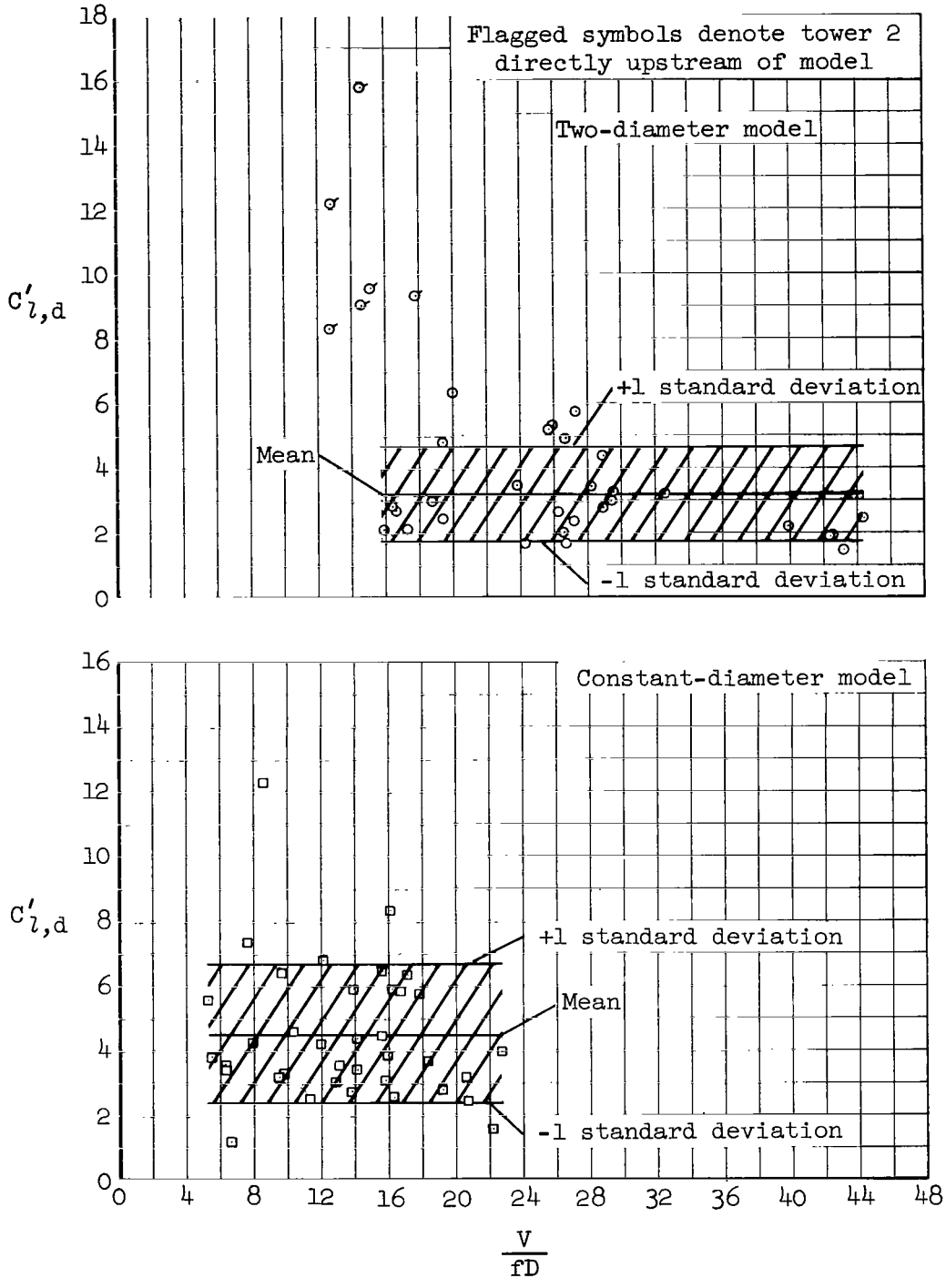

Figure 45.- Representation of selected data samples in terms of the modified dynamic lateral bending-moment coefficient, $C'_{l,d}$.

"The aeronautical and space activities of the United States shall be conducted so as to contribute . . . to the expansion of human knowledge of phenomena in the atmosphere and space. The Administration shall provide for the widest practicable and appropriate dissemination of information concerning its activities and the results thereof."

—NATIONAL AERONAUTICS AND SPACE ACT OF 1958

NASA SCIENTIFIC AND TECHNICAL PUBLICATIONS

TECHNICAL REPORTS: Scientific and technical information considered important, complete, and a lasting contribution to existing knowledge.

TECHNICAL NOTES: Information less broad in scope but nevertheless of importance as a contribution to existing knowledge.

TECHNICAL MEMORANDUMS: Information receiving limited distribution because of preliminary data, security classification, or other reasons.

CONTRACTOR REPORTS: Technical information generated in connection with a NASA contract or grant and released under NASA auspices.

TECHNICAL TRANSLATIONS: Information published in a foreign language considered to merit NASA distribution in English.

TECHNICAL REPRINTS: Information derived from NASA activities and initially published in the form of journal articles.

SPECIAL PUBLICATIONS: Information derived from or of value to NASA activities but not necessarily reporting the results of individual NASA-programmed scientific efforts. Publications include conference proceedings, monographs, data compilations, handbooks, sourcebooks, and special bibliographies.

Details on the availability of these publications may be obtained from:

SCIENTIFIC AND TECHNICAL INFORMATION DIVISION

NATIONAL AERONAUTICS AND SPACE ADMINISTRATION

Washington, D.C. 20546